Universidade de Aveiro Departamento de Engenharia Mecânica
2013

João Nuno Delgado Torrão

Controlo e execução de estampagem incremental com cinemática paralela

Control and execution of incremental forming using parallel kinematics

Universidade de Aveiro Departamento de Engenharia Mecânica
2013

João Nuno Delgado Torrão

Controlo e execução de estampagem incremental com cinemática paralela

Control and execution of incremental forming using parallel kinematics

Dissertação apresentada à Universidade de Aveiro para cumprimento dos requesitos necessários à obtenção do grau de Mestre em Engenharia Mecânica, realizada sob a orientação científica de Ricardo José Alves de Sousa, e Jorge Augusto Fernandes Ferreira, ambos Professores Auxiliares do Departamento de Engenharia Mecânica da Universidade de Aveiro

O júri / The jury

Presidente / President	**Prof. Doutor Francisco José Malheiro Queirós de Melo** Professor Associado do Departamento de Engenharia Mecânica da Universidade de Aveiro
Vogais / Committee	**Prof. Doutor Ricardo José Alves de Sousa** Professor Auxiliar do Departamento de Engenharia Mecânica da Universidade de Aveiro (orientador)
	Prof. Doutor Jorge Augusto Fernandes Ferreira Professor Auxiliar do Departamento de Engenharia Mecânica da Universidade de Aveiro (co-orientador)
	Prof. Doutor António Manuel Ferreira Mendes Lopes Professor Auxiliar da Departamento de Engenharia Mecânica da Faculdade de Engenharia da Universidade do Porto

Agradecimentos / Acknowledgements

Em primeiro lugar gostaria de agradecer aos meus orientadores, o professor Ricardo Sousa e o professor Jorge Ferreira, por toda a paciência e disponibilidade mediante a minha condição de trabalhador estudante, assim como por todo o apoio que me deram.

Em segundo lugar, mas não menos importante, menciono o Professor António Mendes Lopes pela ajuda preciosa relativa à cinemática da plataforma de stewart e por ter aceitado arguir esta dissertação, gostaria de lhe agradecer em meu nome e em nome da equipa SPIF-Aveiro. Equipa essa (Sonia, Miguel e Sá Farias) que sempre se apoiou mutuamente, na batalha que foi construir uma máquina funcional, com um especial obrigado para o Miguel, que mais do que um colega de trincheira, foi o nosso sargento.

Quero também agradecer aos professores, além dos meus orientadores, que sempre estiveram disponíveis para me ajudar não só durante a dissertação, mas também durante o resto do curso e, que sempre primaram pelas boas relações entre o corpo docente e discente, sendo eles o professores Victor Santos, António Bastos, João Oliveira, Hugo Calisto, Robert Valente, Filipe Teixeira-Dias, Carlos Relvas, entre outros. Um obrigado especial também à diretora de Curso, a professora Mónica Oliveira em particular pela paciência que teve com a minha pessoa e pelo zelo que tem pelos melhores interesses dos seus alunos.

Estes mesmos agradecimentos também se estendem aos membros do corpo não docente, o engenheiro Festas, o investigador Victor Neto a dona Cecília, a dona Júlia e a dona Filomena entre outros.

Para finalizar os agradecimentos a esta casa que muito me ensinou gostaria de mencionar os meus colegas e amigos, uma lista infindável, que não cabe nesta página, de pessoas sem as quais o meu percurso académico não teria sido tão gratificante, o pessoal do LAR, unidos na nossa demanda de gozar com o Jorge, a comissão de faina, todos os meus caloiros, os meus colegas de casa, em especial o meu "filho"João Guilherme "freestyle"Ferreira e todos aqueles cúmplices de trabalhos, invenções e brincadeiras, foram vocês que me deram alento para fazer tudo o que fiz no DEM.

Não podia deixar de agradecer à minha família, aos meus pais que desde cedo fizeram todos os sacrifícios para me dar aquilo que nunca tiveram e que eu por vezes pareço não dar valor, aos meus avós paternos cuja memória mantenho viva e que sempre me deram a liberdade de explorar a minha curiosidade, à minha avó materna que nos seus momentos de lucidez ainda tem coisas para me ensinar, e tambem aos meus primos e primas, novos e velhos, pela alegria que conferem à nossa família.

Na minha Figueira também há pessoas merecedoras de aqui serem mencionadas, todos os meus irmãos escuteiros do 235 assim como aqueles amigos de longa data que acham que vou ser responsável pelo carro voador ou pelos robots dominarem a terra, Cátia, Cláudia, Daniel, Grifo, Nuno e vários Luises, obrigado.

E como o melhor é sempre para o fim o meu mais profundo obrigado é para a minha Lili, que me irá sempre gozar por ter sido engenheira uma hora antes de mim, obrigado pela paciência, amizade e força que é uma constante a cada dia que passa.

Palavras-chave

Plataforma de Gough/Stewart; Estampagem Incremental; Medição de forças em três eixos; Lógica Difusa.

Resumo

O projeto SPIF-A é um verdadeiro desafio de engenharia: desenvolver uma máquina totalmente nova e inovadora para conformação plástica de chapa. Trata-se principalmente de um trabalho de equipa, que abrange varias áreas da engenharia mecânica, desde análise estrutural até automação e controlo, passando pela termodinâmica e cinemática, entre outras.

Esta dissertação sendo mais uma peça no puzzle, vai-se focar no seu desenvolvimento, principalmente no estudo da cinemática inversa e directa da plataforma de Stewart, assim como no desenvolvimento do primeiro sistema de controlo de posição.

O referido sistema é um controlador de lógica difusa e será implementado através de software num computador de processamento em tempo real.

Durante o desenvolvimento destes componentes também foram optimizados e/ou actualizados os sistemas hidráulicos, eléctricos e mecânicos da máquina assim como se implementou e calibrou um sistema de medição de forças de trabalho recorrendo ao uso de células de carga.

Keywords Gough/Stewart Platform; Single Point Incremental Forming; Three Axis Force Measurement; Fuzzy Logic.

Abstract

The SPIF-A project is a true engineering challenge: to develop an entirely new and innovative machine for sheet metal forming. It is mostly a team effort, covering various engineering subjects from structural analysis to automation and control but also thermodynamics, kinematics, among others.

This dissertation being another piece of that puzzle, will focus on machine development, namely on defining the machine's Stewart platform inverse kinematics, proposing a solution for the forward kinematics and devising its first position control system.

The referred system will be a fuzzy logic controller and will be implemented via software on a real time targeting machine.

During this work several components like from its hydraulic, electrical and mechanical systems were updated and a force measuring system, using load cells was installed and calibrated.

Contents

List of Tables iii

List of Figures vii

List of Acronyms ix

List of Symbols xi

1 Introduction 1
- 1.1 The SPIF-A Project 1
- 1.2 Motivation 2
- 1.3 Reading Guide 3

2 Sheet Metal Forming Review 5
- 2.1 Forming Processes and Technologies 5
  - 2.1.1 Tube Forming Operations 6
  - 2.1.2 Sheet Forming Operations 7
- 2.2 Single Point Incremental Forming Overview 8
  - 2.2.1 Aplications 9
  - 2.2.2 Forming Parameters 10
  - 2.2.3 Forming Machinery 14

3 The SPIF-A Machine 17
- 3.1 Structure 18
- 3.2 Stewart Platform 19
- 3.3 Spindle 22
- 3.4 Force Measuring System 24
  - 3.4.1 Load cells and signal amplifiers 24
  - 3.4.2 FMS calibration 26
- 3.5 Forming Apparatus 28
  - 3.5.1 Tool development 28
  - 3.5.2 Blank holders 29
- 3.6 Power Systems 30
  - 3.6.1 Hydraulic System 31
  - 3.6.2 Electrical system 33

4 SPIF-A Kinematics 35
- 4.1 Gough/Stewart platform - a brief history 35
- 4.2 Inverse Kinematics 37
- 4.3 Forward Kinematics 41
  - 4.3.1 Numerical method solutions 41
  - 4.3.2 Algebraic solutions 42

4.3.3 Open form solutions . . . 43

5 Motion Control 45
5.1 Fuzzy Logic . . . 45
5.2 SPIF-A's Controller . . . 47
5.3 Tuning and Simulation . . . 48

6 SPIF-A Operating System 51
6.1 User interface . . . 52
6.1.1 Automatic mode . . . 53
6.1.2 Simulation mode . . . 53
6.1.3 Manual positioning . . . 54
6.1.4 Machine setup . . . 55
6.2 Target Machine Implementation . . . 55
6.2.1 Interface input variables . . . 56
6.2.2 Actuator encoder reader . . . 56
6.2.3 Inverse kinematics . . . 57
6.2.4 Motion and pump control . . . 58
6.2.5 Forward kinematics . . . 58
6.2.6 Force Measuring . . . 59
6.2.7 Output to interface . . . 59

7 Experiments and Results 61
7.1 Simple geometries . . . 62
7.1.1 First parts . . . 62
7.1.2 Different forming paths . . . 64
7.1.3 Different materials . . . 65
7.2 Complex geometries . . . 66

8 Conclusions 69
8.1 Future Work . . . 70
8.1.1 SPIF process research . . . 70
8.1.2 Proposal for another SPIF-A machine . . . 71
8.1.3 Stir friction welding . . . 71
8.2 Earned Skills . . . 72

Bibliography 73

A FMS calibration data 79

B Blank holder CAD 81

C Electrical plan 83

List of Tables

1.1 Task schedule for the development of the SPIF-A machine. 4

2.1 SPIF forces. 11

3.1 Actuactor specifications [46]. 21
3.2 Shaft stiffness and fatigue analysis results. 22
3.3 Shaft bearing specifications [2]. 23
3.4 FMS load cells specifications. 25
3.5 LMU specifications. 26
3.6 Testing forces applied by the Shimadzu AG-50kNG. 27
3.7 Voltage to force conversion ratios. 27
3.8 Forming tool geometric properties. 28
3.9 Forming tools heat treatment cycle. 29
3.10 Forming areas used by different researchers/machinery. 30
3.11 Hydraulic pump specifications. 31
3.12 List of electrical components for the electrical system. 33

5.1 Rule base for the SPIF-A's FLC. 48

6.1 List of G-codes compatible with the SPIF-A OS. 51

List of Figures

1.1 SPIF-A during assembly. 2

2.1 Springback in sheet metal bending operations [9]. 6
2.2 Tube bending operations [11]. 6
2.3 Tube press forming [11]. 6
2.4 Progressive Forming tool and strip stages [11]. 7
2.5 Stages of sheet hydroforming [11]. 7
2.6 Spin forming methods [9]. 8
2.7 MPF machinery and process [21]. 8
2.8 SPIF components. 9
2.9 Various shapes obtained with SPIF manufacture [27]. 9
2.10 Aluminium SPIF produced cranial implant [28]. 10
2.11 Different methods for ISF [27]. 10
2.12 Theoretical vertical and horizontal loads [27]. 10
2.13 State of stress and forming limit curves for stamping and SPIF [34]. 12
2.14 Different methods for tool/blank contact interaction. 12
2.15 Types of forming movement: direct and inverse. 13
2.16 Types of forming path: contour milling and spiralling. 13
2.17 Different step size surface effect for the same geometry [39]. 14
2.18 ISF toolpath step types and scallop height definition [34]. 14
2.19 Adapted milling machine for research at University of Oporto [40]. 14
2.20 Serial industrial manipulator preforming SPIF operations [41]. 15
2.21 Amino®Corp. Dieless-NC machine [42]. 15
2.22 Cambridge ISF machine [39] and SFB/TR73 machine [43]. 15
2.23 Tricep performing SPIF operations [44]. 16

3.1 SPIF-A's main components. 17
3.2 First proposed geometry and its deformation simulation result. 18
3.3 Final structural design and its solicitations. 18
3.4 Stress and displacement analysis of the frame and table assembly. 19
3.5 Forming table stiffeners and electrical cabinet supports. 19
3.6 The original proposal for the SPIF-A's stewart platform [3]. 19
3.7 Base and mobile plates for the final platform design. 20
3.8 U-joints used and their geometry [45]. 20
3.9 Cylinder, valve and transducer assembly [46]. 21
3.10 Final design of Stewart platform for the SPIF-A. 21
3.11 Tool holder components (top) and clamping tools (bottom). 22
3.12 Shaft bearing configuration [5]. 23
3.13 Shaft/tool holder clamping system. 23
3.14 Exploded view of the spindle system. 23
3.15 Spindle forces and load cell configuration. 24
3.16 Wheatstone bridge. 25

3.17 Load cell and LMU connections. 26
3.18 Compression and tensile load testing along Z-axis. 27
3.19 Shear load testing mechanism. 27
3.20 Conformation table with blank and blank holder assembly. 28
3.21 Manufactured tools for SPIF operations. 28
3.22 SPIF-A's 230×230mm blank holder components. 30
3.23 Assembled 500×500 mm, and 1000×1000 mm blank holder parts. 30
3.24 Hydraulic plan for the SPIF-A. 32
3.25 SPIF-A's hydraulic pump and heat exchanger installation. 33
3.26 Electrical cabinet after reorganization. 34
3.27 Cabinet for the LMU's on top of the SPIF-A. 34

4.1 Gough Universal Rig [55]. 35
4.2 Parallel and Serial Positioning Systems [59]. 36
4.3 Taylor Spatial Frame used to align two bone fragments [60]. 36
4.4 NASA Docking System and ISS Common Docking Adapter [62]. 37
4.5 Type 3-3, type 6-3 and type 6-6 Stewart Platforms. 37
4.6 SPIF-A's platform geometry and coordinate systems. 37
4.7 SPIFF-A's base plate and mobile platform. 38
4.8 Coordinate system transformation diagram. 40
4.9 SPIF-A dimensions and Kinematic reference points. 40
4.10 Different configurations for the same link length set [69]. 41
4.11 Linearly related [75] and independent platform geometries [68]. 43
4.12 Bonev's extra sensor proposal [70]. 44
4.13 Sensor configuration. 44

5.1 Negative feedback control loop. 45
5.2 Structure of a fuzzy logic based controller[79]. 46
5.3 Fuzzification of a crisp input variable. 46
5.4 Fuzzy rule interference system. 46
5.5 PID and FLC response comparison for a 0.25 step input [80]. 47
5.6 Input and output membership functions. 48
5.7 Output signal surface in order to error and error derivative input. 48
5.8 Matlab™ simulator. 49
5.9 Simulink™ controller model. 49
5.10 Controller outputs for various tested gains. 50

6.1 Worflow between the SPIF-A and its operator. 52
6.2 SPIF-A GUI selection menu. 52
6.3 Automatic mode interface. 53
6.4 Simulation mode interface. 54
6.5 Manual positioning mode interface. 54
6.6 Joystick used for manual positioning. 55
6.7 Machine setup interface. 55
6.8 Control model input variables. 56
6.9 Encoder analyser function block. 56
6.10 SPIF-A kinematic links geometry. 57
6.11 WCS to MCS transformation and inverse kinematic function blocks 57
6.12 Possible forming angle δ versus ideal forming angle β 58
6.13 analog control signal outputs for pump and actuators 58
6.14 Forward kinematics and MCS to WCS transformation blocks. 59
6.15 Load cell analog input signal reader for the FMS. 59
6.16 Output variables for the GUI. 59

7.1 Three axis and five axis forming strategies for a truncated cone [6]. 61
7.2 First path test performed. 61
7.3 Examples of truncated pyramids and cones to be produced. 62
7.4 Centering apparatus. 62
7.5 Visual representation of the sine law. 63
7.6 Ruptured part while attempting 70º wall. 63
7.7 Top and bottom view of a 45º truncated pyramid made by the SPIF-A. 63
7.8 Truncated cones made using 10, 5 and 1 millimetre vertical increments. 63
7.9 Parts made using contour milling and spiralling paths. 64
7.10 Measured forces for different toolpath types. 64
7.11 Truncated cones made from aluminium and dual phase steel. 65
7.12 Measured forces for truncated cones using different materials. 65
7.13 Uniaxial tensile strain-stress curves for DPS780 [88] and AA1050 [89]. 66
7.14 Face masks produced using different size tools. 66
7.15 Cranial implant produced by the SPIF-A. 67
7.16 Volkswagen beetle bonnet produced by the SPIF-A. 67

8.1 Evolution of the SPIF-A during this work. 69
8.2 Springback on solar ovens formed with/without a backing plate [39]. 70
8.3 Stir friction welding process [92]. 72

List of Acronyms

CAD Computer Aided Design

CAM Computer Aided Manufacturing

CDA Common Docking System

CET Cable Extension Transducers

CNC Computer Numerical Control

DOF Degrees of Freedom

FLC Fuzzy Logic Control/Controller

FMS Force Measuring System

GUI Graphical User Interface

ISF Incremental Sheet-metal Forming

ISS International Space Station

LMU Load Monitoring Unit

MAG Metal Active Gas

MCS Machine Coordinate System

MPF Multi-Point Forming

NASA National Aeronautics and Space Administration

NDS NASA Docking System

OS Operating System

PID Proportional-Integral-Derivative (type of controller)

PKM Parallel Kinematic Machine

SPIF Single Point Incremental Forming

SPIF-A Single Point Incremental Forming - Aveiro (machine designation)

SKM Serial Kinematic Machine

SRH Semi Regular Hexagon

TCP/IP Transmission Control Protocol - Internet Protocol

TPIF Two Point Incremental Forming

TTL	Transistor-transistor logic
WCS	Work-piece Coordinate System

List of Symbols

A_c - Cylinder Bore Area

$B_p(i)$ - Base vertex coordinates

c - Specific heat

C_0 - Bearing static load

C_D - Bearing dynamic load

d_{min} - Minimum Diameter

d_{bore} - Bore Diameter

F_v - Vertical Forming Force

F_h - Horizontal Forming Force

F_t - Total force

F_{nZ} - Force at Z axis

F_{hX} - Horizontal force at X axis

F_{hY} - Horizontal force at Y axis

H_{tf} - Hight tool

J^{-1} - Inverse Jacobian matrix

K - Stiffness Matrix

Kde - Error derivative gain

Ke - Error gain

Ku - Output signal gain

L_i - Actuator length

LBM - Base SRH large edge

LBm - Base SRH small edge

LPM - Platform SRH large edge

LPm - Platform SRH small edge

$M_p(i)$ - Platform vertex coordinates

M_x - Moment around X axis

M_y - Moment around Y axis

M_z - Moment around Z axis

$\dot{m}$ - Flow

P_w - Work pressure

P_u - Bearing fatigue load

P_v - Power loss

P - Position matrix

r - Tool Radius

R - Rotational matrix

R_f - Distance between spindle and load center cell

R_n - Resistor

SEi - CET positional coordinates

SLi - CET measured length

t - Initial Blank Thickness

T_f - Transformation matrix

U_{out} - Analog voltage output

v_{lim} - Maximum speed

V_G - Bridge voltage

V_s - Excitation voltage

v_s - Stroke speed

V_{tK} - Oil tank volume

σ_y - Yield Strength

σ_θ - Circumferential Stress

σ_m - Hydrostatic Stress

σ_ψ - Meridional Stress

α - Cone Interior Angle

ϵ_n - Principal Strain

θ_{max} - Maximum distortion

δ_{max} - Maximum displacement

ρ - Density

ϑ_{Bt} - Ideal oil temperature

ϑ_1 - Initial oil temperature

ϑ_2 - Final oil temperature

λ - Wall angle

Chapter 1

Introduction

Mankind is constantly improving production technology, finding new and better ways to suit the needs of industry. In the world of sheet metal products, the main process used is deep drawing with punch presses but, with product diversification, batches tend to get smaller and the initial investment required to make punches and dies tends to make the whole process less cost effective.

To comply with the needs of these small or single piece production series, being rapid tool/prototyping parts, custom built medical components or other unique situations a solution was born: Incremental Sheet-Metal Forming, a process which was patented in 1967 by Edward Leszak [1]. The method of production is easy to understand, instead of using a punch press with a costly specialized tool and die to form a part with each stroke, one or more simple tools (only as complex as small metal rod, with or whitout a round tip) are used to shape a piece over time in a similar fashion to a milling machine, being said forming time ISF's major disadvantage witch is longer when compared to other production methods such as deep drawing and hydro-forming.

1.1 The SPIF-A Project

In order to contribute to the development of the sheet-metal industry, a new machine [2] is being developed at the University of Aveiro aiming to elevate this process to the highest level. It is both a team effort and an engineering challenge; the team is comprised of both students and teachers/researchers working on various domains and, since those domains overlap, problem solving is made from several inputs rather than by a single individual, making it the ideal environment to learn from several specialities of mechanical engineering.

The project took its first major step in 2010 with the work of Sonia Marabuto [3]. Other students have worked in this project being through research, like José Sena who simulated and studied the process on ABAQUS software [4], or actually developing and building the machine, like Miguel Martins who oversaw the structure's in-house construction and power systems' design [5]. Both project and machine have received the name of SPIF-A which stands for Single Point Incremental Forming - Aveiro, since this project is being carried out at the Department of Mechanical Engineering of the University of Aveiro.

This machine brings a new approach to the ISF industry. With the limitations of current machinery in mind, the SPIF-A was outfitted with a custom made Gough/Stewart platform with six top of the line hydraulic cylinders giving it 6 DOF [2], while maintaining the ability to apply high loads.

Many different technologies are already employed and have been adapted and connected together. Several fields were studied: design of kinematic systems, structural design, dimensioning of hydraulic systems, development of the electrical system, development of a force measuring system and a custom spindle.

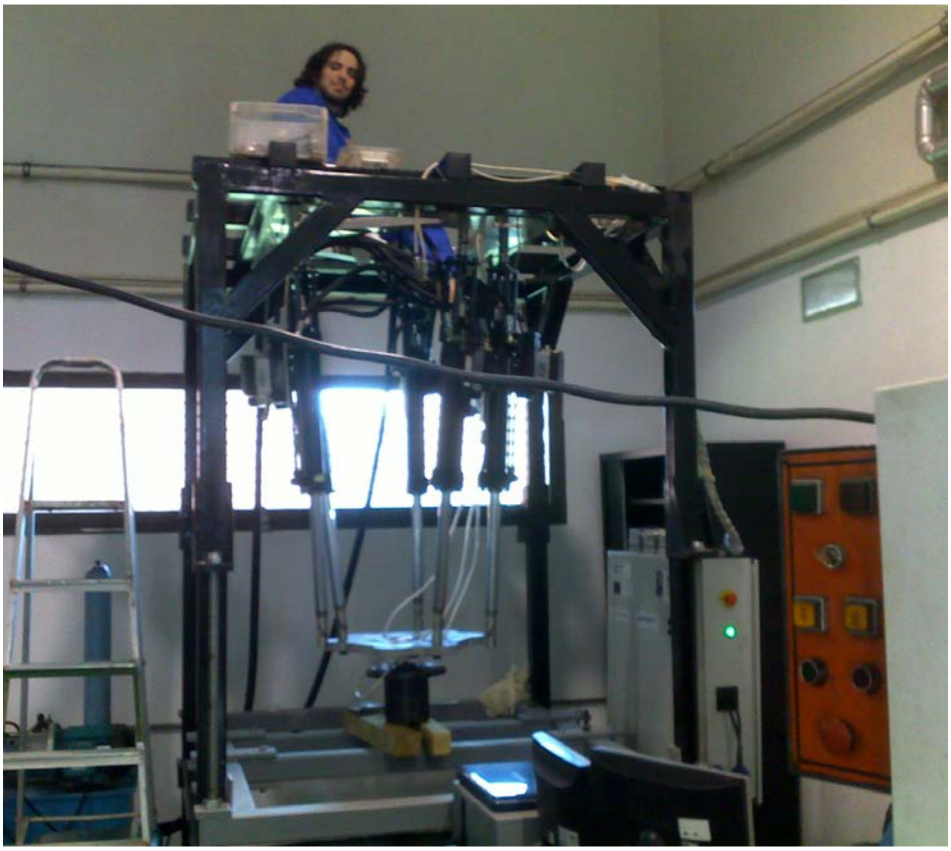

Figure 1.1: SPIF-A during assembly.

This project aims to pave the way for future research and development of the process, both in improving the machine but also in developing and understanding its forming mechanism.

1.2 Motivation

Like the SPIF-A project itself and all other work preceding this thesis, its aim is to continue the development of the SPIF-A machine and to provide a positive contribution to the ISF industry.

Using a custom made hydraulic Gough/Stewart platform, although innovative, presents a series of challenges. First of all there's the matter of designing the machine, most of that hasalready been done in the previous works [3; 5], after that comes the construction of said machine. Part of that work was done throughout this thesis, making it a real hands-on project.

The tasks due were split into three groups with a parallel time frame, hasseen on Table 1.1. One such group focused on literary work: researching and analysing kinematic and control solutions for SKM hydraulic applications and writing the thesis document and the machine's operating manual.

The second task group consists of anything related to the construction of the machine's physical components(welding, painting and milling) and the assembling of its hydraulic and electrical power systems. The third group was about the development of the machine's operating system, the calibration of the measurement systems and designing the user interface. Both this task groups were conducted with the aid and guidance of fellow researcher Miguel Martins, and some of the later tasks, like the G-code reader and Tool manufacture were done side-by-side with João Sá Farias for his PhD [6].

Academically speaking, in order to lay way for future research, the aim is to overcome all the obstacles of machine development, such as:

- obtaining a solution for the kinematic system in order to proper position and navigate the forming tool;
- calibrating a force measuring system in order to study the forming forces involved in producing parts from different materials and/or blank widths;
- making machine operations as straight forward as possible by developing a user-friendly HMI and employing a G-code processor to command tool paths;

In a social/industrial standpoint, since incremental forming industrial solutions aren't yet rectally available, and the return for the investment required to implement the process is very difficult to achieve due to the small production batches involved, having such a technology at the University of Aveiro will attract the attention of clients and companies looking for unique solutions that only ISF can provide, hopefully strengthening the bond between the academic world and local/national industry paving the way for future joint projects and job opportunities for its students.

1.3 Reading Guide

This thesis is divided into eight chapters. Chapter one provides an introduction what the SPIF-A project stands for and how this thesis will further its development, while chapter two is the literary review on sheet-metal forming technologies paying special to the SPIF process, explaining how it differs from other methods, in order to understand the requirements needed when designing equipment to preform it.

Chapter three catalogues all of the machines subsystems and explains how some of some of those of them were further developed and updated during this thesis, namely the power supply, the force measuring system and the forming tools. The Gough/Stewart platform is only briefly addressed in this chapter as chapter four, is used for the study of its kinematics, specially the selection of a solution for its forward kinematics and its simulation on MatLab™, it also features a small introduction explaining the history and applications of the platform. The control strategy of this mechanism is presented in chapter five with the analysis of some control methods in particular Fuzzy Logic.

Chapter six explains the software developed using MatLab™ and Simulink™ used to control and interface with the SPIF-A via the Speedgoat™ Real-Time Target Machine, including its G-Code capabilities, whilst chapter seven yields a qualitative analysis of the first produced parts, to better understand the machine's capabilities.

Chapter eight presents the conclusions, reflects on the skills earned during this thesis, proposes future work to complement the existing systems and to aid in the continuation of the SPIF-A project.

Table 1.1: Task schedule for the development of the SPIF-A machine.

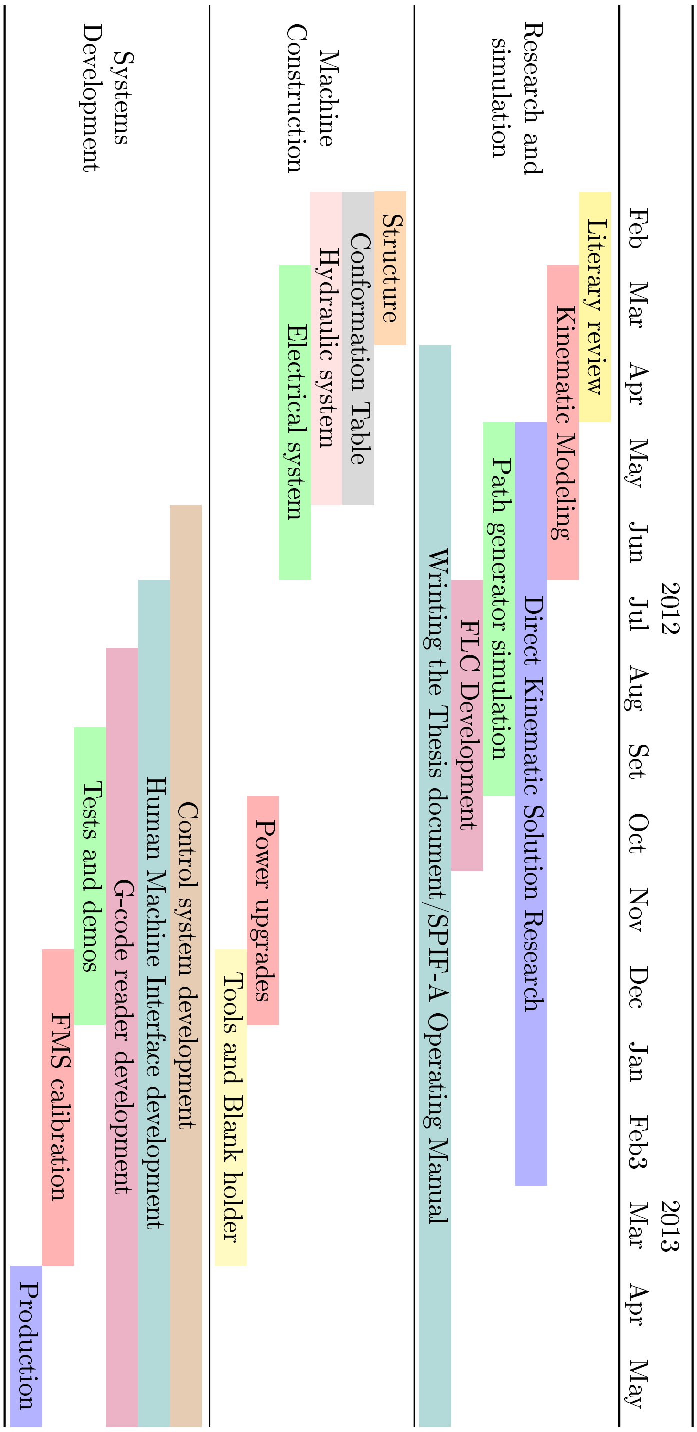

		2012												2013			
		Feb	Mar	Apr	May	Jun	Jul	Aug	Set	Oct	Nov	Dec	Jan	Feb3	Mar	Apr	May
Research and simulation	Literary review	■	■	■													
	Kinematic Modeling		■	■	■	■											
	Direct Kinematic Solution Research				■	■	■	■	■	■	■	■	■	■			
	Path generator simulation				■	■	■	■	■								
	FLC Development						■	■	■	■							
	Writing the Thesis document/SPIF-A Operating Manual			■	■	■	■	■	■	■	■	■	■	■	■	■	■
Machine Construction	Structure	■	■														
	Conformation Table	■	■	■	■												
	Hydraulic system	■	■	■	■												
	Electrical system		■	■	■	■											
	Power upgrades									■	■	■					
	Tools and Blank holder											■	■	■	■		
Systems Development	Control system development					■	■	■	■	■	■	■	■	■	■	■	■
	Human Machine Interface development						■	■	■	■	■	■	■	■	■	■	■
	G-code reader development							■	■	■	■	■	■	■	■	■	■
	Tests and demos								■	■	■	■					
	FMS calibration											■	■	■	■		
	Production															■	■

Chapter 2

Sheet Metal Forming Review

There has been a never ending number of uses for metal parts throughout history and each one as a proper way manufacture. In the metalwork industry four major groups of processes exist:

Casting

Molten metal is shaped in a mold as it cools and solidifies.

Compatible with various materials: iron, steel, aluminium, copper and other metals, used different methods (like die, centrifugal or sand casting) and and molds (permanent or lost/expendable) to comply with material properties and production specifications.

Forming

Also known as plastic forming, it consists of deforming a metal work-piece through the use of mechanical force, sometimes using heat to soften the part and increasing its formability. This is done removing very little to none material, making it very cost effective.

Cutting

Consists of any method do obtain geometries by removing excess material from a work-piece. There are three categories: machining which implies chipping (milling, turning and drilling for example), burning techniques like plasma, laser and oxi-cut that use focused heat to remove material, the third group consists of all technology that doesn't fall in the previous categories like shear cutting in presses and chemical milling. Uses range from the production of blanks for other operations(for milling and forming), to produce whole parts or for finishing operations on parts obtained from casting and forming.

Joining

Two or more parts are assembled together either mechanically (such as rivets or bolts) or thermally by melting the same material (welding) or a different support material (soldering and brazing).

2.1 Forming Processes and Technologies

Plastic forming can be broken down into two major groups: bulk forming and sheet (and tube) forming. In both cases, the surfaces of the deforming material and the tools are in contact, and friction between them may have a major influence on material flow.

In bulk forming, the material starts as a billet, rod, or slab, and is usually pre-heated. The surface-to-volume ratio increases considerably under the action of highly compressive loads during forming, resulting in an appreciable change in shape or cross section, with little to none springback [7]. In sheet forming, the deformation occurs due to tensile loads bending or stretching the blank, a thin piece relative to its width and length, into a three-dimensional shape, often without significant variations in sheet thickness or surface characteristics. Due to these facts, elastic deformation cannot be dismissed in most methods meaning that springback or elastic recovery hasto be accounted for when producing parts and designing equipment to produce them [8].

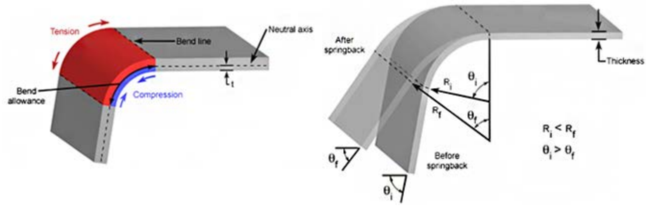
Tension
Bend line
Neutral axis
Bend allowance
Compression
t_t
After springback
Thickness
R_i
θ_i
R_f
θ_f
$R_i < R_f$
$\theta_i > \theta_f$
θ_f
Before springback
θ_i

Figure 2.1: Springback in sheet metal bending operations [9].

2.1.1 Tube Forming Operations

While tubes and sheets share the same forming mechanics, machinery and processes are quite different. In fact each method often requires dedicated equipment or at least specialised tools. When it comes to shaping tubes, the most common operation is bending its shape without altering its cross-section. To achieve this the tube is filled with a medium like sand or a fluid to prevent collapse as mechanical force is exerted [10].

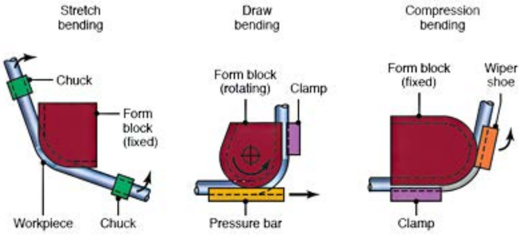
Stretch bending
Draw bending
Compression bending
Chuck
Form block (fixed)
Workpiece
Chuck
Form block (rotating)
Clamp
Pressure bar
Form block (fixed)
Wiper shoe
Clamp

Figure 2.2: Tube bending operations [11].

Other than bending, tubes can also be formed in presses using compressive forces, still using the same filling medium. This type of solicitation is beneficial in forming operations because it delays fracture, but the use of custom molds and dies make the process more expensive and less versatile a bending. One of these specialized process, tube hydroforming, actually uses the fluid inside the tube to apply the necessary pressure to achieve complex forms like exhaust manifolds [12].

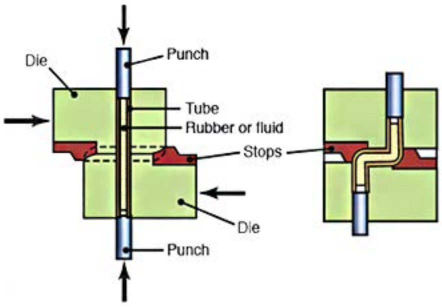
Die
Punch
Tube
Rubber or fluid
Stops
Die
Punch

Figure 2.3: Tube press forming [11].

2.1.2 Sheet Forming Operations

Sheet metal parts range from simple bent and cut pieces to complex shapes, they are most commonly produced in press operations in single or multiple stages by using progressive tools, this technique know as drawing are highly rentable as they produce one part per stroke [13].

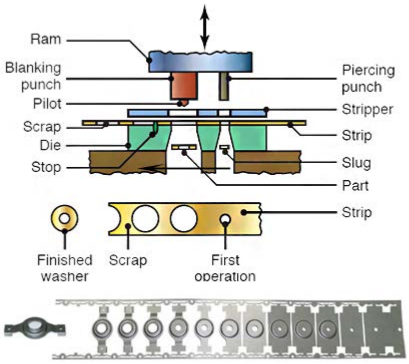

Figure 2.4: Progressive Forming tool and strip stages [11].

Depending on its geometry, namely depth, there is also the process of deep drawing (for example to produce beverage cans) that requires careful planing in order to avoid failure during forming, noting that custom tools and dies are required there is a significant initial investment. Also since changing part geometry implies tool and die alterations, versatility is very limited [14].

To comply with the lack of versatility many techniques have emerged that rely less on costly proprietary tool, requiring only either the punch/tool or the die. One such example is using a thick rubber pad in place of the die to evenly distribute pressure as the punch pushes the blank against it [15], sheet hydroforming swaps the die for a rubber diaphragm back by a fluid pressure vessel that forces the blank to wrap around the punch [16].

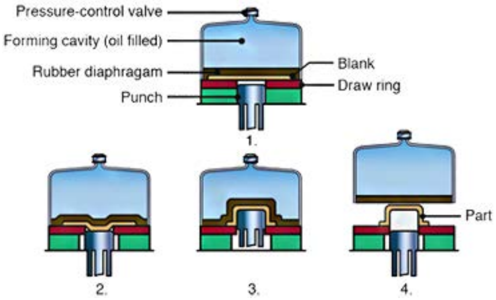

Figure 2.5: Stages of sheet hydroforming [11].

Other methods keep the die as a mold and use fluid mechanics to form the material, in superplastic forming uses extreme heat to soften the sheet and gas pressure to shape it to the geometry of the mold, mush like polymer vacuum forming processes [17]. Magnetic pulse forming employs magnetic field manipulation in order to shape the part and being purely electromagnetic, is not limited to repetition rate by the mechanical inertia of moving parts achieving rates of hundreds of operations per minute, making it one of the quickest production methods [18].

Explosive forming uses water to propagate pressure waves of a controlled explosion resulting in large parts otherwise impracticable in normal forming operations [19] that would otherwise have to be formed in separate sections and subsequently tailor-welded together.

Spin forming is used to produce axisymmetric parts, a sheet metal disc is rotated at high speeds while rollers press it against a tool, called a mandrel, to form the shape of the desired part, two methods exist: conventional spinning, where the blank is bent around the mandrel and shear spinning, where the part is stretch along the mandrel. It can be preformed on existing CNC lathes, making it a low-cost process [20].

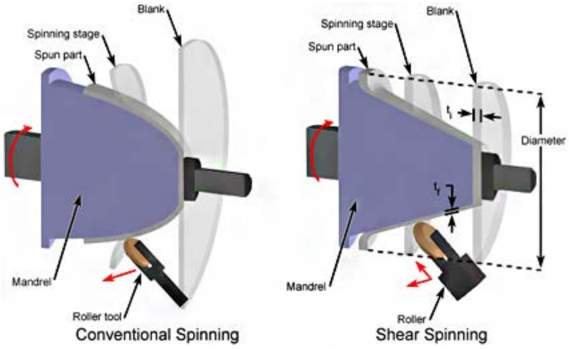

Figure 2.6: Spin forming methods [9].

Multiple Point Forming (MPF) is a flexible 3D manufacturing process, meaning that in the same machine, with the same tools, production of very distinct parts is possible. Instead of a solid punch and die, it uses two matrices made from series of punches adjustable in length whose tip form a discrete die/punch surface.

Large parts can be shaped via sequential MPF and when the deformation path is designed properly, forming defects can be avoided completely achieving large deformation. While the initial investment is rather high due to mechanical complexity, the absence of dedicated punch/die tools make the process cheaper than some press forming technologies [21].

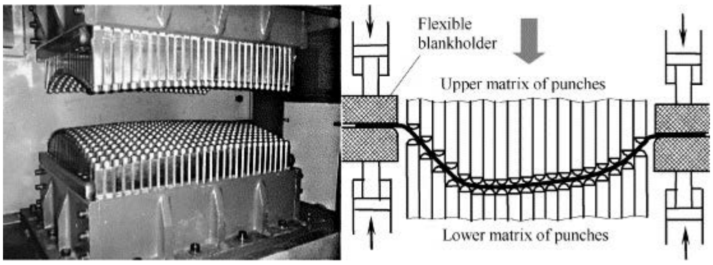

Figure 2.7: MPF machinery and process [21].

Inspired by ancient blacksmithing techniques of hammering pieces to a desired shape some methods were developed to gradually shape a part along a specific contour(ISF). The most straightforward is the incremental Hammering process where a robot arm or a CNC milling machine control the path of a oscillating hammering tool [22], while SPIF does the same but without the hammering motion simply by dragging the tool across the blank. Similar non-contact methods like laser forming, that uses localized heat resulting in thermal stress that induce plastic strain on the part [23], and water jet forming which uses a stream of pressurize fluid as a shaping mechanism that achieves good surface finish [24]. ISF being in its early years already offers a high degree of versatility but technologies need yet to be optimized to compete with the shorter forming times than its counterparts.

2.2 Single Point Incremental Forming Overview

Single Point Incremental Forming is an innovative yet simple process; the forming tool is nothing more than a cylindrical rod with a flat or spherical tip, which will gradually move along a path and press down on the sheet metal restrained on a blank holder, eliminating the need of a specialized die making it a die-less process.

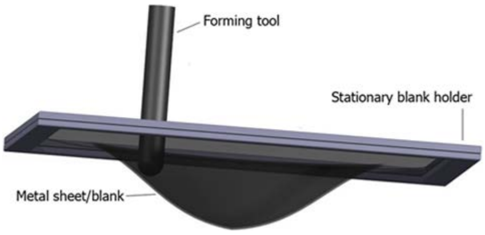

Figure 2.8: SPIF components.

Although this process was patented in 1967 by Edward Leszak [1] only on late 1990's, and thanks to the development of automation and control technologies, has it gained the attention of the industrial community, resulting in various forms of implementation.

The process has been analysed and characterised by several researchers who were able to point out it's advantages and disadvantages [25].

Advantages:

- It is highly flexible, part size and shape can easily changed without the need for new tools.
- Parts can be produced directly from the CAD model, making it one of the few methods to produce metallic rapid prototypes.
- It's incremental nature and bend/stretch deformation mechanism increase formability.
- The process is more silent and its work load is much smaller than other forming processes.

Disadvantages:

- The main hindrance is a longer forming time than its counterpart technologies resulting in smaller production batches in the same timeframe.
- Producing right or near right angles requires multiple steps
- Springback occurs during the forming process, requiring correction algorithms witch are being developed [26].

2.2.1 Aplications

Various geometries can be produced with the aided of CAD/CAM software to obtain complex forms ready to use fresh of machines, adding the fact that it is possible to apply to several different materials its ideal for rapid prototyping and tooling and combined with reverse engineering it can be used to produce replacements for discontinued or unique parts.

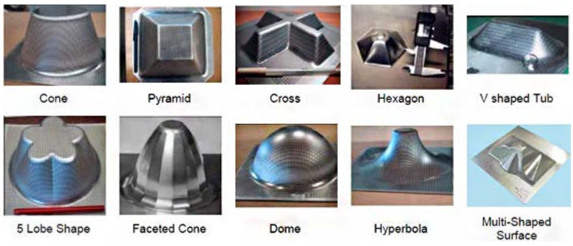

Figure 2.9: Various shapes obtained with SPIF manufacture [27].

Applications range from household appliances, to food processing, automotive and aeronautical parts, and even for medical applications such as prostheses and implants [27]. One such example was presented by Duflou et al. [28] who produced a cranial implant from the scanned model of a patient's skull.

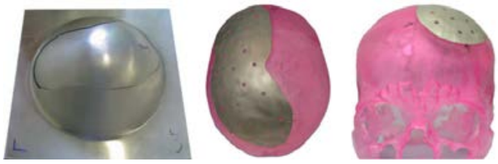

Figure 2.10: Aluminium SPIF produced cranial implant [28].

2.2.2 Forming Parameters

ISF forming mechanism is as follows: it starts by clamping a piece of sheet metal in the blank holder and letting the tool describe a contour path on it, different variants depend on the type of backing used. The most common is SPIF which uses a face plate to limit the edge of the part, instead of this a counter tool can be used on the underside of the forming part to obtain more complex forms but, requiring a more complex system and tool path planning. Another method is TPIF a method that used a partial or full die underneath and by moving the blank holder up or down is able to produce both concave and convex parts, again requiring a more complex system [27]. Parameters like work load, contact interaction and formability are similar in all methods.

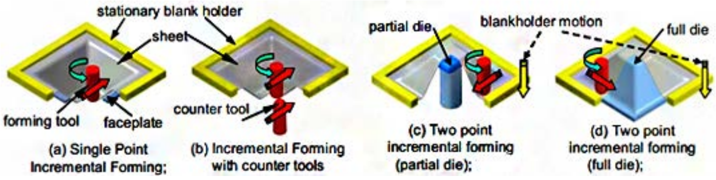
stationary blank holder
sheet
forming tool
faceplate
(a) Single Point Incremental Forming;
counter tool
(b) Incremental Forming with counter tools
partial die
blankholder motion
full die
(c) Two point incremental forming (partial die);
(d) Two point incremental forming (full die);

Figure 2.11: Different methods for ISF [27].

Forming Forces

One of the major components of a deformation process is the forming forces involved. Allwood et al. [27], used a theoretical model for SPIF by splitting the load in two a vertical force from the tool travelling normally to the flat sheet, causing a hemispherical indentation, and a horizontal force as the tool moves tangent to the existing deformed area, creating a one-sided groove known as scallop.

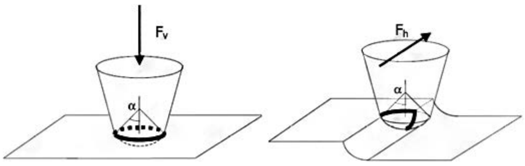

Figure 2.12: Theoretical vertical and horizontal loads [27].

$$F_v = \pi \cdot r \cdot t \cdot \sigma_y \cdot \sin\alpha \tag{2.1}$$

$$F_h = r \cdot t \cdot \sigma_y \cdot (\sin\alpha + \cos\alpha) \tag{2.2}$$

A rough assessment of the forces can be made with some swiftness. For a 1.6 mm thick mild steel blank, with a yield stress of 350 MPa and considering a tool radius of 15 mm with a 30 degree angle, the predicted vertical and horizontal are 13.2 kN and 5.3 kN. Various authors have used different methods to estimate/determine load values for different materials, part thickness and tools, revelling that loads are significantly smaller than integral forming processes.

Table 2.1: SPIF forces.

Researchers	**Force [kN]**	**Method**
Allwood et al. [27]	13 (vertical) & 6.5 (horizontal)	theoretical
Duflou et al. [28]	1.46	experimental
Rauch et al. [29]	0.9	experimental
Jackson et al. [30]	3	experimental
Durante et al. [31]	2	experimental
Bouffioux et al. [32]	1.3	simulation
Decultot et al. [33]	12	experimental
	14	simulation

Some of the authors [28; 29; 30], tested for different step and tool size, thickness and forming angle and concluded that forming forces are directly proportional to these parameters, meaning that they size almost linearly for thicker sheets, steeper angles, wider tools and/or with the increase of step size.

Thickness and Formability

One very interesting feature of SPIF is the increase in the material formability. Formability is the ability of a material to deform plastically without fracturing. In order to achieve higher formability there are several techniques:

- heat treatments, usually formability increases in detriment of mechanical resistance;
- cold deformation, where anisotropy due to texture development can be favourable or not to increase formability depending on strain orientation.
- hybrid strain paths, hasa good combination of strain paths can promote increased formability.

In case of SPIF although the scientific community agrees that there is an increase of formability, compared with other processes like stamping or deep drawing, it is still not clear how the deformation mechanism influences the formability of the process.

A possible answer is often provided in terms of the benefits of concentrating the strain on the deformation zone under the forming tool. However, an alternative answer can be provided by comparing the principal stresses acting in the corner of the rotational symmetric sheet metal parts formed by SPIF and by conventional stamping (or deep-drawing) processes. The circumferential stress σ_θ in stamping is equal to the meridional stress σ_ψ resulting in biaxial stretching. Because the hydrostatic stress σ_m in biaxial stretching is higher than that of plane strain stretching the rate of accumulated damage in stamping is faster and results in failure faster than in SPIF, explaining its higher overall forming limit line [34].

This limiting line is drawn based on experimental data from Jewiet and Young [35] and is parallel to the strain path for pure shear $\epsilon_1 = -\epsilon_2$ as well as to the limiting condition for local necking $\epsilon_1 + \epsilon_2 = n$ of a deforming a material sheet that obeys Hooke's law $\sigma = K\epsilon_n$.

Being SPIF primarily a stretching process, wall thickness would follow sine law prediction [36]. Research from of Hussain et al. [37] showed that thickness result did not follow sine law in

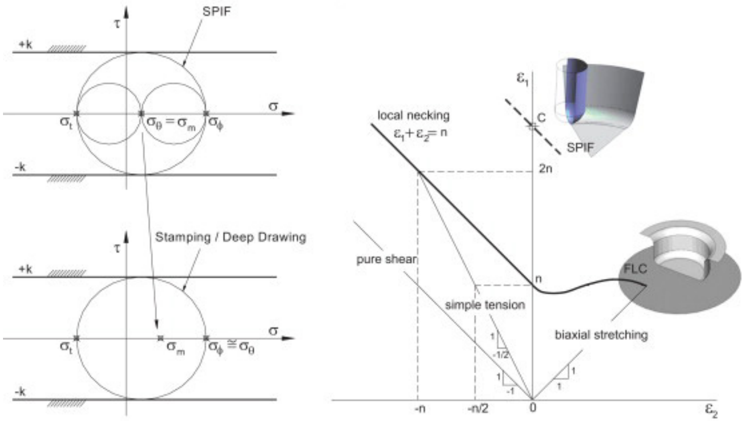
SPIF
τ
+k
σ
σ_t
$\sigma_\theta = \sigma_m$
σ_ϕ
-k
Stamping / Deep Drawing
τ
+k
σ
σ_t
σ_m
$\sigma_\phi \cong \sigma_\theta$
-k
ε_1
local necking
$\varepsilon_1+\varepsilon_2= n$
C
SPIF
2n
pure shear
n
FLC
simple tension
biaxial stretching
1
-1/2
1
-1
1
1
-n
-n/2
0
ε_2

Figure 2.13: State of stress and forming limit curves for stamping and SPIF [34].

conical shape at the area of inner edge of backing plate due to the fact that deformation occurs mainly near the tool rather than in the whole part all at once, with Ham and Jeswiet [38] had concluding that increasing thickness resulted in increased formability because of the presence of more material to draw.

Contact Friction and Lubrication

Interaction between tool and blank is one of the most studied parameters of ISF. It can be characterized in four different ways [3]:

1. the tool is fixed hasit slides on the blank, and the friction heat improves formability;
2. the tool rolls without significant sliding and forming is achieved due to normal pressure and rolling friction;
3. the spindle rotates the tool at constant speed, generating more heat than the fist method due to dynamic friction, further improving formability, but also degrading surface quality;
4. the tool slides and rotates freely due to static contact friction, the spinning is enable by roller bearings in the spindle;

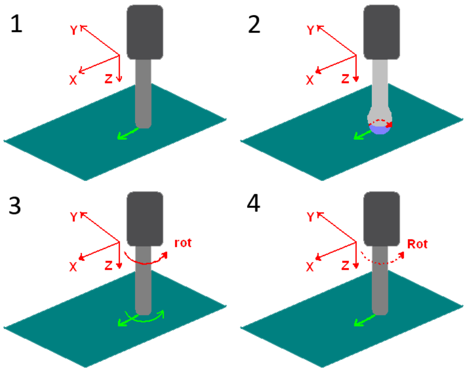
1
Y
X
Z
2
Y
X
Z
3
Y
X
Z
rot
4
Y
X
Z
Rot

Figure 2.14: Different methods for tool/blank contact interaction.

Even if friction heat enables better formability, lubrication hasto be considered in order to obtain good surface quality since in some cases SPIF, is ment to produce ready to use parts, that becomes imperative when forming titanium which tends to adhere to the tool [37]. Another advantage of using lubricants is to prevent excess friction to delay part failure and avoid excessive bending loads on the tool which could result in warping or fracture. Lubricants of all sorts are being tested, like lithium paste [30] and mineral oil [37] in order to find the ideal one for SPIF operations.

Toolpath and Step Size

Forming tool paths are characterized in direction and type of movement. Concerning to direction there are two common designations [34]:

- Direct forming - the punch progressively deforms the blank from the top going towards the maximum depth;
- Inverse forming - the punch is firstly moved down to the maximum drawing depth, and then follows a trajectory in upwards direction until it completes the process.

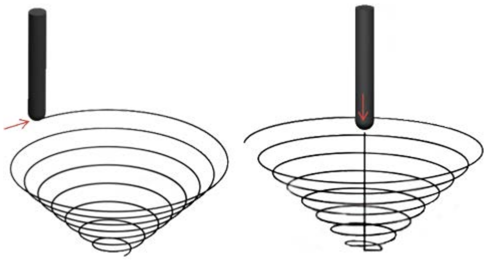

Figure 2.15: Types of forming movement: direct and inverse.

While inverse forming is necessary to obtain step angles the outward movement in relation to its center induces localize thinning that can lead to frailties at the base. Regarding type of movement there are also to types [25]:

- Contour Milling - the path is normally defined as a finishing pass, typically characterized by fixed increments along the Z-axis between consecutive discrete contours, the main disadvantage comes from transition marks between layers, where surface quality decays and force peaks occur;
- Spiraling - the path is continuous with gradually descending along the contour of the part.

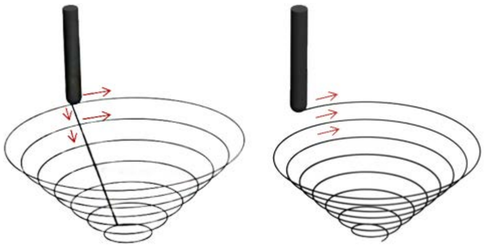

Figure 2.16: Types of forming path: contour milling and spiralling.

In order to obtain a good surface finish and geometrically accurate parts, step sizes need to be adjusted. One common practice is to use a constant increment, however when forming parts with angular variation its sometimes necessary to use instead constant scallop height in order to form the same amount of material at each path, avoiding localized thinning [34]. This is valid for both toolpath strategies.

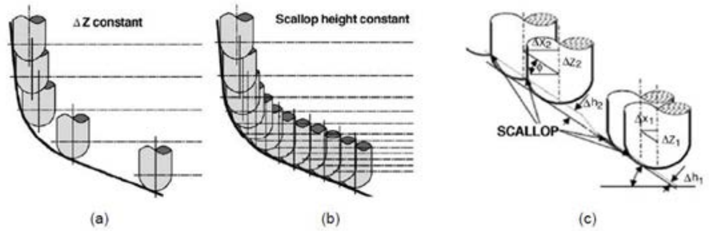

Figure 2.17: Different step size surface effect for the same geometry [39].

Studies have been made on surface quality and roughness for various step sizes in order to obtain ready to use parts at the fastest forming time possible (with less steps).

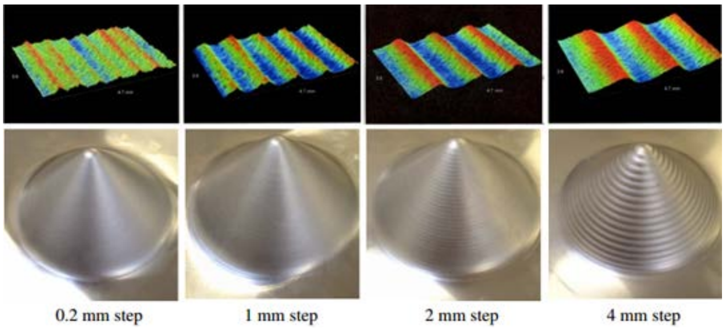

Figure 2.18: ISF toolpath step types and scallop height definition [34].

2.2.3 Forming Machinery

Since the tool path can be described using G-Code and the gradual deformation greatly reduces the work load, conventional CNC milling machines and lathes and even industrial serial manipulators can be used for this process [25]. This allows for easy and low cost research and development, albeit only for thin sheet metal parts.

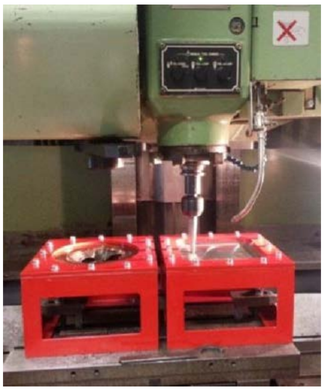

Figure 2.19: Adapted milling machine for research at University of Oporto [40].

While adapted machines and robots may be the cheapest approach, they present various limitations [39]. Both suffer from low structural stiffness and therefore are unable to handle harder and/or thicker materials due to the increased work load. Three axis milling machines also have other limitations such as being unable to use tools at an angle other than its tool axis and due to the worktable limited dimension only small pieces can be produced. As for the serial manipulators their other handicap lies in the lack of precision due the error propagations throughout its actuator joints.

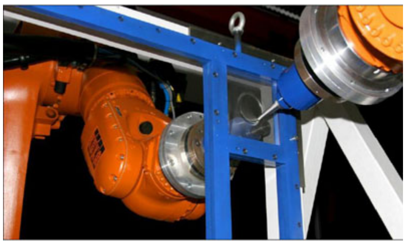

Figure 2.20: Serial industrial manipulator preforming SPIF operations [41].

Purpose built machines or dedicated machines, unlike adapted ones, are designed specifically for incremental forming, and try to have simultaneously high stifness and high flexibility. These systems allow the manufacturing of parts with complex geometries, while maintaining high accuracy and good surface finish.

The Japanese Amino®Corporation pioneered the market with their Dieless-NC machine [42] and now busts an entire range of products from small models for research purposes to large industrial models. They possess three axis but differ from adapted CNC milling machines as they are built to withstand higher workloads, possess instruments to measure not only normal forces but also transversal forces. The work table has its own vertical axis allowing it to produce both concave and convex pieces.

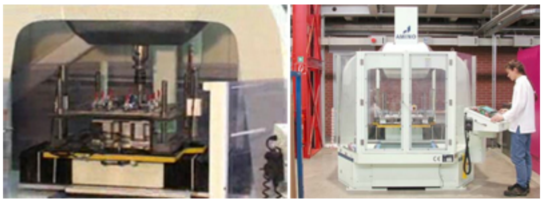

Figure 2.21: Amino®Corp. Dieless-NC machine [42].

A similar machine was being developed at Cambridge University capable of working with harder materials such as automotive grade steel and that will be able to use a second forming tool underneath the work piece [39]. It uses hidraulic actuators to achieve the necessary high loads(up to 26 kN) but its workspace is somewhat limited as its only able to work with 300 by 300 millimetre blanks. Another example of proprietary equipment is the SFB/TR73 designated as a sheet-bulk metal forming, combines a series o spindles and actuators to preform various continuous and interrupted forming operations as well as cutting procedures enabling it produce ready to use parts [43].

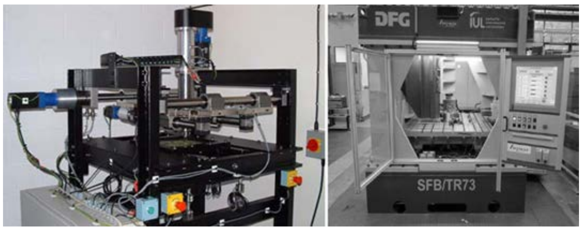

Figure 2.22: Cambridge ISF machine [39] and SFB/TR73 machine [43].

It was also noted that a good solution for incremental forming lays in the world of PKMs due to their stiffness and high workload capacity, namely in to types: Triceps and Stewart platforms [27].

Triceps manipulators consist of three parallel hydraulic cylinders, in order to guarantee precision, and feature a spherical wrist to give it six degrees of freedom, making a hybrid machine part parallel kinematic machine part serial kinematic machine. Due to their high accuracy they are widely used for complex and demanding milling operations and have already been adapted to perform SPIF operations [44]

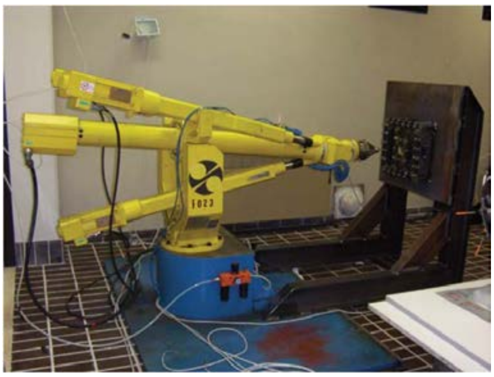

Figure 2.23: Tricep performing SPIF operations [44].

Being parallel manipulators, positioning errors on its actuators tend to balance each other out, rather than propagating like in SKMs, however the parallel configuration give it a complex workspace shape and limit its agility.

Chapter 3

The SPIF-A Machine

Keeping in mind the requirements for SPIF operations in section 2.2.2 and the limitations of existing machinery 2.2.3, the SPIF-A research project [2] opted for a Gough/Stewart platform. Its six parallel linear actuators grant it the same 6 DOF as a tricep but its simpler design makes it easier to build and develop and give it higher structural stiffness. The actuators used are hydraulic cylinders in order to provide the higher loads needed to test harder and/or thicker materials that yet have to be researched.

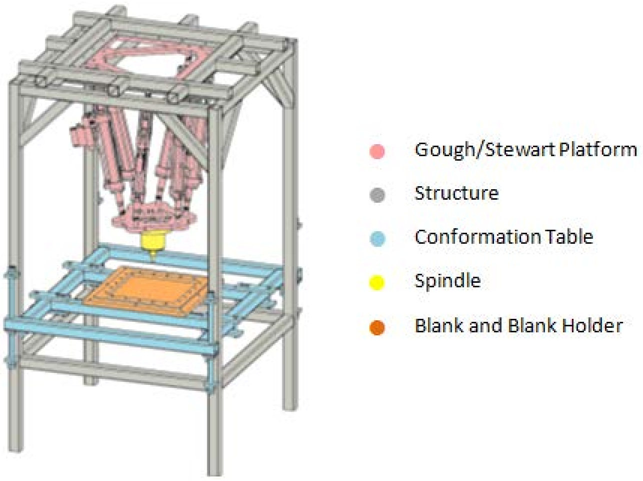

Figure 3.1: SPIF-A's main components.

The machine's configuration is vertical in the sense that its forming table is parallel to the shop-floor and the Z-axis, responsible for giving depth to the part is normal to it, as opposed to Callegari's tricep [44] in Figure 2.23.

This setup was chosen taking the flowing advantages in mind:

- saving floor space;
- favouring larger part production due to easier blank placement and removal;
- since the spindle and platform will tend to sag slightly due to their own mass instead of positioning errors in the X or Y-axis, the weight will contribute to the downward forming force, and reduce wear on the joints;
- similarly in the event of power failure the platform/spindle set will drop damaging only the tooltip and workpiece, while a horizontal assembly would pivot into the structure causing damage in cylinders, joints among other parts.

3.1 Structure

The support structure of a machine must withstand both the static and dynamic loads of its process, its design should guarantee the lowest deflection/bending possible in order to ensure accuracy and stability during operations. Factors such as movement, workload, effective area of work, tool and workpiece change and maintenance should be kept in mind when designing a machine.

The SPIF-A's structure occupies a square of about 1.6 by 1.6 meters and is almost 3 meters tall. The original design was devised and simulated by Sonia Marabuto [3]. The basic element intended to be used were C-shape steel girders welded together.

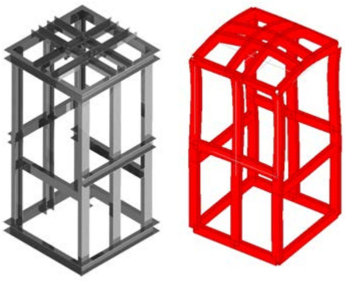

Figure 3.2: First proposed geometry and its deformation simulation result.

The vertical arch frame type inspired by the Amino®[42] and Cambridge ISF [39] machines was chosen in detriment of a pair of wedge structures, one for the platform and the other for the blank holder, in a horizontal configuration, to guarantee alignment and parallelism between platform and forming table, also gaining additional structural stiffness since bending and compression loads are more evenly distributed.

Subsequently the design was modified [5] to comply with an upgraded Stewart platform and a conformation table with adjustable height, this final form was built using squared hollow section A500 K03000 carbon-steel girders and was assembled in-house via MAG welding.

When developing a structure both static and dynamic load need to be taken into account. Static forces are related the weight of different components and result in static deflection that affects accuracy and alignment between various parts. Dynamic forces result from inertial reactions of the movable components the machine operates, these can cause vibrations and dynamic deflection that compromises the stability of operations. Since SPIF is yet a process that involves slow speeds, the major concern lays in static solicitations, therefore the reference loads used to test the current structural geometry was the highest to date according to research (Table 2.1) which is Allwood's model [27] of 13,5 N vertical and 6,5 N horizontal.

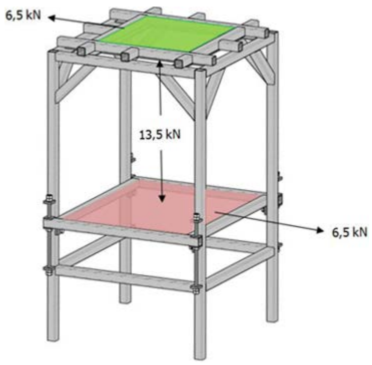

Figure 3.3: Final structural design and its solicitations.

Simulated in CATIA V5 finite element analysis an improvement in structural stiffness and load distribution as noted by the decrease in maximum deflection from 1,388 mm in the original design to 0,286 mm in the current configuration. Also since the yield strength for the alloy used is about 315 MPa, it is safe to assume that higher work loads are allowed.

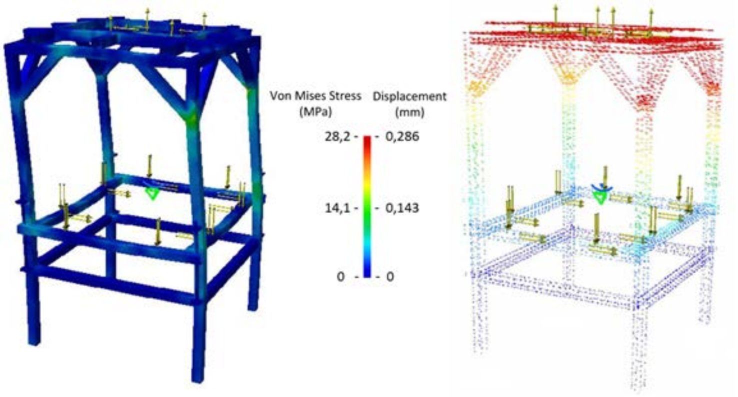

Figure 3.4: Stress and displacement analysis of the frame and table assembly.

Finnish operations on the frame included the welding stiffeners to prevent long term bending on the four corner supports for the forming table, installing supports for the electrical cabinet followed by a thorough sanding and a thick coat of paint for insulation and to prevent corrosion.

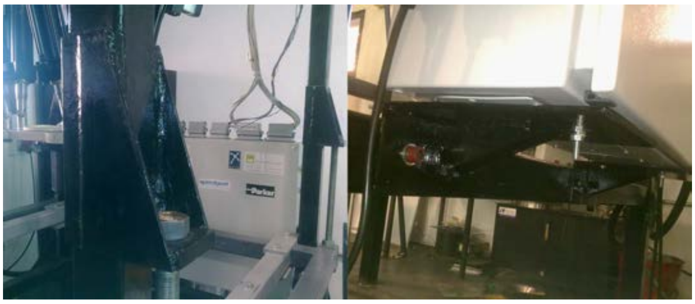

Figure 3.5: Forming table stiffeners and electrical cabinet supports.

3.2 Stewart Platform

A preliminary design was also proposed by Sonia Marabuto [3] using a 6-6 configuration custom made U-joints and circular base and platform made from machined CK45 alloy steel.

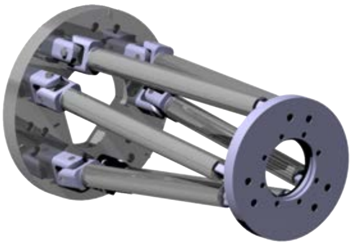

Figure 3.6: The original proposal for the SPIF-A's stewart platform [3].

That same design was modified by Miguel Martins [5] in order to save on weight and production costs but also to provide a sturdier fixture to the structure. The new base and platform plates have a hollow center to save weight and free up space for cabling, hoses and in the case of the platform for the spindle. Both pieces were hydro-jet cut from a single 30 millimetre thick duraluminum plate to save material and machining time. The new base plate is fixed to the structure with eighteen bolts, twice as many as the original design and are spread around its perimeter instead of being clustered near the center transferring the load forces more evenly to the structural frame.

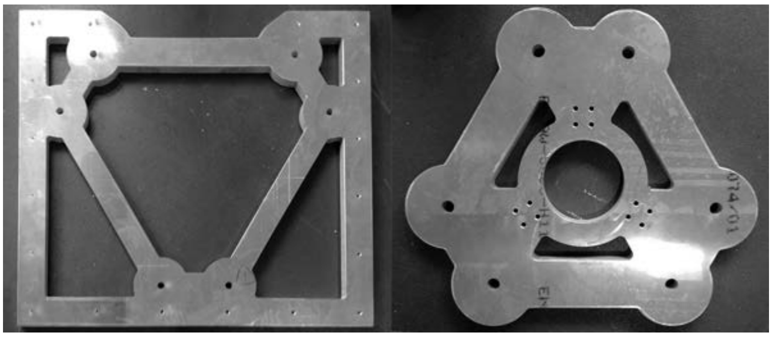

Figure 3.7: Base and mobile plates for the final platform design.

The links that connect the base and mobile plates in these kind of PKMs are commonly referred to as legs and, for this design, consist of two universal joints with a linear actuator between them. To save on fabrication and heat treatment costs (for a total of twelve parts), the custom U-joints were discarded and new ones were acquired from the manufacturer Rotar®. The selected model was the AL110 for its mechanical properties and matching bore with the threads of the chosen actuators and their only drawback comes from a more limiting rotational range of 45º in either direction.

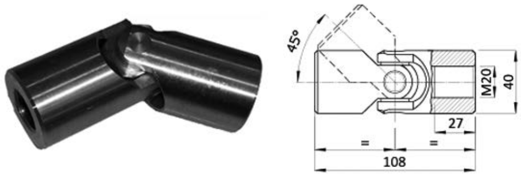

Figure 3.8: U-joints used and their geometry [45].

Linear actuators can be of different natures: electromechanical, piezoelectric, hydraulic or pneumatic. Because of the high work loads electrical systems are discarded to begin with, piezoelectric ones in particular as they have a very small travel range. Fluid power systems on the other hand allow higher work forces, specially hydraulic cylinders, and since precise position control in pneumatic actuators is impossible, except at full stops due to air being a compressive gas, a hydraulic system was selected.

Double effect electro-hydraulic actuators were chosen to enable easy control in both pushing and pulling motions. The required six cylinders were acquired from the Parker Hannifin Corporation [46] the following requirements in mind:

- Suitable work pressure (above 100 bar/10 Mpa) in order to provide the required forming forces (Table 2.1);
- Sufficient travel distance to produce various geometries and different sizes (minimum stroke of 300 mm);

Even though it hassix parallel actuators, there will be instances when not all of them will be exerting forces on the part being produced, therefore the cylinders were dimensioned in the worst case scenario of a single one producing the required work load.

$$\begin{cases} P_w = {}^{F_t}\!/_{A_c} \\ A_c = {}^{\pi}\!/_{4} \cdot d_{\min}^2 \\ F_t = \left\| \overrightarrow{F_h} + \overrightarrow{F_v} \right\| \end{cases} \Leftrightarrow d_{\min} = \sqrt{\frac{4}{\pi} \cdot \frac{\sqrt{\left(13 \cdot 10^3\right)^2 + \left(6.5 \cdot 10^3\right)^2}}{10^7}} = 0.043mm \qquad (3.1)$$

To comply with the above specifications the chosen cylinders were from the HMIX product line, with integrated linear position sensors to provide the necessary feedback for precise motion control and low friction hydrodynamic seals to improve dynamic performance and response time.

Table 3.1: Actuactor specifications [46].

Parker®- TCHMIXRPFS27M - M114 Cylinder

Stroke	Bore diam.	Rod diam.	Retract. length	Max. pressure
400 mm	63 mm	45 mm	883 mm	210 bar

Parker®- D1FP*S - Dfplus valve

Leakage(210bar)	Step response	Dynamics	Dirt sensitivity	Maintenance
<0.6 l/min	<3.5 ms	pressure ind.	low	not required

Temposonics®- RH 550646 C magnetostrictive linear transducer

Output Freq.	Resolution	Output Format	Repeatability	Op. Voltage
8 kHz - 1 MHz	0.002 mm	RS 422 diff.	± 0.0045 mm	24 V DC

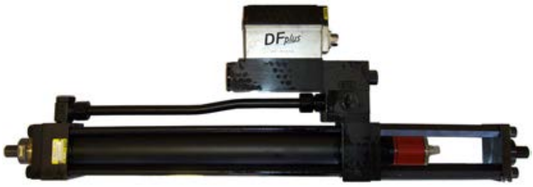

Figure 3.9: Cylinder, valve and transducer assembly [46].

The SPIF-A's platform and its kinematics will be further explained in chapter 4.

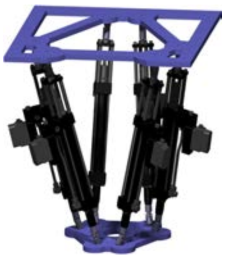

Figure 3.10: Final design of Stewart platform for the SPIF-A.

3.3 Spindle

Due to the current low dissemination of SPIF machinery solutions it was necessary to develop a custom spindle system since no commercial solutions exists. Extensive work was done by Sonia Marabuto [3] to research a develop a system with all the requirement specified in section 2.2.2, and later by Miguel Martins [5] to further adapt it to the final platform design.

The most advantageous type of tool/part interaction for the majority of cases is for the tool-tip to roll over the sheet metal with low friction [47; 48]. As mentioned in section 2.2.2 there are two ways to achieve this, on the tool it self, with a specialized design with a ball bearing on its end and mounted on a fixed spindle; or to let the tool holder rotate freely, requiring a shaft with bearing capable of handling the work forces. Since the ball bearing tool is rather difficult to develop and manufacture, and to keep the option of using high speed rotation in future work open it was decided against the fixed spindle.

Several designs were studied, with different bearing configurations, tool holders and clamping systems and once again the design was adapted in order to save on manufacture costs and allow a compact design. Of the various proposals the spindle shaft selected was the shortest possible in length in order to resist bending without requiring a large diameter, this also allowed for a lighter assembly and with fewer bearings. The material used was quenched and tempered high strength steel (30CrNiMo8), stiffness and fatigue studies were conducted by Sonia Marabuto to validate the design [2].

Table 3.2: Shaft stiffness and fatigue analysis results.

M_z	θ_{max}	δ_{max}
43.33 N.m	10.45 μrad	0.66 μm

A DIN chuck was chosen for being a time tested and highly disseminated system over the more expensive but sturdier HSK chuck, keeping in mind that the SPIF-A is a prototype machine and not an industrial model, future versions may revisit this option to comply with higher work loads and the afore mentioned rotating spindle. With the same line of thought to secure the tool in place a collet system (metal clamps that straddle the tool with the turn of a retention nut) was selected. Although not as rigid an assembly as a contraction (thermal clamping) or hydraulic system they are far more affordable especially when compared with contraction that would require the acquisition of a chuck heater which implies a investment of around four thousand euros.

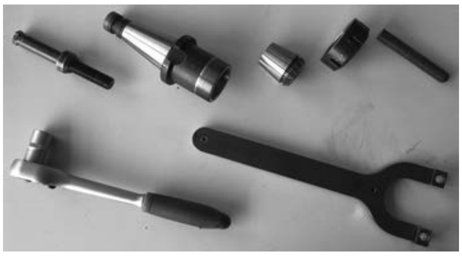

Figure 3.11: Tool holder components (top) and clamping tools (bottom).

In the various proposals various bearing configurations were studied in order to reduce vibrations, guaranty perfect alignment and to better handle the work load, the selected bearings are listed in Table 3.3 and their configuration in Figure 3.12.

With this compact design, the clamping system used to connect the tool holder to the shaft was also cost effective. Since at this stage each SPIF part is produce with the same tool, the selected solution was a threaded rod, in compliance with the DIN 2080 norm, similar to those used in conventional milling machines, and would be assembled manually with a ratchet and

Table 3.3: Shaft bearing specifications [2].

	Needle bearing (A)	Combined needle ball Bearing (B)	Double ball bearing w/ angular contact (C)
Type			
Load	Axial	Axial and Radial	Radial
C_0	186.0 kN	16.7 kN 104.0 kN	80.0 kN
C_D	34.5 kN	9.3 kN 57.2 kN	88.4 kN
P_u	22.4 kN	0.7 kN 13.2 kN	3.4 kN
v_{lim}	4300 rpm	7000 rpm	4500 rpm
Diam.	55 mm	55 mm	70 mm

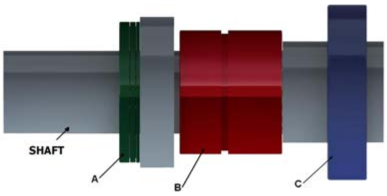

Figure 3.12: Shaft bearing configuration [5].

a custom wrench to secure the chuck (Figure 3.11). This discarded the larger, more complex mechanical/fluid activated systems, resulting in less stresses in the spindle assembly.

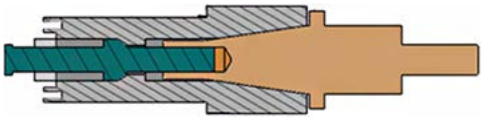

Figure 3.13: Shaft/tool holder clamping system.

The spindle casing was machined from ck45 steel, and also underwent the necessary modifications to make it compatible with Miguel Martins' FMS proposal [5] in which the spindle assembly and the mobile platform would be connected via three load cells in order to study the forming forces during forming operations.

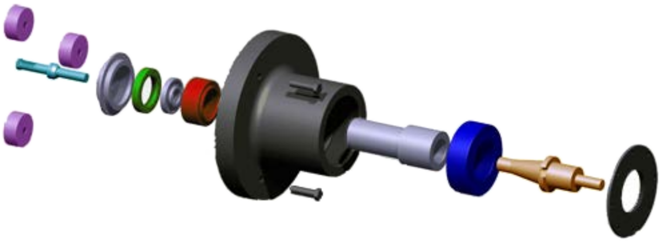

Figure 3.14: Exploded view of the spindle system.

3.4 Force Measuring System

In order to better understand SPIF forming parameters (section 2.2.2) measuring the work loads is essential, therefore a measuring system was devised using load cells [5]. Load cells come in different types: piezoelectric, pneumatic, hydraulic and strain gauges. The latter being the most versatile and commonly used is also the more affordable.

As mentioned in the previous section three load cells connect the platform and the spindle, these are evenly spaced around the base of the spindle casing in such a way that they form an equilateral triangle. The tensile/compressive forces (z-axis) they measure can be converted mathematically into the forming forces between the tool tip and the sheet metal, using static equilibrium Equations (3.2). this is achieved by viewing the spindle as a cantilever anchored in the centroid of the aforementioned triangle, point in which the horizontal force can be broken up into moments in both the x and y-axis .

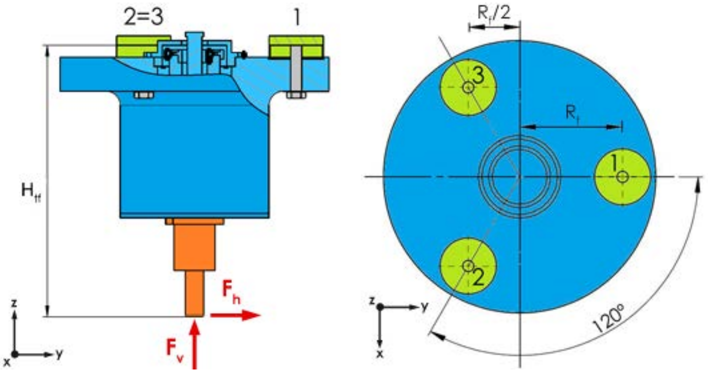

Figure 3.15: Spindle forces and load cell configuration.

$$\sum \overrightarrow{F} = 0 \wedge \sum \overrightarrow{M} = 0 \tag{3.2}$$

$$\sum \overrightarrow{F}_z = 0 \Leftrightarrow F_v = F_{1z} + F_{2z} + F_{3z} \tag{3.3}$$

$$\sum \overrightarrow{M}_x = 0 \Leftrightarrow F_{hx} \cdot H_{tf} = F_{1z} \cdot R_f - (F_{2z} + F_{3z}) \cdot \frac{R_f}{2} \tag{3.4}$$

$$\sum \overrightarrow{M}_y = 0 \Leftrightarrow F_{hy} \cdot H_{tf} = 0 \cdot F_{1z} + F_{2z} \cdot R_f \cdot \cos 30^{\circ} - F_{3z} \cdot R_f \cdot \cos 30^{\circ} \tag{3.5}$$

The three equations (3.3), (3.4) and (3.5) can be rewritten in matrix form:

$$\begin{bmatrix} F_{hx} \\ F_{hy} \\ F_v \end{bmatrix} = \begin{bmatrix} \frac{R_f}{H_{tf}} & -\frac{R_f}{2 \cdot H_{tf}} & -\frac{R_f}{2 \cdot H_{tf}} \\ 0 & \frac{R_f \cdot \cos 30^{\circ}}{H_{tf}} & -\frac{R_f \cdot \cos 30^{\circ}}{H_{tf}} \\ 1 & 1 & 1 \end{bmatrix} \cdot \begin{bmatrix} F_{1z} \\ F_{2z} \\ F_{3z} \end{bmatrix} \tag{3.6}$$

3.4.1 Load cells and signal amplifiers

In order to determine the capacity needed, the highest load scenario on any cell was studied using the most severe forming forces expected (Table 2.1), this occurs when using the longest tool and when the horizontal force F_h at the center of the spindle is lined up with the direction of any cell, by inverting equation (3.6) and using $F_v = 13kN$, $F_{hx} = 6,5kN$ (alignment with load cell 1), $H_t = 280mm$ and $R_f = 110mm$ it was possible to determine the maximum load any cell would be under.

$$\begin{bmatrix} F_{1z} \\ F_{2z} \\ F_{3z} \end{bmatrix} = \begin{bmatrix} -\frac{0.11}{0.28} & \frac{0.11}{2 \cdot 0.28} & \frac{0.11}{2 \cdot 0.28} \\ 0 & \frac{0.11 \cdot \cos 30^{\circ}}{0.28} & -\frac{0.11 \cdot \cos 30^{\circ}}{0.28} \\ 1 & 1 & 1 \end{bmatrix}^{-1} \times \begin{bmatrix} 6500 \\ 0 \\ 13000 \end{bmatrix} = \begin{bmatrix} 15364 \\ -1152 \\ -1152 \end{bmatrix} (N) \tag{3.7}$$

With the minimum cell capacity determined, and to take advantage on a academic campaign with special prices for reconditioned load cells three model TR3D-A-5K from the Michigan Scientific Corporation were chosen. This model is weatherproofed and corrosion resistant making it ideal to use in a machine shop. Since they measure both tensile/compression and shear loads, sensory redundancy can be used to study the horizontal forming forces and to compensate for any eventual load cell failure since since F_{hx} and F_{hy} are equally distributed in cell's shear plane due to the lack of moments around the z-axis.

$$\sum \overrightarrow{M}_z = 0 \tag{3.8}$$

$$\sum \overrightarrow{F}_x = 0 \Leftrightarrow F_{hx} = F_{1x} + F_{2x} + F_{3x} \Leftrightarrow F_{1x} = F_{2x} = F_{3x} = \frac{F_{hx}}{3} \tag{3.9}$$

$$\sum \overrightarrow{F}_y = 0 \Leftrightarrow F_{hy} = F_{1y} + F_{2y} + F_{3y} \Leftrightarrow F_{1y} = F_{2y} = F_{3y} = \frac{F_{hy}}{3} \tag{3.10}$$

Table 3.4: FMS load cells specifications.

TR3D-A-5k load cell		
Max load capacity	5000 lbs (22240 N)	
Full scale output	4.0 mV/V	
Sensor type	3 four-arm strain gage brigdes	
Non-linearity	<0.5% of f.s. output	
Hysteresis	<0.05% of f.s. output	
Repeatability	<0.05% of f.s. output	

The strain gauges inside the load cells are resistors that change their electrical conductance according to variations in their geometry, under tension their section area narrows and resistance increases while when compressed it thickens decreasing resistance. This fluctuations affect the voltage at its terminals and by arranging them in a Wheatstone bridge with other known resistors it is possible to measure the voltage difference which will translate into load forces.

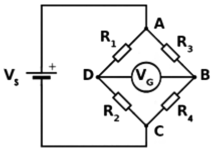

Figure 3.16: Wheatstone bridge.

The four resistors, including one or more strain gauges depending on bridge type, are arranged in to two potential dividers between points A and C and receive an excitation voltage V_S, without any applied loads the voltage across the bridge V_G (from point B to D) will be null since $R_1 = R_3$ and $R_2 = R_4$. However when subjected to mechanical forces the resistance of the strain gauges will vary and case an imbalance on the bridge resulting in a non-zero V_G voltage:

$$V_G = \left(\frac{R_4}{R_3 + R_4} - \frac{R_2}{R_1 + R_2} \right) \cdot V_S \tag{3.11}$$

Taking into considerations that the aforementioned resistance variations are very subtle even at maximum load capacity, loads cells only output a very small voltage, in these case only 4mV for every Volt of excitation voltage as seen on Table 3.4.

To properly evaluate these outputs signal amplifiers are required, the selected option was a package of Magtrol load monitoring units for their versatile configuration and compact, rail mountable design.

Table 3.5: LMU specifications.

Model LMU 209 Load Monitoring Unit		
Supply	18-18V / 70mA	
Voltage output	0 to ±10 V	
Sensitivity	1 mV/V (default)	
Sensitivity range	(1) - 0.5 to 1.5 mV/V (2) - 1.5 to 4.0 mV/V	
Sensitivity adjust.	10-turn potentiometer	
Non-linearity	<0.05%	
Zero fine adjust.	10-turn potentiometer	
Bridge supply	5/10 Vdc (selectable)	

3.4.2 FMS calibration

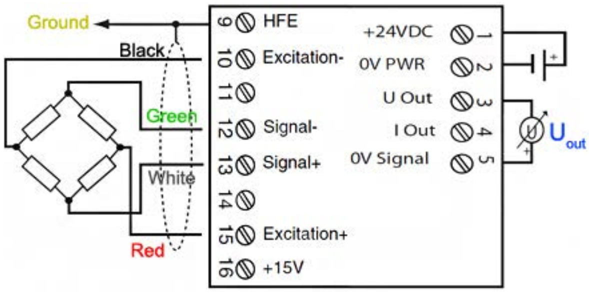

Figure 3.17: Load cell and LMU connections.

With the hardware selected and connected the system needed to be calibrated. The fist step was to adjust the zero offset, if the error is a small percentage of the output signal the error can be adjusted only with the potentiometer, if the value is greater the DIP-switches allow adjustments of ±25% and ±50%. Secondly the sensitivity needed to be set accordingly with the load cell specifications in Table 3.4 which is 4.0 mV/V. The LMU's come with a factory setting of 1mV/V (Table 3.5), adjustable via potentiometer. By pressing the calibrate button, an internal signal of 1mV/V is generated and delivers 10 volts to the output, this value can be adjusted to the full output voltage of the load cells by the following equation:

$$U_{out} = \frac{10\ (\mathrm{V}) \cdot 1\ (\mathrm{mV/V})}{4\ (\mathrm{mV/V})} = 2.5\ \mathrm{Volt} \tag{3.12}$$

To determine the load cell calibration curves, the loads cells were tested against known loads on a Shimadzu AG-50kNG universal testing machine. All three load cell were tested three times on their three axis in both directions for the same load sequence and before every new test the Shimadzu would undergo its electronic calibration cycle to present hysteresis errors.

Measuring compression forces along the Z-axis was the most straightforward scenario and tensile forces required only small adaptations, on the other hand shear forces (X and Y-axis) proved to be more difficult since the cells can't handle significant moments and their round geometry did not guarantee the proper alignment.

Table 3.6: Testing forces applied by the Shimadzu AG-50kNG.

Load test sequence [N]											
0	20	50	100	200	500	1000	2000	5000	10000	15000	20000

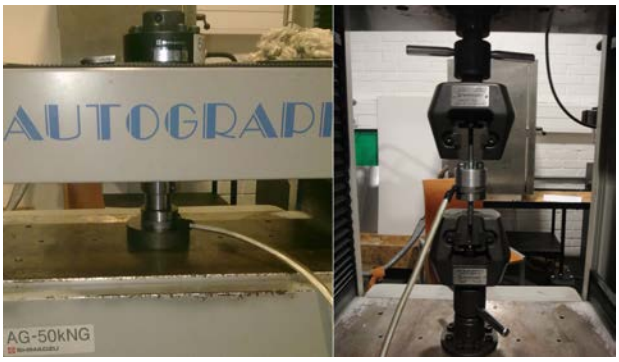

Figure 3.18: Compression and tensile load testing along Z-axis.

In order to enable shear force measurements a custom angle support, to assemble on the testing machine, was manufactured with welded stiffeners to prevent bending. Alignment with the X and Y-axis was guaranteed by the four fixation bolts on the back plate of the load cell, however the steel casing on the top plate was not sturdy enough to handle the full scale load. To effectively transfer the load without causing high moments that would damage the cell a rowlock and a bolt were also manufactured.

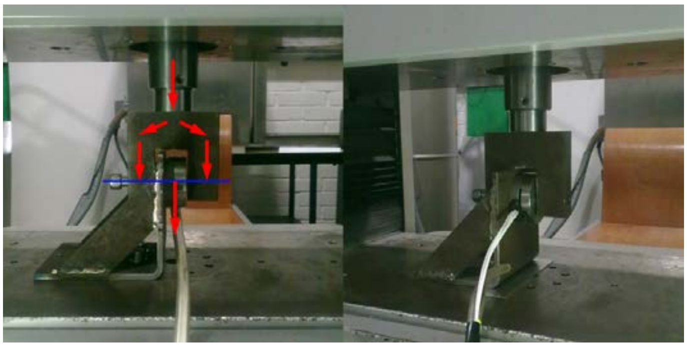

Figure 3.19: Shear load testing mechanism.

With the collected data the conversion factors from voltage to force were calculated and subsequently used to estimate forming forces during SPIF operations.

Table 3.7: Voltage to force conversion ratios.

	Load Cell #1	**Load Cell #2**	**Load Cell #3**
X force	$2391.4 \cdot U_{out}$	$2456.7 \cdot U_{out}$	$2497.9 \cdot U_{out}$
Y force	$2376.6 \cdot U_{out}$	$2441.7 \cdot U_{out}$	$2401.9 \cdot U_{out}$
Z force	$2302.6 \cdot U_{out}$	$2298.4 \cdot U_{out}$	$2218.2 \cdot U_{out}$

3.5 Forming Apparatus

The forming apparatus consists of the components directly involved in forming operations, even though the motion and forces came from the Stewart platform, it is the tool that preforms the operation on the blank, restrained in the blank holder which is mounted on the forming table, like many other components these needed to be custom built to suit the propose of the SPIF-A machine.

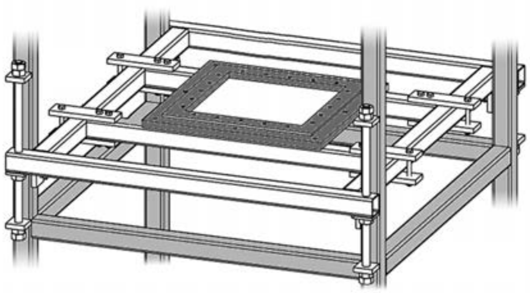

Figure 3.20: Conformation table with blank and blank holder assembly.

3.5.1 Tool development

Despite their simplicity SPIF tools require a careful development, specially in the case of the SPIF-A that aims to test thicker and/or harder materials. While simple steel tools are more than adequate to work with thin aluminium sheets for higher loads sturdier are required, one way of achieving this is to coat the steel tools with cemented carbide [25], effectively increasing its hardness and lifetime, however the cost poses an issue specially when wanting to preform experiments with various tool sizes and geometries, the solution was to develop tools out of heat treatable steel.

The initial tool batch developed consisted of five tools, three with a rounded tool tip and different dimensions, and two with flatten tips with dimensions similar to the larger spherical ones.

Table 3.8: Forming tool geometric properties.

SPIF-A forming tools					
Tip geometry	Spherical			Flat	
Diameter [mm]	5.0	10.0	15.0	10.0	15.0
Length [mm]	43.0	70.0	100.0	70.0	100.0

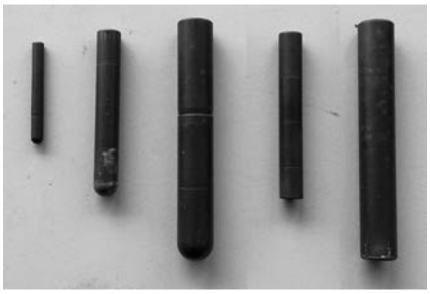

Figure 3.21: Manufactured tools for SPIF operations.

They were produced in house on a Kingston CNC lathe from RL200 cold-working tool steel. The RL200 or X210Cr12, is a high alloy steel that contains 2.1% carbon and 12.0% of chromium among small traces of other elements, due to its composition it allows quenching all the way to its core [49]. Because of the high percent of chromium, it's considered a type D3, according to the AISI norm, meaning that it suffers almost no dimensional variations when heat treated. It is also a stainless steel as it forms a thin layer of chromium oxide on its surface that gives it exceptional corrosive resistance.

Due to these characteristics it is employed on several cold-working applications that require wear resistant tool such as punches and dies, shear press blades and measurement apparatus.

The RL200 in its standard state comes with a hardness of 248 HB (equivalent to 25 HRC) therefore in order to use these tools to preform SPIF operations on more resistant materials it was necessary to harden the tools. With its high carbon percentage this steel can be quenched to reach about 65 HRC effectively making it harder than the parts produced.

This was achieved according to Pinto Soares' methodology [49] for quenching:

- Thin parts (<20mm) should remain at the constant austenization temperature of 970ºC from 15 to 20 minutes, making the ferrite in the steel grains change phase converting it into austenite ;
- When the quenching temperature the range of 900-1000ºC two heating stages are used to promote better heat distribution between core and surface.
- A control atmosphere without oxidants with required, if this is not possible the parts should be wrapped and package to prevent oxidation of the alloy elements.
- Following the final heating stage parts should be emerged in an oil bath at room temperature, the rapid cooling will not allow the austenite to revert back into ferrite, instead forcing the martensitic transformation which is responsible for the change in mechanical properties

After quenching, due to rapid cooling parts tend to become brittle to increase tenacity they undergo a tempering process in which the martensitic structure is homogenized relieving internal tensions at the cost of some of its hardness. This is done by reheating the parts to 160-280ºC (avoiding temperatures from 280 to 470ºC that promote frailty in this type of steel [49]). The temperature should remain constant about 1.5 hours for a 10 mm thick part and one hour more for every additional 10 mm, afterwards by letting them cool naturally, tenacity improves.

Table 3.9: Forming tools heat treatment cycle.

Quenching					**Tempering**		
heating	600ºC	heating	970ºC	oil bath	heating	250ºC	air cooling
2 h.	10 min.	2 h.	15 min.	-	2 h.	2 h.	-

The resulting tools were measured in a hardness tester and yielded 58 HRc, enabling SPIF operations on materials like dual phase steels.

3.5.2 Blank holders

SPIF is a stretch forming operation, therefore the sheet metal blanks need to be restrained along its edges, this is usually done by clamping the blank prior to operations. This type of fixture limits the maximum forming area which varies from researcher to researcher.

The SPIF-A employs the same method, using a blank holder that is bolted to the forming table (Figure 3.11). The first one used is meant for 230x230 mm blanks, its frame was hidrojet cut out of CK45 steel, with a recess for square or round plates and four clamps (also CK45) that are fixed to the frame with four CHC M8x15 bolts each.

Table 3.10: Forming areas used by different researchers/machinery.

Author	**Forming area** [mm]
Obikawa et al. [50]	20×20 (mini-forming)
Hussain et al. [37]	140×140
Ambrogio et al. [51]	290×210
Dejardin et al. [52]	300×300
Allwood et al. [39]	300×300
Amino®Corporation [42]	300×300 / 500×500 (research models) up to 2500×1750 (industrial models)

The baking plates, made from 6mm thick CK45 steel, are placed underneath the blank and serve to define the parts approximate shape, they also limit forming area, the square plate is used 180×180 mm parts while the round plate allows a circular area with 90 millimetres in diameter. These allow to compare results with some authors, and served for the preliminary forming tests.

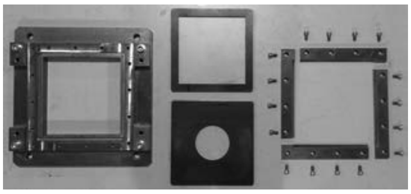

Figure 3.22: SPIF-A's 230×230mm blank holder components.

To take full advantage of the machine's large frame two more blank holders were developed, to support 500×500 and 1000×1000 mm blanks. To assemble them the forming table was outfitted with new fixation points. In order to save on material and machining costs their base frame, unlike their smaller counterpart, the new ones were built in house as multiple parts from CK45 steel, and only assembled together on the forming table. This multi part design means that the 1000 mm blank holder can use the clamps from 500 mm one and also allows for easy storage when not in use.

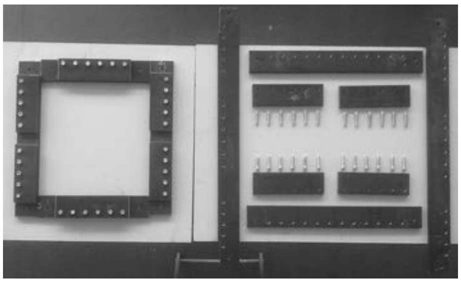

Figure 3.23: Assembled 500×500 mm, and 1000×1000 mm blank holder parts.

3.6 Power Systems

The SPIF-A is an electro hydraulic machine in the sense that while the forming force come from a fluid circuit, the components that regulate it, like the pump and the cylinder valves, are driven by electrical signals, which are also used to relay sensory information to the control unit. It is therefore divided into two subsystems, that were initially devised by Miguel Martins [5] and have since then remodelled and updated.

3.6.1 Hydraulic System

As mentioned in Section 3.2 the linear actuators for the Stewart platform are hydraulic cylinders, due to their bore diameter of 63mm they require significant oil flow to move at moderate velocity, however, since for testing purposes, SPIF-A operations will be conducted at low speeds a small hydraulic power plant will suffice. The first installation was a Bosch Rexroth PV7 40/45, available on campus, with a 45 cc displacement pump powered by a 1500 rpm three phase motor, capable of supplying a 60 litter per minute flow at a maximum of pressure of 160 bar, it also contained an accumulator to compensate for pressure losses. With its flow split by the six cylinders this allowed for an average stroke speed oh about 1 mm/s.

$$\dot{m} = 6 \cdot \frac{d_{bore}^2 \cdot \pi}{400} \cdot v_s \cdot 60 \Leftrightarrow v_s = \frac{\dot{m} \cdot 40}{d_{bore}^2 \cdot \pi \cdot 36} \simeq 0.005 m/s \tag{3.13}$$

However due to its wear, the actual performance of the pump had decayed and it was later swap by a more recent and powerful unit, a Marzocchi ALP3-D-120, almost doubling the allowed forming speed.

Table 3.11: Hydraulic pump specifications.

Marzocchi ALP3-D-120	
Displacement	78 cc/rev
Flow	112 l/min (1500 rpm)
Max pressure	160 bar (constant)
	175 bar (intermitent $<$ 20 s)
	190 bar (peak $<$ 2 s)
Max speed	2300 rpm

$$v_s = \frac{112 \cdot 40}{63^2 \cdot \pi \cdot 36} \simeq 0.010 m/s \tag{3.14}$$

The new power plant differs from its predecessor by lacking an accumulator but featuring a larger tank with 120 litter capacity, and its own electrical power circuit to control its motor.

With this more reliable set-up longer operations could be undertaken, however this posed a problem as the oil would heat up and the associated change in viscosity would affect its performance. A heat exchanger was then required, the capacity for such system can be calculated according to heat power dissipation [53]. This can be done either by temperature measurement or by using an approximate solution based on the pump's efficiency, to ensure a more careful analysis the first method was used. At a room temperature of $\vartheta_u = 25^oC$ the oil in the circuit (SHELL Thelus M 32) with specific heat of $c = 1.88^{kJ}\!/_{Kg \cdot K}$ and density $\rho = 0.875^{Kg}\!/_{L}$ took approximately 40 minutes to reach the excessive temperature $\vartheta_2 = 80^oC$, meaning a power loss of 4.52 kilowatts.

$$P_v = \frac{V_{tk} \cdot \rho \cdot c \cdot (\vartheta_2 - \vartheta_1)}{t \cdot 60} = \frac{120 \cdot 0.875 \cdot 1.88 \cdot (80 - 25)}{40 \cdot 60} = 4.52 kW \tag{3.15}$$

The calculated power loss can be used to calculate the specific cooling capacity that is required for the selection of the cooler:

$$P_{01} = \frac{P_v}{\vartheta_{BT} - \vartheta_u} = \frac{4.52 \cdot (1 - 0.95)}{50 - 20} = 0.181^{kW}\!/_{K} \tag{3.16}$$

To comply with this an EMMEGI MG2030K by-pass heat exchanger with a 220 V ac fan with a capacity of 0.189 kW/K was selected, by installing it to the cylinders, as parts of a re-circulation system, succeeding operations were able to last longer without needing interruptions to allow the system to cool down.

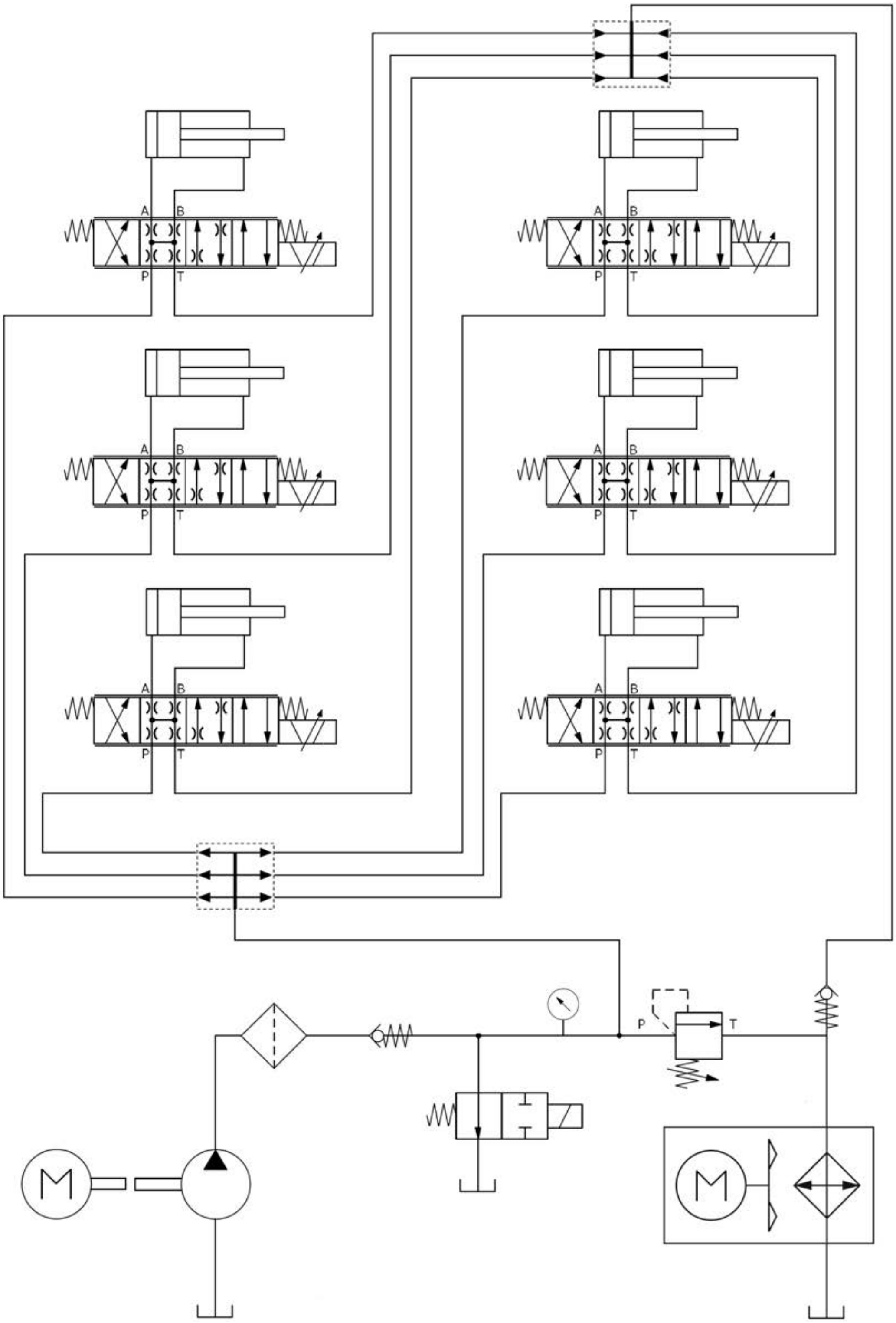
A
B
P
T
A
B
P
T
A
B
P
T
A
B
P
T
A
B
P
T
A
B
P
T
P
T

Figure 3.24: Hydraulic plan for the SPIF-A.

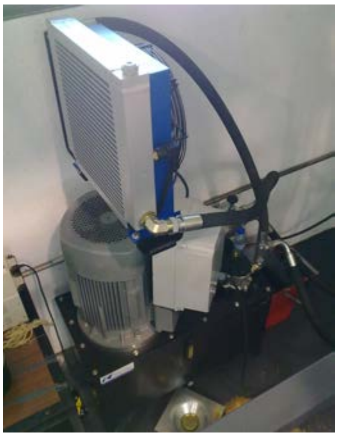

Figure 3.25: SPIF-A's hydraulic pump and heat exchanger installation.

3.6.2 Electrical system

When designing and developing electrical systems for machinery certain precautions should be taken when selecting and assembling components in order to ensure operation and operator safety.

For its multiple systems the SPIF-A uses different types of electrical currents (both AC and DC) with different intensity and voltage depending on each system power supply requirements. With this in mind the electrical plan assumed a modular architecture to allow different subsystems to modified or replaced with ease [5].

The different modules include the 24V DC - 20A supply for the solenoid valves, this module due to its high variations in current requirements which produce electrical noise and interference, was separated from the supply circuit for the LMU's and position sensors which runs on 24V DC - 2.5A. A power outlet module is there to power the external equipment like the real time machine equipped with input output modules to control and supervise all other systems.

Table 3.12: List of electrical components for the electrical system.

Component	Specifications/Reference	Qt.
Main disconnect switch	Rockwell - 194E-E25-1753 (400V ac -25 A)	1
DC linear power supply	DRP-480-24 (85-264V ac - 24V dc 2.5A	1
DC switching regulator	MDR-60-24 (85-264V ac - 24V dc 20A	1
Emergency stop switch	Shneider Electric ZBE-102 10A	1
Indicator light	ABB CL-523G LED -230V ac	1
220 V outlet	IP44 16A 2P+T	2
Fuses	4.0 A	6
	3.0 A	3
Motor control relay	Finder 55.32.9	1
Residual-current device	Shneider RCCB 4P 25A	1
Safety relay	Sick EU 23-2MF	1
Circuit breacker	Merlin Gerin C60N	4

In the initial design the machine would use a three phase power supply, this was mainly because the first hydraulic pump lacked a control switchboard and could only be turned on/off by regulating its supply, with the new pump system which comes with its own control circuit with external power supply only requires the usage of a relay to command it. This fluid system upgrade enabled to reorganize the wiring and changing the switch board supply to use standard

220 V single phase current, reducing power consumption and electrical interference on the analog lines.

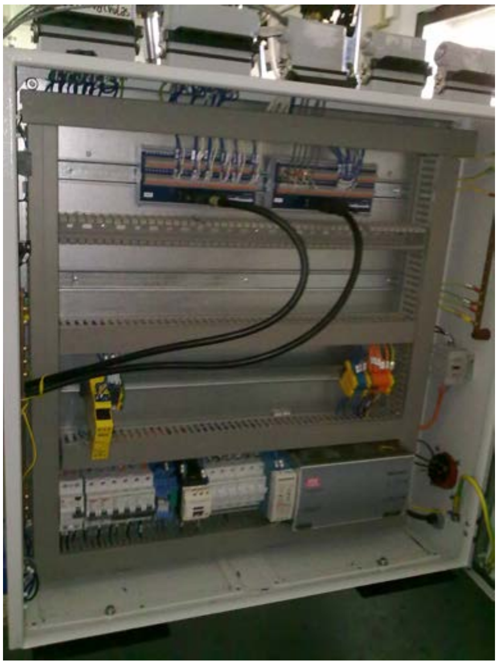

Figure 3.26: Electrical cabinet after reorganization.

To further shield the FMS the LMU's were placed in a separate electrical cabinet on top of the machine, these modifications freed substantial space inside the main cabinet that can be used for extra input/output modules and future subsystems.

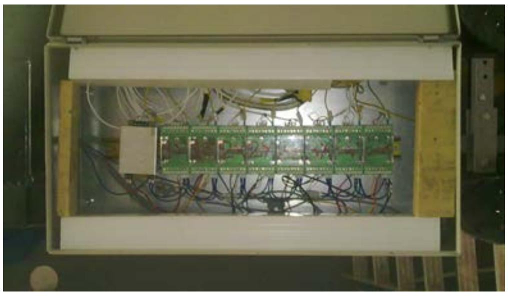

Figure 3.27: Cabinet for the LMU's on top of the SPIF-A.

Chapter 4

SPIF-A Kinematics

4.1 Gough/Stewart platform - a brief history

In the world of PKMs the Gough/Stewart platform is well known for its simple yet robust construction.

Although mechanically simple, its mathematical model, the Articulated Octahedron [54], is somewhat complex. It consists on two parallel faces from said octahedron being rigid, one of those faces will be fixed in space and the other one is able move/rotate in 3D space, giving it 6 DOF: three linear movements x, y, z (lateral, longitudinal and vertical), and the three rotations roll, pitch and yaw (Euler angles). While Moving about the two faces remain connected by six edges which vary in length,

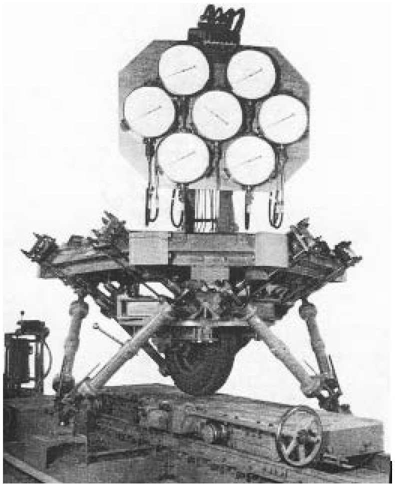

Figure 4.1: Gough Universal Rig [55].

Even though Augustin Louis Cauchy studied this model during the 19th century, it was only in the early 1950s that Eric Gough, a British automotive engineer, built his Universal Tire-Testing Machine at Birmingham's Dunlop tire factory, based on Cauchy's model [55]. It used six hydraulic jacks as actuators to move the platform, making it the first successful construction, since the motion is due to the mutual interaction of all jacks the device is also known as a synergistic motion platform.

Gough's design would later be published in 1965 by D. Stewart to the Institution of Mechanical Engineers, theorizing its application as a flight simulator [56]. The platform was also put to use in the construction of 5 axis milling machines [57], and due to its six jacks which resembled six legs the term "Hexapod" was trademarked by Geodetic Technology [58].

Despite its more complex cinematic model due to its synergistic nature, it has certain advantages over serial kinematic machines [59]:

- In a PKM the parallel links support a common lightweight platform while in a SKM each actuator hasto support all those that follow which results e higher dynamic loads.
- Due to the previous in a PKM the error from one actuator is evened out by the others while in a SKM position errors will accumulate. Also the fact that in a SKM there are multiple moving cables leading to each actuator, cable tension may increase the chance of positioning errors occurring thus giving the PKM better repeatability and reliability.

Taking into account both facts with a PKM it is possible to build a lighter machine with higher stiffness and lower inertia.

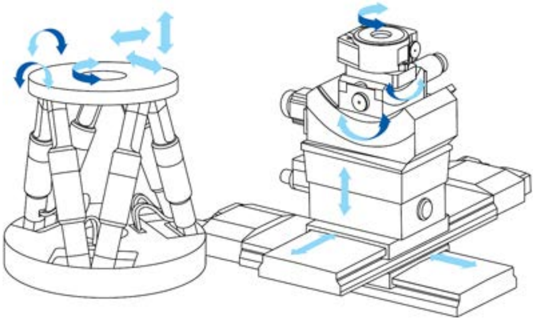

Figure 4.2: Parallel and Serial Positioning Systems [59].

Its unique features have led to some interesting implementations. In medicine Dr. Charles Taylor took advantage of the structure's allow interior and used it to treat complex fractures and bone deformities [60].

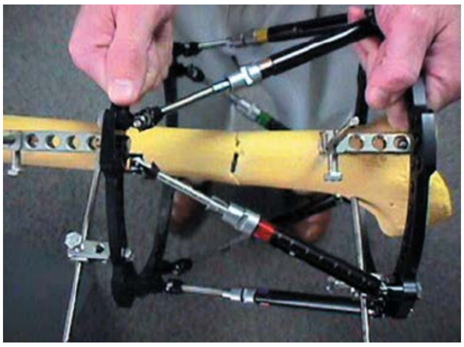

Figure 4.3: Taylor Spatial Frame used to align two bone fragments [60].

Gough/Stewart Platforms also captivated astronomers and space engineers, while they are already used for telescope and antennae positioning [61], A brand new project is being undertaken, the Low Impact Docking System for the International Space Station and its visiting space craft. It consists of two modules, the ISS already features two Common Docking Adapters on several nodes. NASA is developing the NASA Docking System for its new generation of space ships [62].

The NDS is nothing more than a hexapod which will align and clamp to the ISS - CDA when the craft is close enough instead of relying solely on the propulsion, reducing impacts and structural strain. Like with Dr. Taylor, NASA has taken advantage of the hollow core and used it for the airlock system to move between the craft and the station.

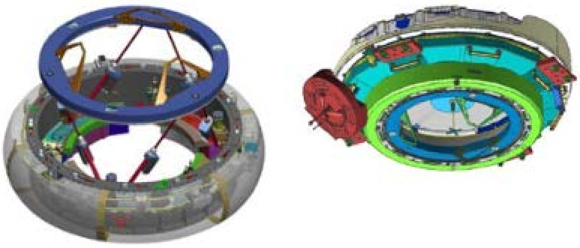

Figure 4.4: NASA Docking System and ISS Common Docking Adapter [62].

4.2 Inverse Kinematics

The inverse or reverse kinematics of a Gough/Stewart platform are fairly simple and a single solution unlike it's serial manipulator counter parts.

Referring to Cauchy's model [54], for any given configuration of the mobile face there is given length of the edges connecting it to the fixed face, while this model portraits the 3-3 type platform it is also valid for type 6-3 and 6-6 platforms and other more unorthodox variations [63].

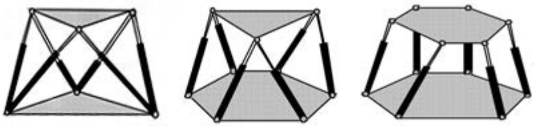

Figure 4.5: Type 3-3, type 6-3 and type 6-6 Stewart Platforms.

The SPIF-A uses a special kind of 6-6 Platform, as described in Section 3.2. It uses a coplanar semi regular hexagon (SRH) geometry providing it high stiffness while still using standard universal joints avoiding the more complex and expensive joints for type 3-3 platforms.

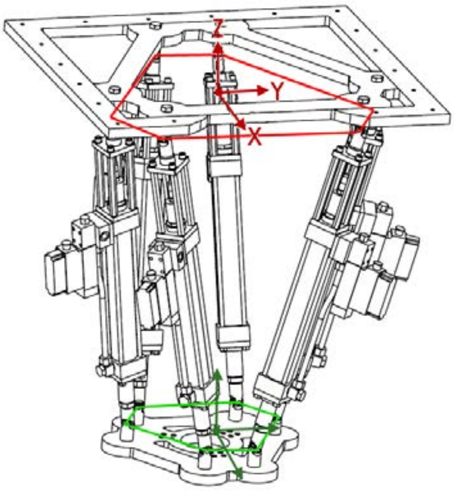

Figure 4.6: SPIF-A's platform geometry and coordinate systems.

The first thing to take into account when studying an inverse Kinematic function is that the base and platform plates used in calculations, for simplification purposes, are not the physical ones, but instead are the hexagons defined by the center points of the universal joints directly connected to them. The coordinate systems were defined in the same way as in milling machines, since the SPIF-A is meant to be used in a similar manner.

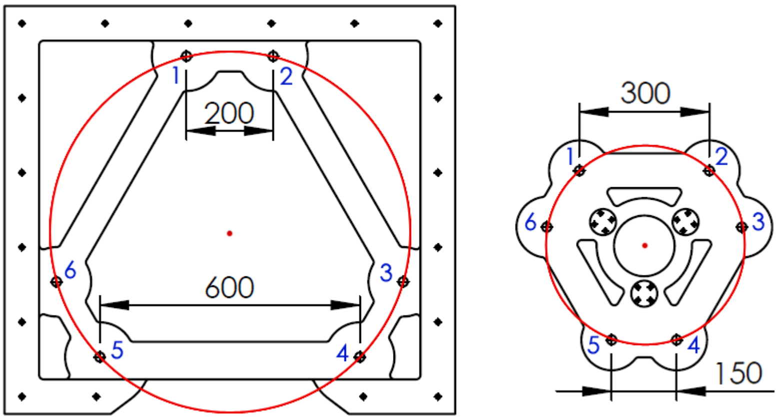

Figure 4.7: SPIFF-A's base plate and mobile platform.

The coordinates for both SRH can be calculated in relation to the length of their sides. For the coplanar base plate the vertex points $B_p(i) = [x_i, y_i, 0]^T$ with $i \in \{1,2,3,4,5,6\}$:

$$L_{BM} = 600mm \wedge L_{Bm} = 200mm \tag{4.1}$$

$$x_{a1} = \left({}^{L_{Bm}}\!/_{2} + L_{BM}\right) \cdot \tan(30^{o}) = 404.145mm \tag{4.2}$$

$$x_{a2} = {}^{(L_{BM}-L_{Bm})}\!/_{2} \cdot \tan(30^{o}) = 115.470mm \tag{4.3}$$

$$x_{a3} = \left({}^{L_{BM}}\!/_{2} + L_{Bm}\right) \cdot \tan(30^{o}) = 288.675mm \tag{4.4}$$

$$y_{a1} = {}^{L_{Bm}}\!/_{2} = 100mm \tag{4.5}$$

$$y_{a2} = {}^{(L_{BM}+L_{Bm})}\!/_{2} = 400mm \tag{4.6}$$

$$y_{a3} = {}^{L_{BM}}\!/_{2} = 300mm \tag{4.7}$$

$$Bp = \begin{bmatrix} -x_{a1} & -x_{a1} & x_{a2} & x_{a2} & x_{a3} & x_{a3} \\ -y_{a1} & y_{a1} & y_{a2} & y_{a3} & -y_{a3} & -y_{a2} \\ 0 & 0 & 0 & 0 & 0 & 0 \end{bmatrix}^T \tag{4.8}$$

For the mobile plate the result is similar, for $M_p(i) = [p_i, q_i, 0]^T$ with $i \in \{1,2,3,4,5,6\}$:

$$L_{PM} = 300mm \wedge L_{Pm} = 150mm \tag{4.9}$$

$$p_{a1} = \left({}^{L_{PM}}\!/_{2} + L_{Pm}\right) \cdot \tan(30^{o}) = 173.205mm \tag{4.10}$$

$$p_{a2} = {}^{(L_{PM}-L_{Pm})}\!/_{2} \cdot \tan(30^{o}) = 43.301mm \tag{4.11}$$

$$p_{a3} = \left({}^{L_{Pm}}\!/_{2} + L_{PM}\right) \cdot \tan(30^{o}) = 216.506mm \tag{4.12}$$

$$q_{a1} = {}^{L_{PM}}\!/_{2} = 150mm \tag{4.13}$$

$$q_{a2} = {}^{(L_{PM}+L_{Pm})}\!/_{2} = 225mm \tag{4.14}$$

$$q_{a3} = {}^{L_{Pm}}\!/_{2} = 75mm \tag{4.15}$$

$$Mp = \begin{bmatrix} -p_{a1} & -p_{a1} & -p_{a2} & -p_{a2} & p_{a3} & p_{a3} \\ -q_{a1} & q_{a1} & q_{a2} & q_{a3} & -q_{a3} & -q_{a2} \\ 0 & 0 & 0 & 0 & 0 & 0 \end{bmatrix}^T \tag{4.16}$$

When the the platform is moved according to a spatial transformation, either a translation, rotation or both, the euclidean distance between corresponding vertex points on the base and platform hexagons, corresponds to the link length required to achieve that particular position (x,y,z) and orientation (ϕ, θ, ψ). The spacial transformation for the mobile plate can be done by using linear transformations, in which the product between a rotational matrix R (dependent on ϕ, θ andψ) and Mp is added the position $P = [x, y, z]^T$ allowing the actuator length L_i by subtracting Bp:

$$L_i = \sqrt{(P + R \cdot Mp_i - Bp_i)^T \cdot (P + R \cdot Mp_i - Bp_i)}\ ,\ i = \{1, 2, 3, 4, 5, 6\} \tag{4.17}$$

where the rotational matrix R is one of the twelve possible Euler angle configurations commonly referred to as Roll-Pitch-Yaw, it consists of a first ϕ rotation around the x-axis (Yaw), followed by a rotation θ around the y-axis and finally a ψ rotation around the Z-axis [64], simplifying the cosine (cos) as C and the sine (sin) as S:

$$R = RPY(\phi, \theta, \psi) = rot(z, \psi) \times rot(y, \theta) \times rot(x, \phi) \tag{4.18}$$

$$rot(z, \psi) = roll(\psi) = \begin{bmatrix} C\psi & -S\psi & 0 \\ S\psi & C\psi & 0 \\ 0 & 0 & 1 \end{bmatrix} \tag{4.19}$$

$$rot(y, \theta) = pitch(\theta) = \begin{bmatrix} C\theta & 0 & S\theta \\ 0 & 1 & 0 \\ -S\theta & 0 & C\theta \end{bmatrix} \tag{4.20}$$

$$rot(x, \phi) = yaw(\phi) = \begin{bmatrix} 1 & 0 & 0 \\ 0 & C\phi & -S\phi \\ 0 & S\phi & C\phi \end{bmatrix} \tag{4.21}$$

$$R = \begin{bmatrix} C\psi \cdot C\theta & C\psi \cdot S\theta \cdot S\phi - S\psi \cdot C\phi & C\psi \cdot S\theta \cdot C\phi + S\psi \cdot S\phi \\ S\psi \cdot C\theta & S\psi \cdot S\theta \cdot S\phi + C\psi \cdot C\phi & S\psi \cdot S\theta \cdot C\phi - C\psi \cdot S\phi \\ -S\theta & C\theta \cdot S\phi & C\theta \cdot C\phi \end{bmatrix} \tag{4.22}$$

Euler angles while simple to work with, come with the limitation of rotation singularities [65], events in which to rotational axis become aligned, in this degenerated state known as gimbal lock in gyroscopes, its impossible to discern rotations around de coincident axes and occurs when $\theta = \pm 90^o$, however such configurations will not occur on the SPIF-A due to mechanical limitations of the links' u-joints.

Another way of representing spacial transformations is to use an affine map, which combine the rotational matrix and the position array in a single 4 × 4 transformation matrix:

$$T_f = \begin{bmatrix} & & & \\ & [R] & & [P] \\ & & & \\ 0 & 0 & 0 & 1 \end{bmatrix} \tag{4.23}$$

the three zeros in the lower right corner are relative to perspective projection, which is to be kept null for rotations and/or translations and the 1 at the lower left corner is the global scale factor of the geometry after the transformation. To use this method with our current geometry an extra constant coordinate needs to be added to $B_p(i) = [x_i, y_i, 0, 1]^T$ and to $M_p(i) = [p_i, q_i, 0, 1]^T$ enabling Equation 4.17 to be rewritten:

$$L_i = \sqrt{(T_f \cdot Mp_i - Bp_i)^T \cdot (T_f \cdot Mp_i - Bp_i)}\ ,\ i = \{1, 2, 3, 4, 5, 6\} \tag{4.24}$$

When producing parts in machine tools the input coordinates are derived from a reference point on the part on the work table, known as the work coordinate system ${}^{Ws}[T]_{Pt}$, since the base and platform geometries used to obtain the inverse kinematics are in different systems, its necessary to define the transformations between the different coordinate systems, from the mobile platform to the tool-tip/contact point ${}^{Mp}[T]_{Pt}$, from the table to the part reference point ${}^{Tb}[T]_{Ws}$, and from table to the fixed base on top ${}^{Tb}[T]_{Bp}$, in order to obtain the ${}^{Bp}[T]_{Mp}$ need to calculate the link lengths in Equation 4.24

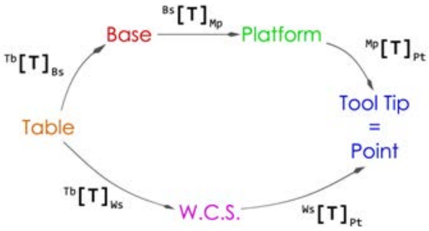

${}^{Bs}[T]_{Mp}$
Base
Platform
${}^{Tb}[T]_{Bs}$
${}^{Mp}[T]_{Pt}$
Tool Tip
=
Point
Table
${}^{Tb}[T]_{Ws}$
W.C.S.
${}^{Ws}[T]_{Pt}$

Figure 4.8: Coordinate system transformation diagram.

$$
{}^{Tb}[T]_{Ws} = \begin{bmatrix} 1 & 0 & 0 & X_{WCS} \\ 0 & 1 & 0 & Y_{WCS} \\ 0 & 0 & 1 & Z_{WCS} \\ 0 & 0 & 0 & 1 \end{bmatrix} \tag{4.25}
$$

$$
{}^{Ws}[T]_{Pt} = \begin{bmatrix} & & & x \\ & [R_{RPY}] & & y \\ & & & z \\ 0 & 0 & 0 & 1 \end{bmatrix} \tag{4.26}
$$

$$
{}^{Tb}[T]_{Bs} = \begin{bmatrix} 1 & 0 & 0 & 0 \\ 0 & 1 & 0 & 0 \\ 0 & 0 & 1 & Tbl \\ 0 & 0 & 0 & 1 \end{bmatrix} \tag{4.27}
$$

$$
{}^{Mp}[T]_{Pt} = \begin{bmatrix} 1 & 0 & 0 & 0 \\ 0 & 1 & 0 & 0 \\ 0 & 0 & 1 & -(338+T_L) \\ 0 & 0 & 0 & 1 \end{bmatrix} \tag{4.28}
$$

$$
{}^{Bs}[T]_{Mp} = \left({}^{Tb}[T]_{Bs}\right)^{-1} \cdot {}^{Tb}[T]_{Ws} \cdot {}^{Ws}[T]_{Pt} \cdot \left({}^{Mp}[T]_{Pt}\right)^{-1} \tag{4.29}
$$

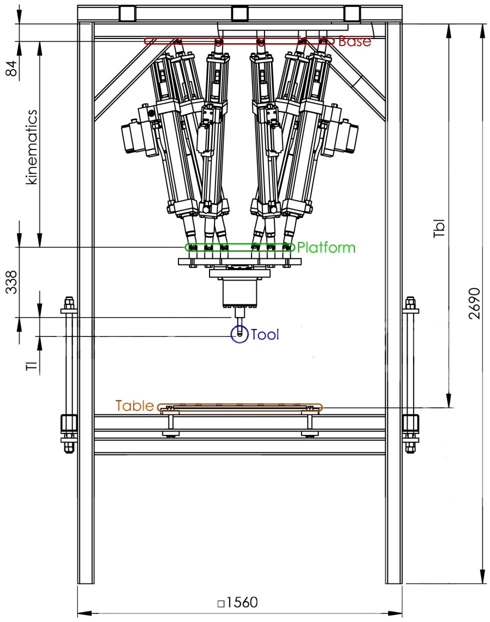

84
kinematics
338
Tl
Base
Platform
Tool
Table
Tbl
2690
□1560

Figure 4.9: SPIF-A dimensions and Kinematic reference points.

4.3 Forward Kinematics

The Forward or Direct Kinematic formulation of a Stewart platform is one of its bigger hindrances. While for a given point and orientation there is only one link configuration (inverse kinematic solution), for a given set of link lengths, there on several solutions for a generic platform there can be up to 64 complex solutions [66], this number can be cut short by optimizing the geometry, when using coplanar base a platform plates the number of solutions comes down to 40 [67], and when using SRH like the SPIF-A its estimated to drop to 24 [68]. To add to the problem the calculations to reach them using only link lengths result leads to non-linear system of equations difficult to solve.

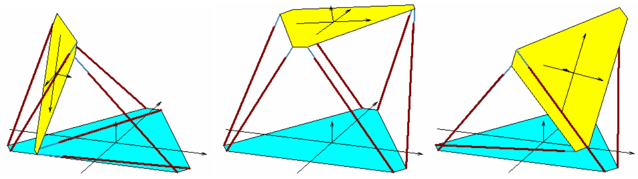

Figure 4.10: Different configurations for the same link length set [69].

This poses a problem to check if the machine is on target and if a force feedback control strategy is to be employed in the future, because of this it's a important piece of the control system that needs to be resolved. There are some methods to tackle this, and are divided into open-form solutions which employ extra sensors [70] and closed-form solutions that either use numerical methods [69; 71; 72] or polynomial based algebraic elimination formulations [66; 67; 68], a consensus is yet to be reached by the scientific community as every methods as its advantages and disadvantages.

4.3.1 Numerical method solutions

Numerical iterative methods require less computational power than their analytical and algebraic counterparts, they are although, dependent on the initial approximation. Since these methods produce a single solution, carefully choosing this initial value will determine which one will be obtain, how many iterations will it take to reach it and if will converge at all, therefore a common practice is to use the last know position as the initial approximation.

The more common methods for this is the Newton-Rapshon [71] method and the first order Newton method [69; 72], Antonio Mendes Lopes [73] compared them both on his PhD thesis, and proposed a algorithm using Newton's method based on its faster convergence rate due to less iterations and because it uses the inverse euler jacobian matrix J_E^{-1} which will be useful in future work to study SPIF-A's differential kinematics. His algorithm is as follows:

1. Select the initial approximation to the platforms position/orientation $Pw_0 \equiv Pw_k$ and the admissible error ϵ;

2. Determine the inverse jacobian $J_E^{-1}(Pw_k)$;

3. Determine the error between the measured actuator lengths L and the length calculated using the reverse kinematics K^{-1} on the position/orientation candidate $\big(L - K^{-1}(Pw_k)\big)$;

4. Solve the new candidate $Pw_{k+1} = Pw_k + J_E^{-1} \cdot \big(L - K^{-1}(Pw_k)\big)$;

5. Calculate error for new candidate $\epsilon_{k+1} = \big|L - K^{-1}(Pw_{k+1})\big|$, if it surpasses the admissible error, return to step 2.

In robotics the kinematic jacobian consists of a matrix that correlates link speeds on the joint space with the manipulators end effector speed on the euclidean work space. The inverse euler jacobian used in aforementioned algorithm can be obtain via the inverse of the kinematic one, as explained by Mendes Lopes [73].

On Equation 4.17 the actuator length is obtain by calculating the norm of the vector three dimensional vector that connects both vertices on tbe base and platform:

$$L_i = \|Lv_i\| \ , i = \{1,2,3,4,5,6\} \tag{4.30}$$

$$Lv_i = P + R \cdot Mp_i - Bp_i = \begin{bmatrix} e_{ix} & e_{iy} & e_{iz} \end{bmatrix}^T \tag{4.31}$$

$$\begin{bmatrix} e_{ix} \\ e_{iy} \\ e_{iz} \end{bmatrix} = \begin{bmatrix} x \\ y \\ z \end{bmatrix} + \begin{bmatrix} r_{11} & r_{12} & r_{13} \\ r_{21} & r_{22} & r_{23} \\ r_{31} & r_{32} & r_{33} \end{bmatrix} \cdot \begin{bmatrix} Mp_{ix} \\ Mp_{iy} \\ Mp_{iz} \end{bmatrix} - \begin{bmatrix} Bp_{ix} \\ Bp_{iy} \\ Bp_{iz} \end{bmatrix} \tag{4.32}$$

the rotational matrix R is shown with a simplified notation but it's the same euler angle configuration used previously dependent on the desired orientation (ϕ, θ, ψ).

The inverse kinematic jacobian is used to calculate the necessary actuator speeds $\dot{L}_i$ known the intended end effector linear and angular speed v_{ee} [64]:

$$\dot{L}_i = J_C^{-1}.v_{ee} \tag{4.33}$$

$$v_{ee} = \begin{bmatrix} \dot{P} & \omega \end{bmatrix}^T \tag{4.34}$$

It needs to be stated that the speed of the platform's vertices differs from the end effector in the center in terms of angular speed. Said speed according to its base coordinate system is:

$$v_{pv} = \dot{P} + \omega \times (R \cdot Mp_i) \tag{4.35}$$

The 6×6 inverse kinematic jacobian is obtained from the inverse kinematic Equation 4.31:

$$J_C^{-1}(i, 1:6) = \begin{bmatrix} \frac{(Lv_i)^T}{\|Lv_i\|} & \frac{((R \cdot Mp_i) \times Lv_i)^T}{\|Lv_i\|} \end{bmatrix} \ , i = \{1,2,3,4,5,6\} \tag{4.36}$$

Using the the angular speed to obtain the first euler angle derivative:

$$w = J_A \cdot \dot{P}_{ang} \tag{4.37}$$

$$J_A = \begin{bmatrix} 0 & -S\psi & C\theta \cdot C\psi \\ 0 & C\psi & C\theta \cdot S\psi \\ 1 & 0 & -S\theta \end{bmatrix} \tag{4.38}$$

The inverse euler jacobian which correlates link length variations to positional and euler angle variations can be calculated from the inverse kinematic jacobian. By representing the 6×6 J_C^{-1} as four 3×3 matrices Equation 4.33 is rewritten:

$$\dot{L}_i = \begin{bmatrix} J_{C11}^{-1} & J_{C12}^{-1} \\ J_{C21}^{-1} & J_{C22}^{-1} \end{bmatrix} \cdot \begin{bmatrix} \dot{P} \\ \omega \end{bmatrix} \tag{4.39}$$

and using Equation 4.37

$$\dot{L}_i = \begin{bmatrix} J_{C11}^{-1} & J_{C12}^{-1} \cdot J_A \\ J_{C21}^{-1} & J_{C22}^{-1} \cdot J_A \end{bmatrix} \cdot \begin{bmatrix} \dot{P} \\ \dot{P}_{ang} \end{bmatrix} \tag{4.40}$$

$$J_E^{-1} = \begin{bmatrix} J_{C11}^{-1} & J_{C12}^{-1} \cdot J_A \\ J_{C21}^{-1} & J_{C22}^{-1} \cdot J_A \end{bmatrix} \tag{4.41}$$

4.3.2 Algebraic solutions

Algebraic methods use such strategies as polynomial systems to describe the non linear equations for the forward kinematics, with the multiple roots for the polynomials being the various possible configurations in the complex domain [67]. While being able to calculate all possible solutions may have advantages when researching the mathematical formulations by providing a better insight on the variable's behaviour, the higher computational burden and the need for a post processor to choose the correct configuration, gives this method little compatibility with real time control applications. While some authors claim that they have recently simplified the formulations, using Gröbner basis and univariate polynomials, their implementation is too complex, highly dependent on the number of significant digits and still not as quick as iterative methods [67]. One particular method used a SRH geometry similar to the SPIF-A [68] however the article was not clear enough on how to reach some of the necessary equations to reach the 14th degree univariate polynomial to solve the system, and contacting the author yielded no feedback.

Another way is to use quaternions to parametrize the rotation matrix, while non-regular geometries tend to be associated with complicated expressions, using regular and/planar geometries and symmetries when designing the platform simplifies the formulation [74]. This was demonstrated by Ji and Wu [75] who used a linearly dependent configuration, and using quaternions to represent the transformation matrix, whose formulation returns eight possible configurations and avoids unnecessary complex roots automatically.

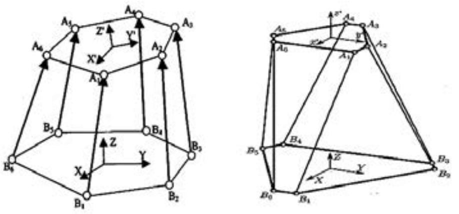

Figure 4.11: Linearly related [75] and independent platform geometries [68].

A platform is considered linearly dependent if the platform geometry can be obtained from the base by using a linear transformation, usually scaling, however Bruyninckx [76], in response to Ji and Wu [75], advises against implementations using linearly related platform geometry because they tend to have various singularities which result in loss of stiffness, this is primarily because these configurations diverge from Cauchy's octahedral geometry [54] and are more similar to a truncated hexagonal pyramid.

After the literary assessment and reviewing mathematical models on Maple™ and MatLab™, the algebraic strategy for solving the SPIF-A's forward kinematic problem was discarded, for now in favour of the more straightforward iterative strategy on Section 4.3.1 .

4.3.3 Open form solutions

Open form solutions use extra sensory data other than the link lengths, the main drawback for this method is extra hardware that will imply additional costs. The extra sensors can be used used to determine one or more unknowns, the more extreme scenario is to discard the link length and use three positional sensors and a gyroscopic sensor to obtain the the platform's coordinates and orientations.

Bonev [70] proposes the use a three extra linear position that will act as passive links and together with the input from the active links yield a formulation, albeit rather complicated, to determine the single solution for the position and orientation.

The sensors used are cable extension transducers (CETs) which are spring loaded wire spools connected to an encoder in order to read linear displacement, and are placed away from the core of the platform structure in order to avoid interfering with the actuators.

Taking into account the geometrical constraints of the SPIF-A machine steep angles aren't achievable, therefore three CETs, can be mounted on its base and connected to the center point of the kinematic system platform, the same point used for position calculation. This would form a tetrahedron and by knowing the coordinates of the base vertices (sensor positions on the base plate) and the length of the edges leading $(SL1, SL2, SL3)$ to the top vertex $SE4$, it is

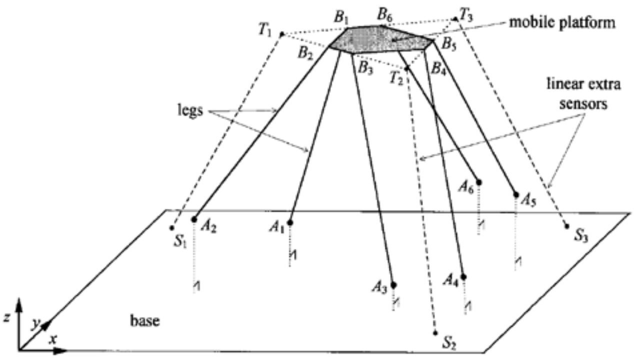
T_1
B_1
B_6
T_3
mobile platform
B_2
B_5
B_3
T_2
B_4
legs
linear extra sensors
A_6
A_5
A_2
A_1
S_1
S_3
A_3
A_4
S_2
base
z
y
x

Figure 4.12: Bonev's extra sensor proposal [70].

possible to obtain its coordinates. To simplify this formulation the coordinate system for the set of sensors coincides with the position of one of the CETs and requires a simple coordinate system transformation afterwards.

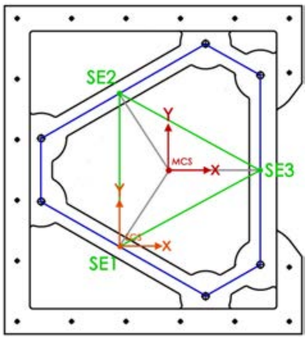
SE2
Y
MCS
X
SE3
Y
X
SE1

Figure 4.13: Sensor configuration.

$$\begin{cases} SE1 = (0,0,0) \\ SE2 = (0,c,0) \\ SE3 = (a,b,0) \\ SE4 = (x_{se}, y_{se}, z_{se}) \end{cases} \tag{4.42}$$

$$x_{se} = \frac{(c^2 + SL1^2 - SL2^2)}{2 \cdot c} \tag{4.43}$$

$$y_{se} = \frac{a^2 + b^2 + SL1^2 - SL2^2 - 2 \cdot q \cdot b}{2 \cdot a} \tag{4.44}$$

$$z_{se} = \sqrt{SL1^2 - p^2 - q^2} \tag{4.45}$$

This method although less complex than Bonev's [70], only retrieves the position of the platform but not the orientation, but it can be used as the initial approximation for the iterative method.

Chapter 5

Motion Control

The main purpose of a controller is to provide proper corrective actions that will result in system stability. To overcome the limitations of open-loop controllers, control theory introduces feedback to close the loop, by comparing a measured system output with the reference value, in order to stabilize dynamical systems. In the case of positional control, for a given path that a system is suppose to take, sensors are used to measure its position, and the read values are continuously compared with the reference, by subtracting them the positional error is obtained, and depending on its magnitude and direction the controller can take action accordingly, this is known as negative feedback [77].

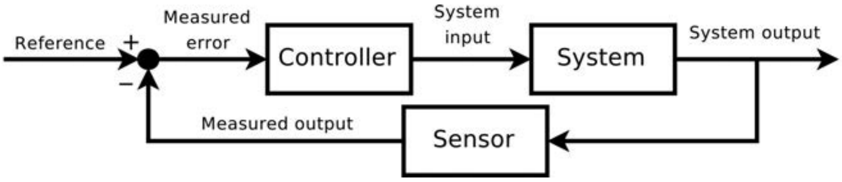

Figure 5.1: Negative feedback control loop.

The most simple control strategies are for systems with linear dynamics, however for real systems, like robotics and aeronautics, this is seldom the case and, to cope with these non-linear situations, various methods were developed.

One of these techniques is adaptive control, where de control variables are adjusted based on changes of the system's parameters. In the case of the SPIF-A this could be done by implementing a PID controller and adjusting the proportional, integral and derivative gains accordingly, however to properly design it, measuring the load on each cylinder would be required, and since the FMS was yet to be installed and calibrated this option was left on standby.

Another way to deal with non-linear systems is by the use of intelligent controllers that rely on various artificial intelligence computing approaches. An example of intelligent control is fuzzy logic, it was first introduced by Zadeh [78] and consists conditional statements as expressions with the form "IF A THEN B", where A and B have fuzzy meaning in the sense that describe the input and output. These statements known as fuzzy rules are the basis for a FLC and can be defined empirically by knowing how a system behaves without needing to define its dynamical model mathematically, for this reason this type of control strategy was chosen for the first motion controller for the SPIF-A.

5.1 Fuzzy Logic

A fuzzy logic controller, FLC for short, consists of three steps, fuzzification of input variables, running the fuzzy interference machine against a rule database to compute the resulting action to be taken, and the defuzzification to turn the results back into usable output variables [79].

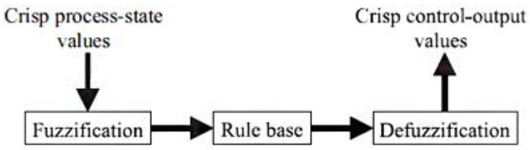

Figure 5.2: Structure of a fuzzy logic based controller[79].

Unlike classical logic where proposition are either true or false, in fuzzy logic deals in propositions with variable answers, one such example the speed of a car, while someone might say that 70 km/h is a moderate velocity others may agree that it is fast. The meaning of each of term (moderate or fast) can be represented by a fuzzy set, also known as membership functions and each of these assume zero to one values according to the term they describe, in the form of a slope, a Gaussian curve curve, among others.

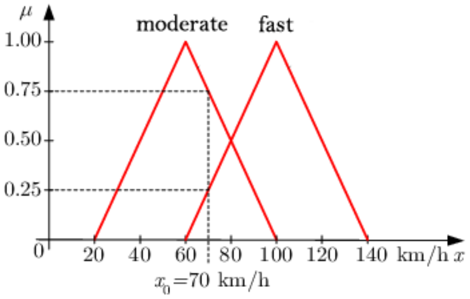

Figure 5.3: Fuzzification of a crisp input variable.

A FLC commanding the car's breaking system will apply a more or less aggressive braking force depending on the car's speed, first it compares the measured speed with the membership functions, in a process known as fuzzification.

As for every input membership function there is a conditional output function, during fuzzification, the weight of the measured variable in the various input fuzzy sets is used to determine their leverage on the output (fuzzy interference machine), the output fuzzy set obtained then needs to be converted to a crisp variable output that can be used to control the system.

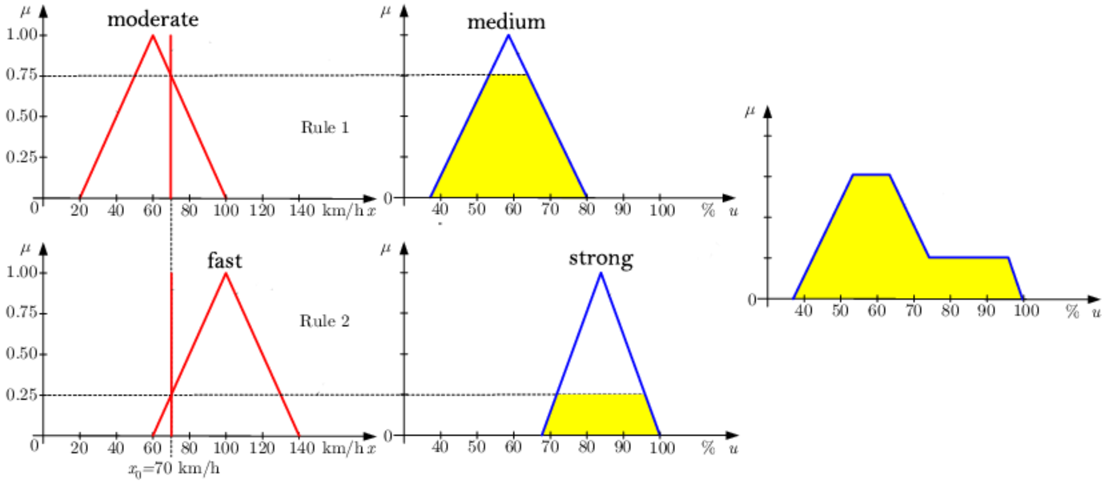

Figure 5.4: Fuzzy rule interference system.

This process is known as defuzzification and there are some methods of achieving this, like the Maximum method which takes into account the highest value of μ the output set, which means that the rule with the maximum activity always determines the value, and therefore shows a discontinuous and step output with a continuous input, not at all suitable for controllers. Another way is the Center of Gravity method, which uses the centroid of the output set, this way the rule with more activity still hasmore weight in the output but with less discontinuities.

5.2 SPIF-A's Controller

There are many types of fuzzy controllers: Takagi-Sugeno, Mamdani, among others, that have been used by several authors to control hydraulic cylinders for Stewart platforms [79; 80; 81; 82], and shown to have better response than pure PID controllers, with faster response times and avoiding overshoot phenomena.

To avoid a complex control scheme at this early stage, the strategy employed was to use a single input, single output controller for each cylinder, meaning that the positioning system would be controlled in the joint space and not the modal space, using the inverse kinematics defined in Setion 4.2 to make the transition.

Based on Sulc's method [79], a Mandani type FLC was developed for the SPIF-A, while Takagi-Sugeno type controllers reduce the computational effort by using constant values as the output instead of variable fuzzy sets, they tend to sometimes have step outputs, Mamdani type controllers, similarly to the example on Section 5.1 use membership functions allowing smoother responses.

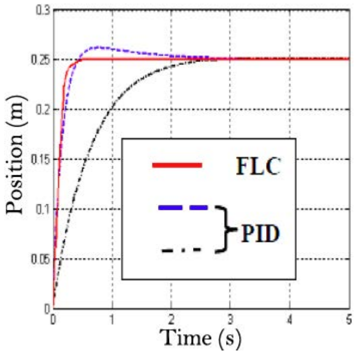

Figure 5.5: PID and FLC response comparison for a 0.25 step input [80].

To design the FLC, MatLab™'s Fuzzy Logic Toolbox™ was used since its GUI allows for easy rule and membership function input, and the outputed .fis file is compatible with Simulink™.

The rule base was defined similarly to one used by Omurlu [82], the inputs used are the cylinder position error and its derivative, which is related to its speed, and each hasseven membership functions depending on its signal (positive or negative) and magnitude (big, medium or small), the output, which after defuzzification will be used to command the cylinder valves, is defined by another seven membership functions.

A total of 49 control rules were used by the combining the error and error derivative membership functions, for example in case of a large negative error and a small derivative (low actuator velocity) the output will be large in the positive direction, while if for that same error, the derivative would be large in the positive direction the output only needs to be minimal in the same direction.

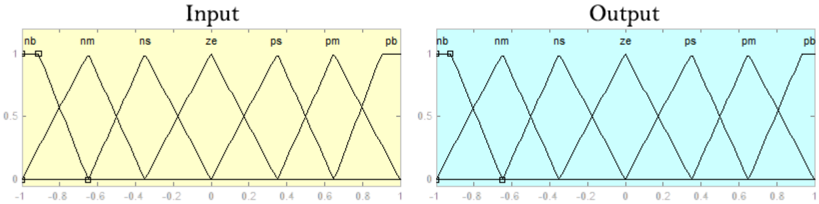

Figure 5.6: Input and output membership functions.

Table 5.1: Rule base for the SPIF-A's FLC.

		error derivative						
		nb	**nm**	**ns**	**ze**	**ps**	**pm**	**pb**
	nb	pb	pb	pb	pm	pm	ps	ze
	nm	pb	pb	pm	pm	ps	ze	ns
	ns	pm	pm	ps	ps	ze	ns	nm
error	**ze**	pm	ps	ze	ze	ze	ns	nm
	ps	pm	ps	ze	ns	ns	nm	nm
	pm	ps	ze	ns	nm	nm	nb	nb
	pb	ze	ns	nm	nm	nb	nb	nb

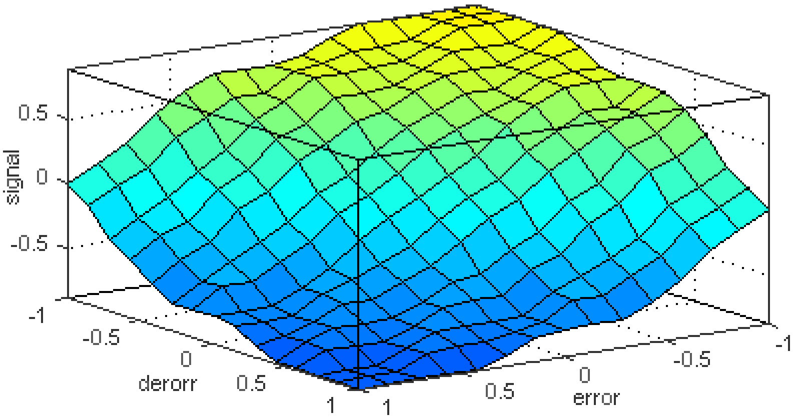

Figure 5.7: Output signal surface in order to error and error derivative input.

5.3 Tuning and Simulation

With the basis for the controller done, it was necessary to test and fine tune it before using it on the actual hardware in order to prevent hazardous situations in cause of eventual flaws in the controller.

For this purpose the MatLab™ simulator, used to study and test the kinematics of the Stewart platform was also used to generate an input signal consisting of the actuators' length along a specific toolpath.

While Simulink™ hasa FLC function block that can use the .fis file directly, it is rather slow since it also runs the Fuzzy logic toolbox simultaneously to allow rule adjustment. The solution found to improve processing time was to use the output signal surface (Figure 5.7), in the form of a two dimensional lookup table [83], in order not to degenerate the result it hastwenty one points ranging from -1 to 1 for both inputs making it a 21x21 matrix, the defuzzification is now achieved by interpolating between the closest known input points.

The controller was then tested using a transfer function from the manufacturers catalogue

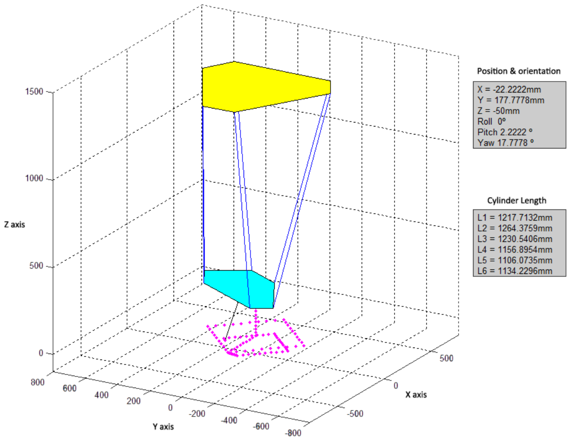

Position & orientation

X = -22.2222mm
Y = 177.7778mm
Z = -50mm
Roll 0°
Pitch 2.2222 °
Yaw 17.7778 °

Cylinder Length

L1 = 1217.7132mm
L2 = 1264.3759mm
L3 = 1230.5406mm
L4 = 1156.8954mm
L5 = 1106.0735mm
L6 = 1134.2296mm

Figure 5.8: Matlab™ simulator.

[46], with the actuators length along the forming path of a truncated pyramid for input. To better tune the controller there is the possibility of adjusting the gain for the error (K_e) and error derivative (K_{de}) inputs [80] in order to achieve better stability and response times, since the inputs need to be on the -1 to 1 range, saturation function blocks are in place to prevent excessive values. As the output only ranges from -1 to 1, the signal needs to be amplified to the -10 to 10V range the valves use (K_u), again and to ensure that excessive voltage isn't applied there is another saturation block as a safeguard. Several gain values were tested for both the error and its derivative, as for the error the faster responses without losing stability happened using gain of 10, the derivative gain proved more sensitive therefore tuning was more challenging. What was discovered was that the gain needed to be very small, under 0.2, since the system would gradually start to oscillate around the target position, but discarding the derivative all together (using a null gain) shown oscillations at the beginning of the planned path, therefore the most stable configurations tested used a 0.1 derivative gain.

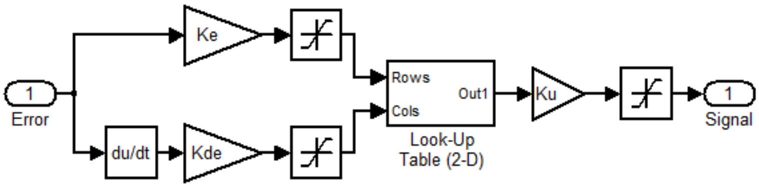

Figure 5.9: Simulink™ controller model.

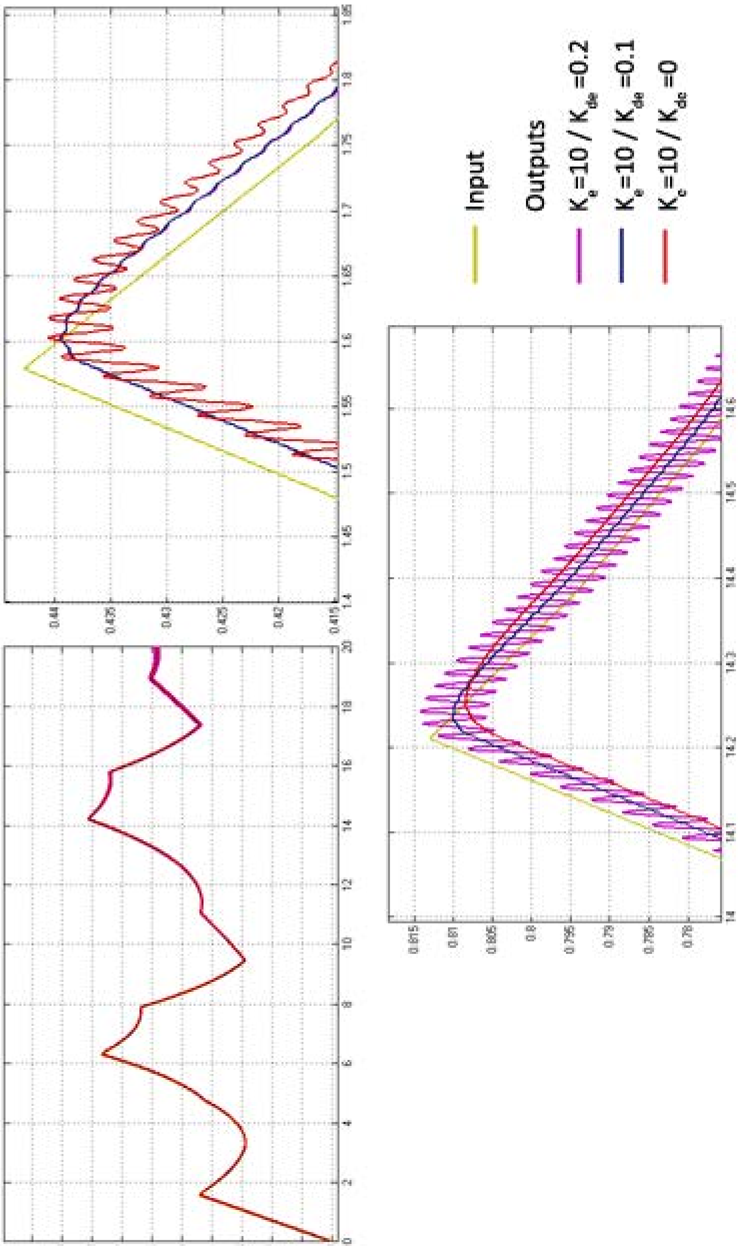

Figure 5.10: Controller outputs for various tested gains.

Chapter 6

SPIF-A Operating System

The majority of forming machinery mentioned in Section 2.2.3 uses G programming language, which is widely implemented on CNC machine tools throughout the industrial world.

It essentially tells the machine where to move to and what path to take, this is done by specifying the target point (X,Y,Z) preceded by a preparatory function identified by the letter G and followed by a number that corresponds to a particular action.

There are a lot of preparatory functions, some universal, other from specific implementations, there are also auxiliary functions denoted by letter M that govern for example spindle rotation direction, coolant oil and program stops.

On this early stage, for the preliminary version of the SPIF-A's operating system, only a few fundamental G-code instructions are recognized, however they are sufficient for production of various types of geometries.

Table 6.1: List of G-codes compatible with the SPIF-A OS.

SPIF-A G-codes	
G01	Linear Interpolation
G02	Clockwise circular interpolation
G03	Counterclockwise circular interpolation
G43	Turn on tool length offset compensation
G49	Turn off tool length offset compensation
G53	Movement using machine coordinate system
G54-G57	Movement using work coordinate systems
G90	Absolute coordinate positioning
G91	Incremental coordinate positioning
M30	End of program

To obtain the code for the parts to be produced CAD/CAM methods are employed, the part is designed using CAD software like Solidworks™ or CATIA V5® and afterwards imported by a dedicated CAM software in this case EdgeCAM® where the G-code is generated according to the machining strategy used.

The SPIF-A OS comes into play by bridging the part's G-code with the hardware that will manufacture it namely the SPIF-A machine. For this purpose a real time target machine is used to communicate with the hardware using two input/output modules, on it a Simulink™ control model is running that receives inputs from the host that reads the G-code file.

The real time machine used is a Speedgoad™ SN1584 [84], a brand whose equipments are developed with compatibility with Simulink™ and MatLab™ in mind. They come with easy to install/implement communication protocols using MatLab™'s xPC Target™ toolbox, making them a valuable academic/research tool for the development and continuous verification/validation

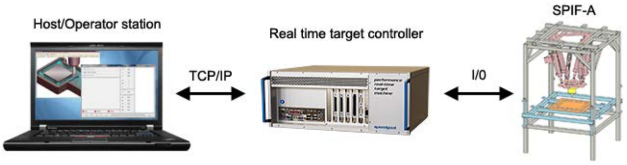

Figure 6.1: Worflow between the SPIF-A and its operator.

of controllers, since they can preform such tasks as hardware-in-the-loop simulation, where a real time machine emulates the mechanism to be controlled using its dynamic model, in case of the absence of the physical system or to avoid risks, and rapid controller prototyping by being connect to the actual hardware and interacting with it, which is the case for the SPIF-A.

The xPC Target software is prepared for two methods of connecting the host and target machine: Ethernet TCP/IP and RS232, although the real time target machine supports both, Speegoat™ recommends the first option to take advantage of its Gigabit Ethernet card, that has less limitations on data bandwidth than the RS232 serial link which is also more susceptible to electrical interference.

6.1 User interface

The GUI was developed using MatLab™'s graphical user interface development environment GUIDE™. It hasseveral roles, its main purpose being to read .txt files containing the G-code and to and verify if their production is possible, it also allows manual positioning, to set up the necessary WCS reference points and tool lengths. It also collects information from the target machine, such as current position and forces being exerted to be stored back for further analysis.

In order to keep it user friendly the GUI is initialized as a simple selection menu where it is possible to choose from automatic mode, path simulation, manual positioning and machine setup.

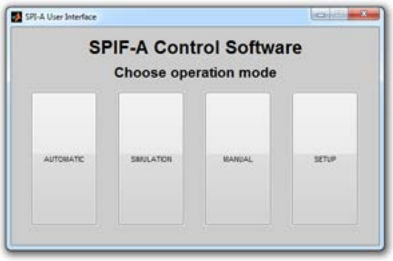

Figure 6.2: SPIF-A GUI selection menu.

The initial idea was for the interface simply to verify if a G-code command was valid and to use the real time machine to interpret it and generate the path accordingly using and embedded MatLab™ function or a dedicated S-function. However since Simulink™ only supports numerical values, sending each code line as a string is automatically excluded, and for the time being the G-code is processed by the interface program, which has the disadvantage of being slower than the the real time target machine, an issue that will be addressed in future work.

For this first version of the SPIF-A OS two MatLab™ functions are used to comunicate with the real time target:

SignalRead.m responsible for checking if the target machine is connected, if true checks connection to the SPIF-A hardware and returns various sensory data regarding pump status, position and workload;

SignalWrite.m responsible for setting/changing the variables on the target machine that control the positioning system, namely the hydraulic pump, the tool and WCS offsets and the desired tool position and orientation.

6.1.1 Automatic mode

The automatic mode is responsible for analysing the G-code files generated using CAD/CAM software and to plan the tool paths according to which type of interpolation (Table 6.1), in order for the SPIF-A to produce parts.

When pressing start the user is prompted to choose a text file containing the part's G-code, after checking for file compatibility the program then checks for connection to the target machine, returning an error message in case of any failure. If a connection is achieved the color of the indicators on the status change and part production beings, using the write function to provide the necessary forming path.

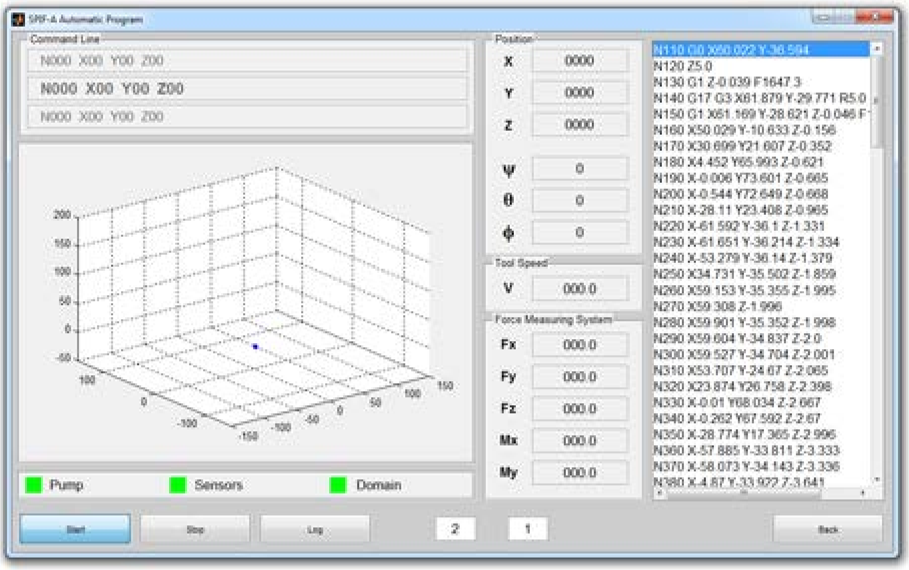

N000 X00 Y00 Z00
N000 X00 Y00 Z00
N000 X00 Y00 Z00

X 0000
Y 0000
Z 0000
ψ 0
θ 0
ϕ 0
V 000.0
Fx 000.0
Fy 000.0
Fz 000.0
Mx 000.0
My 000.0

2
1

```
N110 G0 X50.022 Y-36.594
N120 Z5.0
N130 G1 Z-0.039 F1647.3
N140 G17 G3 X61.879 Y-29.771 R5.0
N150 G1 X61.169 Y-28.621 Z-0.046 F
N160 X50.029 Y-10.633 Z-0.156
N170 X30.699 Y21.607 Z-0.352
N180 X4.452 Y65.993 Z-0.621
N190 X-0.006 Y73.601 Z-0.665
N200 X-0.544 Y72.649 Z-0.668
N210 X-28.11 Y23.408 Z-0.965
N220 X-61.592 Y-36.1 Z-1.331
N230 X-61.651 Y-36.214 Z-1.334
N240 X-53.279 Y-36.14 Z-1.379
N250 X34.731 Y-35.502 Z-1.859
N260 X59.153 Y-35.355 Z-1.995
N270 X59.308 Z-1.996
N280 X59.901 Y-35.352 Z-1.998
N290 X59.604 Y-34.837 Z-2.0
N300 X59.527 Y-34.704 Z-2.001
N310 X53.707 Y-24.67 Z-2.065
N320 X23.874 Y26.758 Z-2.398
N330 X-0.01 Y68.034 Z-2.667
N340 X-0.262 Y67.592 Z-2.67
N350 X-28.774 Y17.365 Z-2.996
N360 X-57.885 Y-33.811 Z-3.333
N370 X-58.073 Y-34.143 Z-3.336
N380 X-4.87 Y-33.922 Z-3.641
```

Figure 6.3: Automatic mode interface.

This is done by the function **Gcode.m**, it reads the code file one line at a time to get the intended destination and interpolation type. To properly define a path several points are required and since G-Code only references endpoints various middle points need to be calculated. Using the position returned by **SignalRead.m** as the initial position and the endpoint from the code, it is possible to determine various points along the linear or circular path with their amount dependent on the path length. These points are then continuously relayed to the controller via the **SignalWrite.m** function and displayed on a figure. If any point is not reachable a warning message is returned and machine operations halt.

Prior the start of an experiment/part production it is possible to chose to log the position and workload data by pressing the Log button which will save all information returned by the **SignalRead.m** function in a text file in matrix form for later analysis. The first column stores the time stamp, columns two through seven store position/orientation and columns eight through twelve are for the works loads.

6.1.2 Simulation mode

The simulation mode serves for off-line analysis of G-code text files, its purpose to check if a generated file is compatible with the SPIF-A OS and if its part is feasible taking into account the

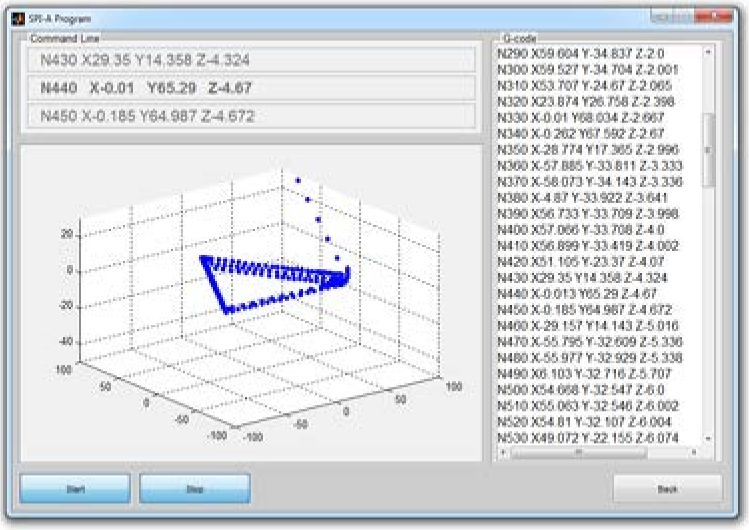
SPIF-A Program
Command Line
G-code
Start
Stop
Back
20
0
-20
-40
100
50
0
-50
-100
-100
-50
0
50
100

Command Line:

```
N430 X29.35 Y14.358 Z-4.324
N440  X-0.01  Y65.29  Z-4.67
N450 X-0.185 Y64.987 Z-4.672
```

G-code:

```
N290 X59.604 Y-34.837 Z-2.0
N300 X59.527 Y-34.704 Z-2.001
N310 X53.707 Y-24.67 Z-2.065
N320 X23.874 Y26.758 Z-2.398
N330 X-0.01 Y68.034 Z-2.667
N340 X-0.262 Y67.592 Z-2.67
N350 X-28.774 Y17.365 Z-2.996
N360 X-57.885 Y-33.811 Z-3.333
N370 X-58.073 Y-34.143 Z-3.336
N380 X-4.87 Y-33.922 Z-3.641
N390 X56.733 Y-33.709 Z-3.998
N400 X57.066 Y-33.708 Z-4.0
N410 X56.899 Y-33.419 Z-4.002
N420 X51.105 Y-23.37 Z-4.07
N430 X29.35 Y14.358 Z-4.324
N440 X-0.013 Y65.29 Z-4.67
N450 X-0.185 Y64.987 Z-4.672
N460 X-29.157 Y14.143 Z-5.016
N470 X-55.795 Y-32.609 Z-5.336
N480 X-55.977 Y-32.929 Z-5.338
N490 X6.103 Y-32.716 Z-5.707
N500 X54.668 Y-32.547 Z-6.0
N510 X55.063 Y-32.546 Z-6.002
N520 X54.81 Y-32.107 Z-6.004
N530 X49.072 Y-22.155 Z-6.074
```

Figure 6.4: Simulation mode interface.

SPIF-A's spacial limitations. It works in the same way as the Automatic mode but, due to its off-line nature does not rely on the read position as a starting point, instead using the previous endpoint as the start for a new path and using the origin of the coordinate system as the starting point for the first iteration.

6.1.3 Manual positioning

The manual mode works in a similar manner as the automatic, when pressing the Start is attempts to connect using the **SignalRead.m** function and the **SignalWrite.m** is used to relay the desired position.

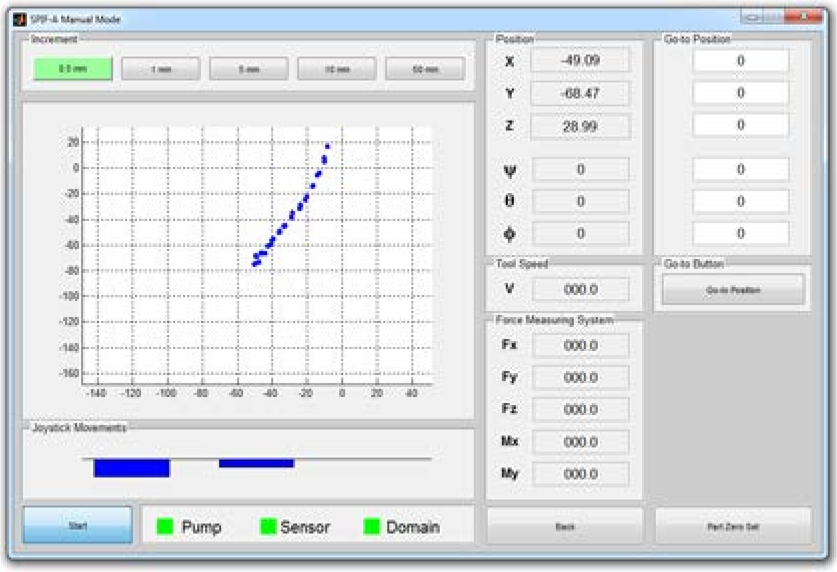
SPIF-A Manual Mode
Increment
0.5 mm
1 mm
5 mm
10 mm
50 mm
Joystick Movements
Start
Back
Part Zero Set
Go-to Button
Go-to Position
20
0
-20
-40
-60
-80
-100
-120
-140
-160
-140
-120
-100
-80
-60
-40
-20
0
20
40

🟩 Pump 🟩 Sensor 🟩 Domain

Position		Go-to Position
X	-49.09	0
Y	-68.47	0
Z	28.99	0
ψ	0	0
θ	0	0
ϕ	0	0

Tool Speed

V 000.0

Force Measuring System

Fx 000.0
Fy 000.0
Fz 000.0
Mx 000.0
My 000.0

Figure 6.5: Manual positioning mode interface.

There are two ways to manually position the SPIF-A's tool, the first option is to enter the desired position on the top right corner of the interface and pressing the Go to Position button while the second method for manual movement is by using a joystick. Its object is defined by the **vrjoystick.m** function and to read its movements the **readjoystick.m**, which come as standard for MatLab™ is employed, the increment each movement contributes to the current position can be selected on the top left of the interface to allow more precision or wider range.

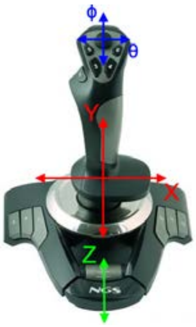

Figure 6.6: Joystick used for manual positioning.

One other feature of this mode is allowing to set the current position as the origin of the WCS, by simply pressing the Part Zero Set button.

6.1.4 Machine setup

The setup interface is the menu where up to four WCS origin point offsets can be defined, in relation to the MCS. Different tool lengths can be stored as well, these values are to be set prior to starting any operation as they are required for the coordinate system transformations in the kinematic system (Equations 4.25 and 4.28).

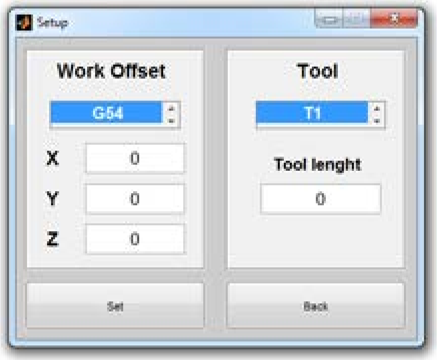

Work Offset
G54
X 0
Y 0
Z 0

Tool
T1
Tool lenght
0

Figure 6.7: Machine setup interface.

6.2 Target Machine Implementation

The target machine works by running a preloaded Simulink™ model whose variables are read and/or altered by the **SignalRead.m** and **SignalWrite.m** functions via the TCP/IP connection.

To communicate with the hardware there are two different modules [85]:

IO101 a 16-bit analog module with 32 single-ended or 16 differential analog input, 8 analog output, and 8 digital input and 8 digital output TTL channels, manufactured by Acromag™;

IO401 a digital input module with provides 6 individual channels of 32-bit counters to connect incremental and absolute encoder sensors, it supports both TTL and RS422 (differential) encoder outputs selectable via DIP switches, manufactured by TEWS®.

In order to read input or generate output signals, Speedgoat™ provides a custom library with a wide range of functions from analog input readers and output generators to specialized digital input applications such as absolute encoder readers, usable in Simulink™ models.

6.2.1 Interface input variables

As mentioned before the movement commands come from the GUI, in the model running on the real time target machine they are defined as constants whose value can be set by **SignalWrite.m**.

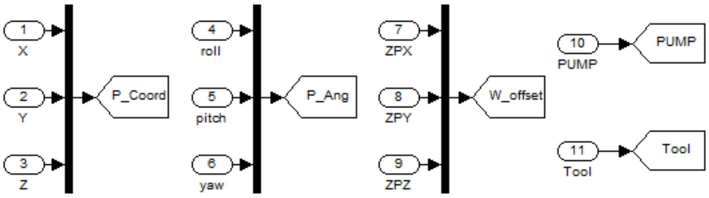

Figure 6.8: Control model input variables.

When the Start button on either the Manual (Section 6.1.3) or the Automatic mode (Section 6.1.1) is pressed, in the event of a successful connection all variables are altered. While the first six variables, tool position and orientation, are continuously updated during part production, variables seven through nine, WCS offset, and variable eleven, tool length, are only updated at the beginning of the program and should be set prior to operations using the Machine Setup interface (Section 6.1.4). Variable number ten which commands the hydraulic pump state assume the value of 1 and when the Stop button is pressed it returns to 0.

6.2.2 Actuator encoder reader

As noted in Table 3.1, the SPIF-A's cylinders come equipped with absolute linear transducers, that produce a RS422 differential output. Their position is read by an absolute encoder model from Speedgoat™'s library, and the values returned by all six transducers are analysed by an embedded MatLab™ function.

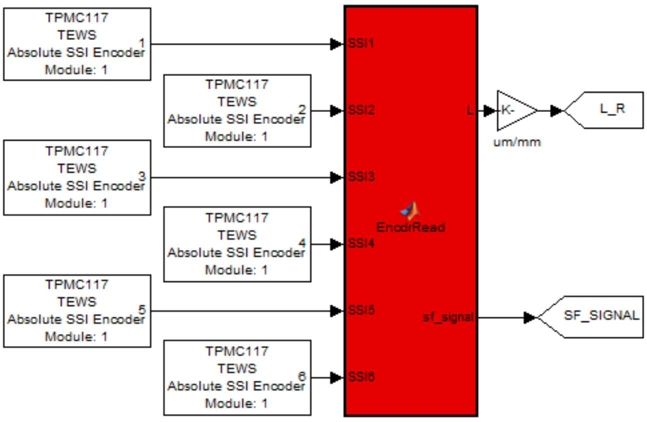

Figure 6.9: Encoder analyser function block.

These magnetostrictive transducers measure the displacement of a sensor on the cylinders rod relative to the transducer module, due to their absolute nature and the fact that they are assemble at the rear of the cylinder, they return a position of about 52000 micrometers with the rod at its stowed position. What the encoder analysis block does is check if the read position are within the correct range from 0 to about 452000 micrometers return a sensor error output if any of the transducers fails this check. The function also subtracts the stowed position offset and output the displacement of all six rods which are then converted to millimetres (ranging from 0 to 400), to be used by other functions.

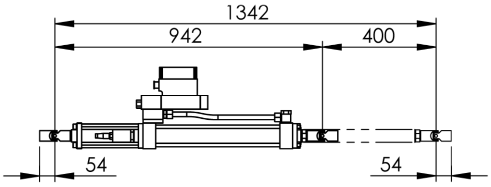

Figure 6.10: SPIF-A kinematic links geometry.

6.2.3 Inverse kinematics

As specified on Section 4.2, in order to obtain the actuator length combination for a specific position and orientation, the inverse kinematics need to be calculated. Since the kinematic formulation is made relative to the MCS the input coordinates, which have the WCS as reference, need pass through coordinate system transformation block.

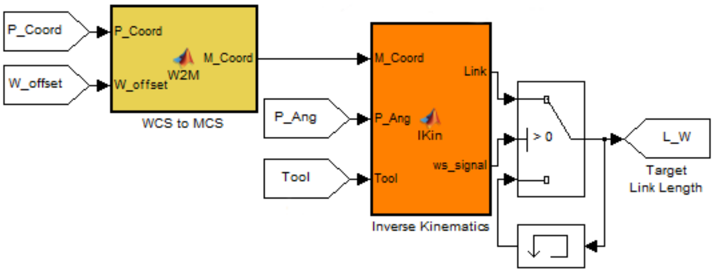

Figure 6.11: WCS to MCS transformation and inverse kinematic function blocks

The embedded function used for the inverse kinematics is very similar to the one used in the motion simulator on Section 5.3, in terms of formulation, but differs on the returned output. The first distinction is that the length output is not the distance between u-joints but instead the required rod position between the aforementioned 0 a 400 millimetres, this is so to compare the intended position with the measured value when controlling the positioning system, and its obtainable simply by subtracting the stowed length of the actuator which is 942 millimetres as seen of Figure 6.10.

This block also performs two separate checks to see if a target configuration is possible. The first is right before the actuator length calculations and serves to determine if the intended position is inside the machine frame meaning that for safety reasons X and Y values can not be outside the -500 to 500 millimetre range.

Due to the U-joints limits the intended orientation is also checked, pitch and yaw angles cannot exceed the -30º to 30º degree interval, this limitations mean that using the ideal forming angle, in which the tool is perpendicular to the wall it's forming is not achievable for steep geometries however this restriction also insures that collisions between the tool holder/spindle, and the work table are less likely to occur. When it comes to roll (rotation around the spindle

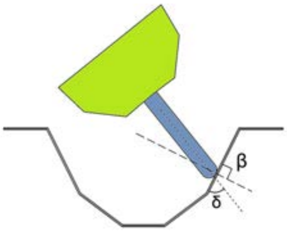

Figure 6.12: Possible forming angle δ versus ideal forming angle β

axis) only zero degree values are accepted since it would result in a twisted configuration that could damage the whole platform system.

If the target configuration does not meet the previous requirements the function block outputs the variable "ws-signal" as zero and skips the inverse kinematic calculations, and the system remains at the last valid position, otherwise the link lengths are deduced. After their calculation, the function again checks if the length value for any of the six cylinders is outside the 0 to 400 millimetre interval and if any exceeds the range of action, same as before, the "ws-signal" variable assumes the value zero otherwise it assume the value of one, triggering the switch which will allow movement.

6.2.4 Motion and pump control

The hydraulic circuit that governs the movements of the SPIF-A is controlled by analog signals. As the pump is either on or off it can be controlled by a constant 10 volt output that activates a relay, since the input "PUMP" variable either assumes the values one or zero, depending on its state the control signal can be generated via a proportional gain of ten.

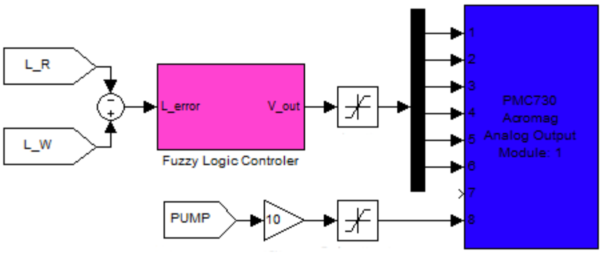

Figure 6.13: analog control signal outputs for pump and actuators

In order to control the valves that drive the cylinders the FLC developed in Chapter 5 is employed using the calculated length from the inverse kinematics as the reference value, and the values read from the transducers to close the loop and calculate the error value used in the controller that outputs an electrical signal ranging from -10V to 10V.

In order to prevent excessive voltage on the analog module and/or the cylinders valves, a saturation block that limits the voltage to the aforementioned interval is in place.

6.2.5 Forward kinematics

The forward kinematics use the read actuator lengths to obtain the tool tip's position and orientation along a given path. The method used is the iterative solution explained in Section 4.3.1, for the initial estimate the last known configuration is used and since the result is relate to the MCS a second function block is for the coordinate transformation to the WCS.

This calculated configuration is then used to determine if the tool is on target in order to move to the next movement interpolation.

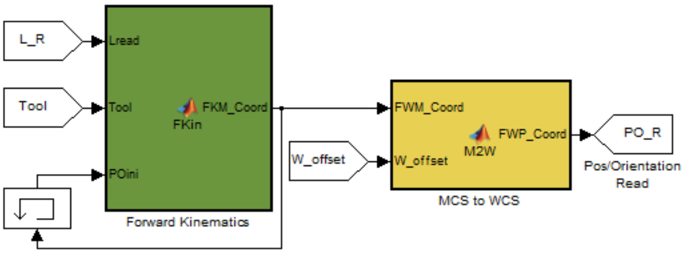
L_R
Tool
Lread
Tool
POini
FKM_Coord
FKin
Forward Kinematics
W_offset
FWM_Coord
W_offset
FWP_Coord
M2W
MCS to WCS
PO_R
Pos/Orientation Read

Figure 6.14: Forward kinematics and MCS to WCS transformation blocks.

6.2.6 Force Measuring

At this stage the FMS serves only to monitor and study the forming forces and is not yet included in the control strategy.

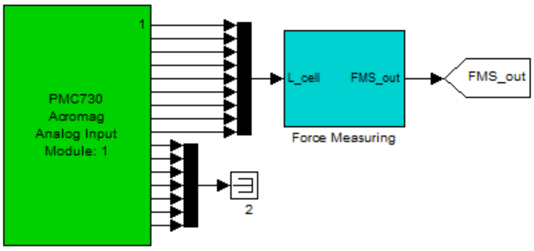
1
PMC730
Acromag
Analog Input
Module: 1
L_cell
FMS_out
Force Measuring
FMS_out
2

Figure 6.15: Load cell analog input signal reader for the FMS.

The work loads exerted by the tool are calculated through the formulation from Section 3.4 and by reading the LMU's voltage using the analog input module.

6.2.7 Output to interface

As the Simulink™ model runs continuously at the end of each cycle it relays Variables back to the GUI via the **SignalRead.m** function.

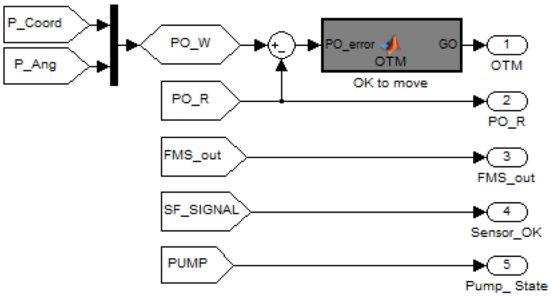
P_Coord
P_Ang
PO_W
+
-
PO_error
GO
OTM
OK to move
1
OTM
PO_R
2
PO_R
FMS_out
3
FMS_out
SF_SIGNAL
4
Sensor_OK
PUMP
5
Pump_ State

Figure 6.16: Output variables for the GUI.

The first output is a boolean variable that is the result of an embedded function that compares the intended position with the actual configuration and will only assume the value of 1 if the SPIF-A's tool is on target, and only after this will the GUI send a new destination. The second and third outputs are the position/orientation configuration and the work loads calculated previously for display and logging purposes, while the fourth and fifth refer to the state of the sensors and the pump to be displayed in the interface's indicator panel.

Chapter 7

Experiments and Results

One of the features that set the SPIF-A apart from other forming machinery is its stewart platform, with the extra DOF's it has over adapted milling machines [40] and purpose built machinery [39; 42], while having the necessary stiffness that allow reaching higher work loads than SKM and tricepts [41; 44].

With its novel design the SPIF-A will allow to study the influence of using both three axis and five axis strategies for producing parts in order to study the influence of the pressing direction, which is theorized to be more favourable to the forming process if the tool is close to perpendicular to the wall being formed [86].

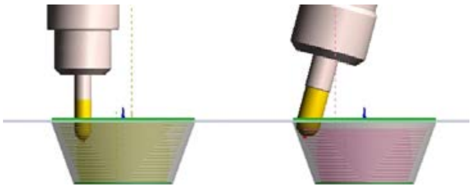

Figure 7.1: Three axis and five axis forming strategies for a truncated cone [6].

In order to test the SPIF-A's positional accuracy a series of tests were done. The first operations were conducted without the forming table in place, to provide more room should any errors or problem arise.

Without any mishaps, for the next test, the forming table was mounted but instead of a a blank holder a white board was used and instead of a forming tool a marker was assembled on the spindle. The purpose of this test was to see if the machine would behave the same way along a specific path using three or five axis and the results show were favourable in both case with only small deviations from the intended path when using five axis.

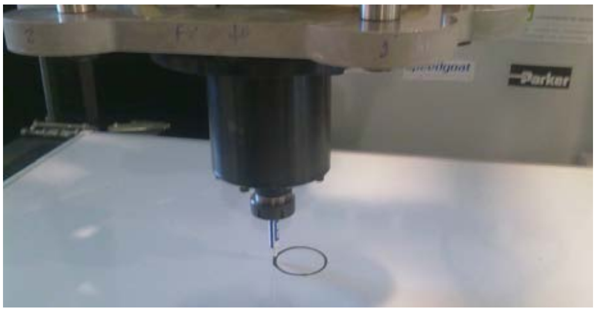

Figure 7.2: First path test performed.

7.1 Simple geometries

The second stage of tests consisted of using simple geometries like truncated pyramids and truncated cones different using one millimetre thick 230x230mm aluminium blanks (AA1050), and varying parameters like dimensions, wall angle and vertical step size for the preliminary experimental work for the Phd Thesis regarding the SPIF-A [6; 87].

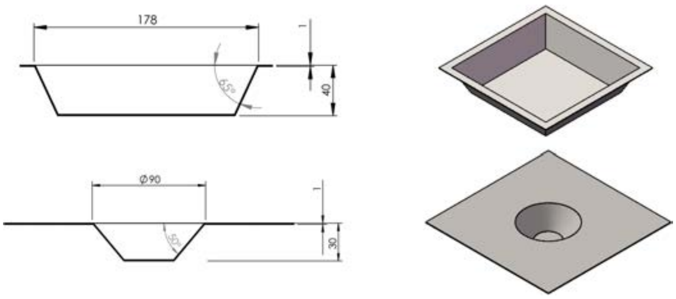

Figure 7.3: Examples of truncated pyramids and cones to be produced.

For these parts the WCS reference point was the center of the blank, due to the forming table's adjustable configuration the blank holders aren't mounted on a fixed location, therefore a way to obtain the central reference point was devised. For the smaller blank holder, the one used in these operations, a special piece, machined on a lathe, that fits snugly on the circular baking plate, has a center hole where different bushings with the inner diameter for different tools are mounted. Then, in manual positioning mode, one simply needs to align the mounted tool with it, set the WCS offset, and after clamping the blank, the machine is now ready for forming operations.

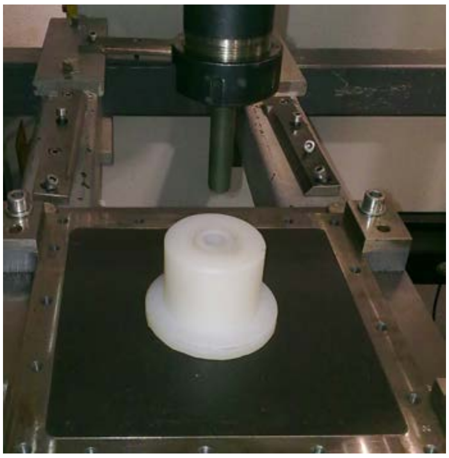

Figure 7.4: Centering apparatus.

7.1.1 First parts

One of the problems encountered during tests was that some parts would rupture during operations, this occurred mainly while forming steep walls.

The reason behind this is that since SPIF is a stretch forming process the thickness of the part is governed by the sine law which states that the final thickness is related to the wall angle λ:

$$t_f = t \cdot \sin(90^o - \lambda) = t \cdot \cos(\lambda) \tag{7.1}$$

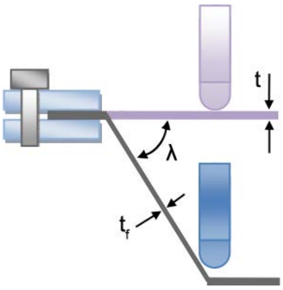

Figure 7.5: Visual representation of the sine law.

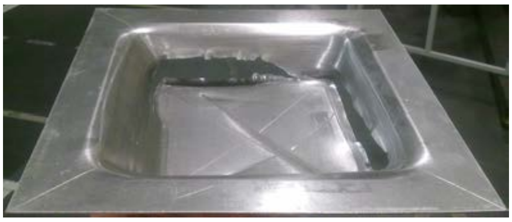

Figure 7.6: Ruptured part while attempting 70º wall.

Equation 7.1 was verified as it predicted a wall thickness of about 0.35 mm and the measured values along the torn edge were ranged from 0.30 to 0.40 mm. These types of failures are most likely to be related to localized necking phenomena and will be the target of more comprehensive studies in the near future.

By reducing the wall inclination, this problem was avoided and even with large vertical increments, which imply higher work loads, but less forming time, various successful parts were achieved.

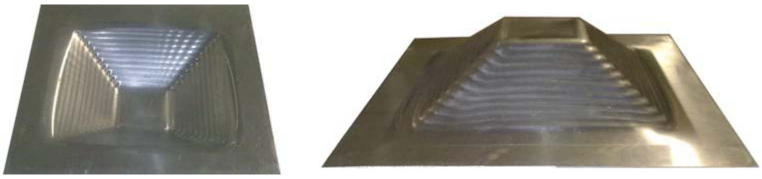

Figure 7.7: Top and bottom view of a 45º truncated pyramid made by the SPIF-A.

However the time saved, comes at the cost of the surface quality, as large vertical increments imply fewer passages, that are further apart, resulting in a rough surface finish, that is undesirable when producing ready to use parts, such as those intended for medical applications [28].

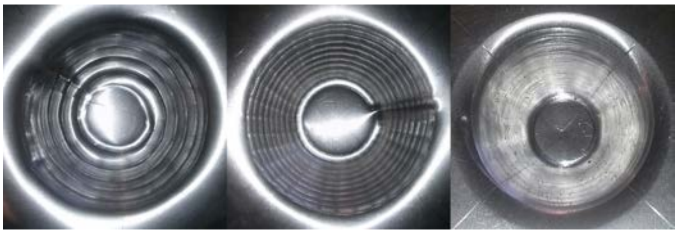

Figure 7.8: Truncated cones made using 10, 5 and 1 millimetre vertical increments.

7.1.2 Different forming paths

Due to its soft and formable nature, the aluminium blanks used allowed using large vertical increments, however this bright up certain surface finish imperfections to light, and one of these defects is related to the type of forming path used.

As mentioned in Section 2.2.2, there are two types of forming paths. The main advantage of contour milling is that the G-code, that describes it, is more straightforward and easily programmable by a human operator. However, at each step change there is a visible transition indentation in the surface. On the other hand spiralling toolpaths imply a more complex code that can only be generated on CAD/CAM software, this is due to its continuous step decent, opposed to the discrete step movement in contour milling, however this avoids abrupt transitions and results in a better surface finish.

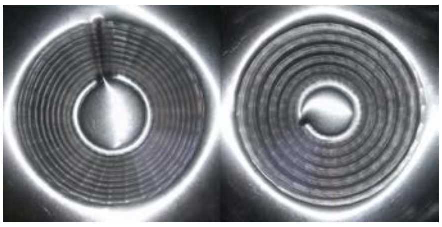

Figure 7.9: Parts made using contour milling and spiralling paths.

There are improvements for both cases, for contour milling since the issue is on the point where each level begins and ends, the ridge that forms could possibly by avoided by overlapping the end point after the initial. In the case of spiralling toolpath, since the vertical descent is continuous, the only issue is that the end point on the bottom of the part will not match the contour of the intended geometry properly, a solution for this would lie on executing a single pass contour path to ensure geometrical accuracy and avoid the snail like effect seen of Figure 7.9.

While performing these tests the FMS was also tested, to measure normal and transverse forces (explained in Section 2.2.2) during the forming operation. It was verified that forces when using different forming toolpaths, using contour milling force spikes appear in the Z-axis, at each vertical step increment, while when using spiralling toolpaths forming forces are more constant.

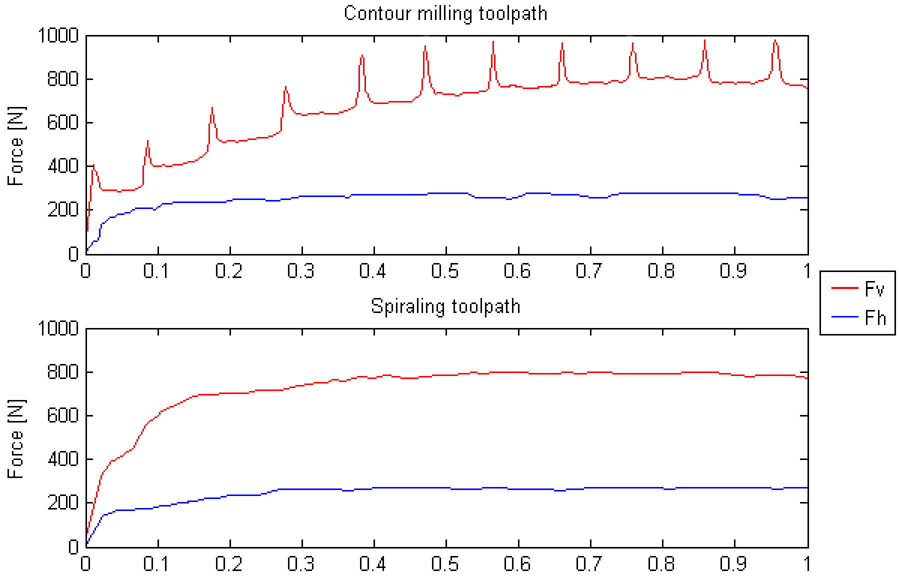

Figure 7.10: Measured forces for different toolpath types.

7.1.3 Different materials

Most experimental research to date, being limited by the work load, focuses either on softer materials like aluminium [28; 35; 38] and plastics [30], or very thin steel [39]. One of the aims of the SPIF-A project is to study harder materials, for this reason production a a steel part was attempted. The test involved a one millimetre thick dual phase steel (DPS780) blank, this type of material, was developed in the 1970s and in its microstructure there is both soft ferrite and hardened martensite, which together result in a high strength steel with higher formability than other hard materials [88].

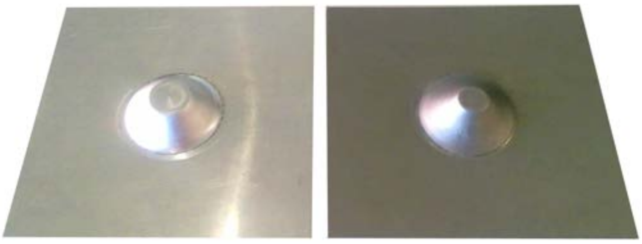

Figure 7.11: Truncated cones made from aluminium and dual phase steel.

The FMS was also used to compare both materials, for the aluminium parts the measured forces of arround 1 kN are consistent with the existing research [28; 29; 32] while the DPS780 is yet to be tested in such applications.

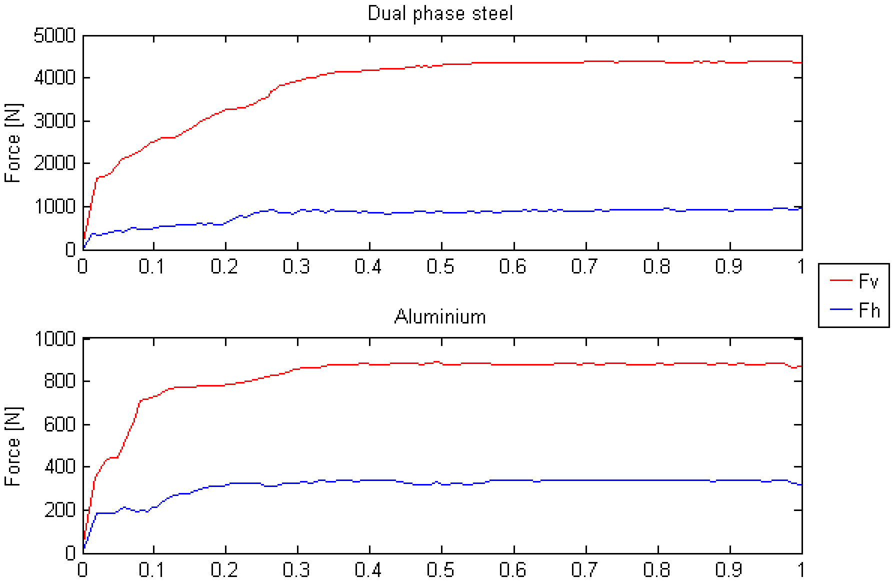

Figure 7.12: Measured forces for truncated cones using different materials.

Observing the tensile test strain-stress curves for both materials, on Figure 7.13, to obtain the same geometry, with the same blank thickness, the necessary load for forming DPS780 parts is expected to be ten times greater for when working with AA1050, this was not verified as the measured load as only about five times greater. This is probably due to the unique forming mechanism for SPIF, which was described in Section 2.2.2, the scientific community hasn't reached consensus upon and needs to be further studied.

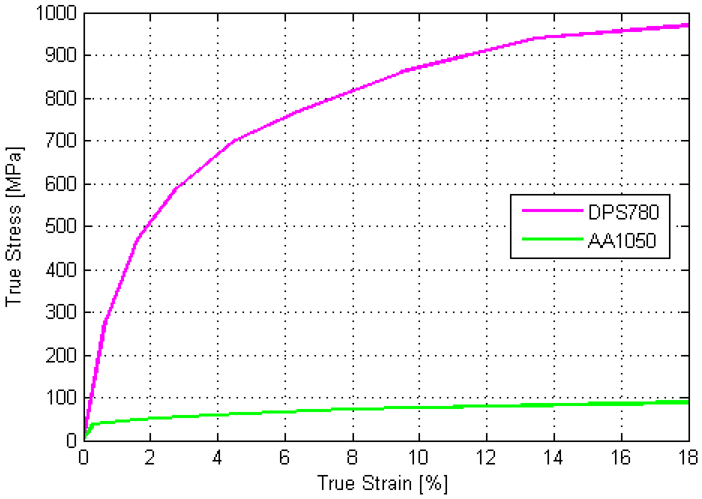

Figure 7.13: Uniaxial tensile strain-stress curves for DPS780 [88] and AA1050 [89].

7.2 Complex geometries

Production of parts with complex is also possible, although not the key objective at this stage of development, since the various forming parameters referred in Section 2.2.2, need to be further studied in simpler cases. Because of this only a few parts were produced to show the SPIF-A's potential.

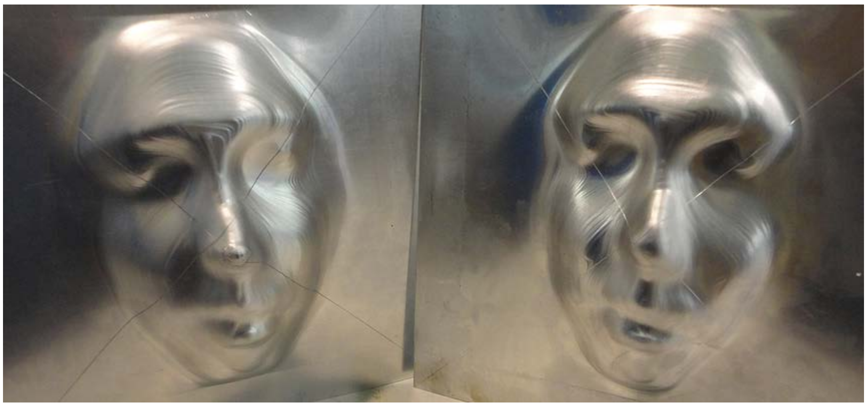

Figure 7.14: Face masks produced using different size tools.

These parts, due to their intricate contours, take longer to produce than they less complex counterparts, for example the face masks required a small vertical step size of one millimetre in order to achieve the intended level of detail. The two parts were produced with different size tools, as seen on Figure 7.14 the part on the left, which was produced with the 5mm rounded tip tool is more detailed namely in the nose than the part on the right made with the rounded 10 mm tool, however when using the smaller tool the grooves on the surface are more pronounced due to its small radius and therefore it is not as smooth as when using the larger tool.

One of the uses for SPIF lies in medical applications, similarly to the work of Duflou [28], seen on Figure 2.10, the SPIF-A is able to produce cranial implants, needing only the CAD file with the patient skull geometry.

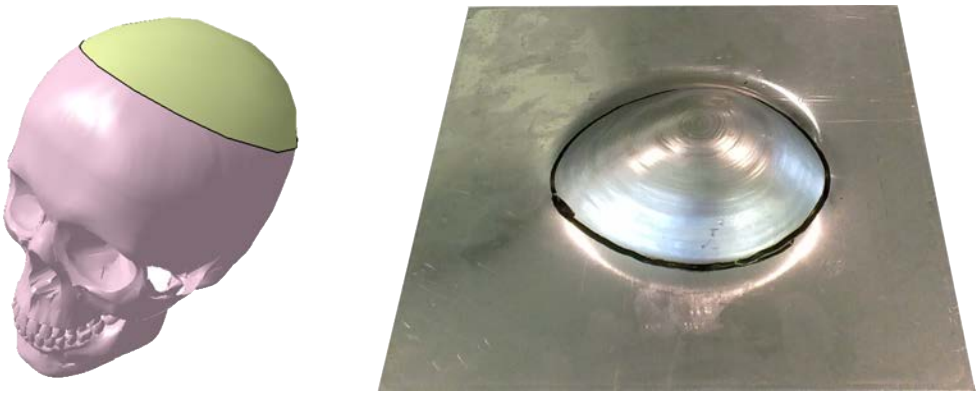

Figure 7.15: Cranial implant produced by the SPIF-A.

Another use for incremental forming is to produce small batches of discontinued parts, for example for the automotive industry, on this scope, the largest part produced to date on the SPIF-A is the bonnet for a Volkswagen Beetle. It was produced using a square meter of 1.5 millimetre thick AA1050 aluminium, and took full advantage of the SPIF-A's large work space.

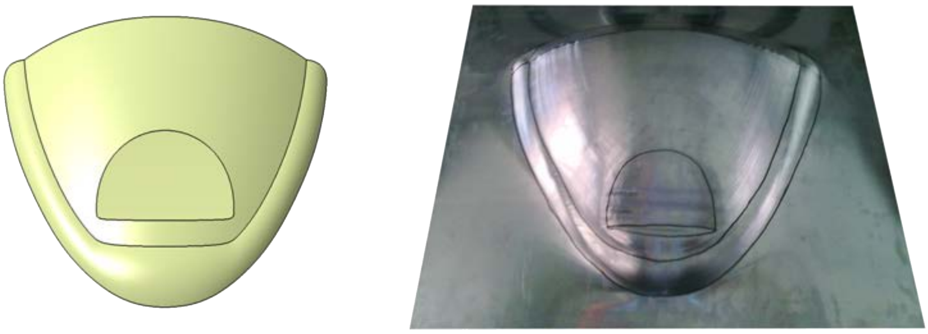

Figure 7.16: Volkswagen beetle bonnet produced by the SPIF-A.

Chapter 8

Conclusions

From what was read in the publications of several authors, single point incremental forming is a recent technology, with a great field of applicability, but still needs to be developed to take advantage of its full potential.

The main goal of this thesis was to get the SPIF-A up and running in order to become a powerful tool for researching this process. This task was achieved thanks to the various systems developed and installed, that enabled motion control and force measuring, allowing to start research on hardened steel and 5-axis forming, to fill a gap in the available in SPIF literature.

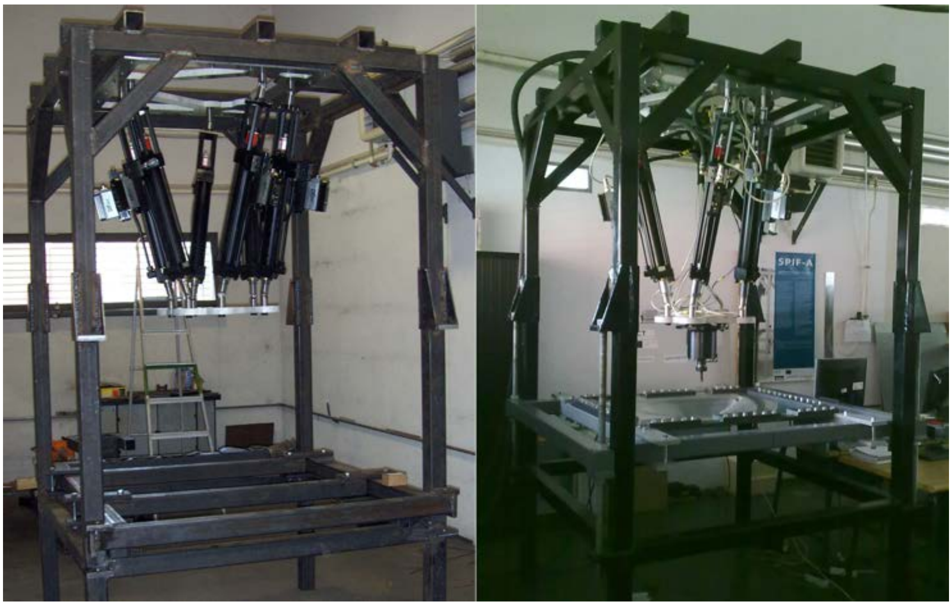

Figure 8.1: Evolution of the SPIF-A during this work.

There were however some setbacks, primarily from the amount of hardware involved so, getting all the systems and mechanisms in working order, meant that there was less time to develop the machine's software, and that will need to be addressed in future work.

Nevertheless the overall results are positive, teamwork played an important part so far and will be a key factor in taking advantage of the full potential the SPIF-A holds.

8.1 Future Work

Regarding the machine's operational system, it can be further improved by converting the embedded MatLab™ functions used, into the dedicated S-functions using C or C++, which run significantly faster. Also it is also necessary to create more functions in order to allow compatibility with other G-code functionality like tool radius compensation, and fixed cycles for common geometries.

Using the differential kinematics defined in Section 4.3.1 and the loads measured on the FMS, it is now possible to use the kinematic jacobian to calculate actuator forces τ [64]:

$$F = \left(J_C^{-1}\right)^T . \tau \Leftrightarrow \tau = \left(J_C\right)^T \cdot F \tag{8.1}$$

This allows to try different control methods like designing a PID for positional control and comparing its performance with the FLC in use, and implementing force control strategies to help correct springback issues.

One of the major drawback of SPIF process is its lengthy forming times, for the SPIF-A the forming speed is currently limited by its hydraulic pump. In order to use high speed forming the first system to be update must be the hydraulic circuit, namely by using a high capacity variable displacement pump, and installing one or more accumulators to ensure the flow necessities at constant high pressure during operations. Using higher speeds means that even thou the stewart platform has low inertia, dynamical forces will no longer be negligible and therefore, studying its dynamical model is a priority. Also, to ensure operational stability, vibration pads need to be dimensioned and, a motor would need to be installed, capable of producing the high rotational tool speed required for high speed forming [90].

One variable that is not yet controlled at this stage, is the forming speed at the tool tip. Even without the modifications for high speed forming, the next controller should pay special attention to it in order to ensure constant forming speeds and smooth speed changes throughout the forming process, and allow studying how different values influence the process.

8.1.1 SPIF process research

This project holds more research opportunities one such example is a doctoral thesis by Sonia Marabuto that will study and attempt to predict and correct springback throughout the forming process, one of the main issues on incrementally formed parts. Success in this task would enable great dimensional/geometrical accuracy, greatly widening the field of applications for SPIF parts, it is currently a topic of interest for several [28; 39] that are studying how the different forming parameters affect it.

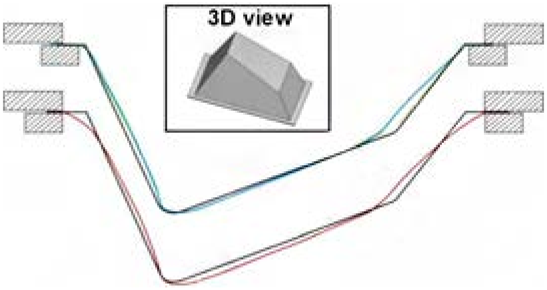

Figure 8.2: Springback on solar ovens formed with/without a backing plate [39].

Another research topic closely related to the aforementioned one, is the pressing direction of the tool during the forming process, most equipments to date, use 3 axis strategies, and so the tool is always perpendicular to the work table. Testing Zhu's hypothesis [86], on the benefits of using 5 axis strategies to ensure a pressing direction perpendicular to the geometry being formed is the Phd work of João Sá Farias [6]. To aid in both this topics, using blanks with an etched grid, to study deformation locally is required. Another dissertation in the near future would do well to focus on studying the influence of the aforementioned parameters like forming speed, toolpath type, tool geometry, among others and organizing the various tests in a database to be used in future research and to support Phd work.

8.1.2 Proposal for another SPIF-A machine

The SPIF-A, being the first dedicated SPIF machine prototype built in Portugal, was developed with industrial applications in mind. Since incremental forming is only used for small or unitary production batches, it means that the return on the investment for such an equipment is much slower than machines with higher production rates, and therefore it needs to affordable while still keeping up with process requirements.

What was learned during this dissertation and its preceding work [3; 5], is that adapting/combining existing solutions can, in most cases, meet the necessary requirements of a particular problem without the need for developing a proprietary system which is more time consuming and sometimes ends up being either more expensive or less robust than the already tried and tested commercial solutions.

The Key system in the SPIF-A is its stewart platform, which was wholly developed in house, mainly because the lack of known existing systems capable of meeting the required workload specifications (Table 2.1), during the course of this work a possible solution was found in the form of Stewart platforms manufactured by Bosch Rexroth for heavy duty flight simulators [91]. There are two particularly relevant solutions, the hydraulic powered Micro Motion System® which is capable of a 6 kN workload whose range would allow it to use 300×300mm blanks, adding this to its compact size it would be ideal for a smaller version of the SPIF-A. The second platform is the electrical powered E-Motion-1500®, it is about the same size as the one developed for the SPIF-A and with its work load of 15 kN it could be used in a similar version, but without needing and hydraulic circuit. Both solutions come with its power supply and control unit discarding the need to develop the platforms kinematic formulation and controller, therefore in terms of software, the only lacking component would be a G-Code reader.

To date the Amino Corporation® [42] is the only supplier of dedicated incremental forming machinery, one interesting feature of their models is the ability to produce both concave and convex parts. This is achieved not by SPIF but by TPIF, and its due to the forming table being capable of ascending and descending movement and having a partial or full die underneath, which is the secondary forming point. To allow more versatility in part production the new version of the SPIF-A should be outfitted with a movable forming table, either with hydraulic or electrical actuators, although this would require a careful control strategy to cope with the combination of table and platform movements.

8.1.3 Stir friction welding

An alternate use for the SPIF-A would be to use it to research stir friction welding [92], a novel solid-process for joining parts of same or different materials. It consists of pressing two parts at the seem and using a rotating refractory tool designated as probe, to drill into and move across the seem, this softens the material to the point it's malleable enough to be mechanically mixed, and since the melting point isn't reached material properties are not significantly affected.

A viability study for implementing this on the SPIF-A, would be require to check if the structural components are capable to withstand the work loads, and some components would require an upgrade, specially the spindle which would require a motor capable of supplying the required speed.

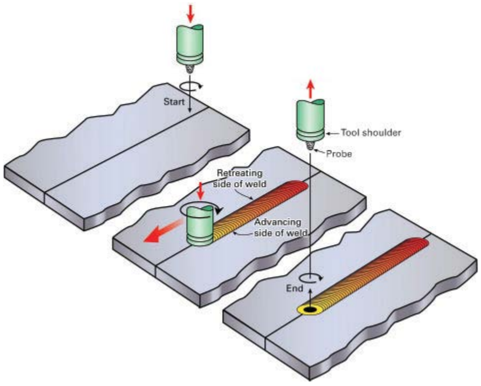

Figure 8.3: Stir friction welding process [92].

8.2 Earned Skills

On a personal level, working on the SPIF-A proved extremely beneficial.

While it allows development of the research skills needed to solve complex problems of machine theory, actually building and troubleshooting its prototype serves as excellent motivator. Even thou developing hardware and working with physical systems adds its own set of problems it also provides with the needed dexterity to solve issues that come quite close to those found in the industrial world.

Team work crucial during the course of this work, the ability to solve problems in unison and debating solutions as a group not only enabled mutual learning but also proved that the collective insight allowed to spot tiny reasoning flaws that were holding back solutions for certain problems.

Hard skills earned on earlier semesters played a important part during this work and were honed in the process, such examples include the use of hardware like Universal testing machines, lathes, milling and welding machines, as well as other tools. In terms of software, aptitude for problem solving using MatLab$^{\text{TM}}$, Simulink$^{\text{TM}}$ and Maple$^{\text{TM}}$ improved, as did for using Eplan$^{\text{TM}}$ for electrical plans, CATIA V5® and Solidworks$^{\text{TM}}$ for CAD and drafting. Writing this document allowed to widen the knowledge of the English language, in particular technical vocabulary, an invaluable tool in the modern engineering world, and to learn how to elaborate documents using LaTex.

In terms of technical knowledge, it provided an invaluable understanding on hydraulic, electrical and instrumentation systems, as well on machine kinematics and component development.

To conclude it was an exciting challenge that comprised various fields of engineering, both theoretical and experimental, essential to prepare an engineer for the real world, that yielded very positive results, both for the SPIF-A project and for personal development.

Bibliography

[1] Leszak E., "Apparatus and Process for Incremental Dieless Forming", E. Patent US3342051A1, 1967.

[2] Marabuto S. R., Afonso D., Ferreira J. A. F., Melo F. Q. M., Martins M. A. B. E., Sousa R. J. A., "Finding the best machine for SPIF operations", Key Engineering Materials, Volume 473, pp. 861-868, 2011.

[3] Marabuto S. R., "Desenvolvimento de uma máquina para operações de estampagem incremental", Master Thesis - Universidade de Aveiro, 2010.

[4] Sena J. I. V., "Estampagem Incremental: Um Novo Conceito de Produção", Master Thesis - Universidade de Aveiro 2010.

[5] Martins M. A. B. E., "Projecto e Construção de uma Máquina para Estampagem Incremental", Master Thesis - Universidade de Aveiro, 2011.

[6] Farias J., Martins M. A. B. E., Afonso D., Marabuto S. R., Torrão J., Ferreira J. A. F., Sousa R. J. A., "CAD/CAM strategies for a parallel kinematics SPIF machine", in Proceedings Esaform Conference 2013, Aveiro, Portugal

[7] Semiatin S. L., "Introduction to Bulk-Forming Processes", ASM Handbook, Volume 14A, Metalworking: Bulk Forming, ASM International, 2005

[8] Wagoner, R., "Fundamental aspects of springback in sheet metal forming" in Proceedings Numisheet 2002, edited by D. Yang et.al., pp 13-19, 2002

[9] http://www.custompartnet.com/wu/sheet-metal-forming, last visited on the 8th of April 2013

[10] Semiatin S. L., "Bending and Forming of Tubing", ASM Handbook, Volume 14B, Metalworking: Sheet Forming, ASM International,pp 457-478, 2005

[11] Kalpakjian S; Schmid S; "Manufacturing Processes for Engineering Materials", 5th edition, Pearson Education, 2008

[12] Koc M, Altan T, "An overall review of the tube hydroforming (THF) technology", Journal of Materials Processing Technology, Volume 108, Issue 3, pp 384-393, 2001

[13] Semiatin S. L., "Forming of Steel Strip in Multiple-Slide Machines", ASM Handbook, Volume 14B, Metalworking: Sheet Forming, ASM International, pp 250-263, 2005

[14] Semiatin S. L., "Deep Drawing" , ASM Handbook, Volume 14B, Metalworking: Sheet Forming, ASM International, pp 263-299, 2005

[15] Jiang X., Tian M., Zhang J., "The Application of the Polyurethane Rubber in the Field of Stamping Technology", Defense Industry Academic Press, Beijing 1989

[16] Lang L. H.; Wang Z. R.; Kang D.C.; Yuan S. J.; Zhang S. H.; Danckent J.; Nielseni K. B.,"Hydroforming highlights: sheet hydroforming", Journal of Materials, Volume 151, pp 165-177, 2004

[17] Lorenz R, "Apparatus and method for superplastic forming", US Patent 4,951,491, 1990

[18] Semiatin S. L., "Electromagnetic Forming" , ASM Handbook, Volume 14B, Metalworking: Sheet Forming, ASM International, pp 420-439, 2005

[19] Semiatin S. L., "Explosive Forming" , ASM Handbook, Volume 14B, Metalworking: Sheet Forming, ASM International, pp 401-420, 2005

[20] Semiatin S. L., "Spinning" , ASM Handbook, Volume 14B, Metalworking: Sheet Forming, ASM International, pp 317-331, 2005

[21] Li M, Cai Z, Sui Z, Yan Q," Multi-point forming technology for sheet metal", Journal of Materials Processing Technology,Volume 129, Issue 1-3, pp 333-338, 2002

[22] Schafer T., S.R.D., "Incremental sheet metal forming by industrial robots using a hammering tool," Assises Europeennes se Prototypage Rapide, Paris, France, 2004

[23] Santos E.,Shiomi M.,Osakada K.,Laoui T., "Rapid manufacturing of metal components by laser forming", International Journal of Machine Tools and Manufacture ,Volume 46, pp 1459-1468, 2006

[24] Iseki H., "Flexible and Incremental Bulging of Sheet Metal Using High-Speed Water Jet", JSME International Journal, 2001

[25] Jeswiet J,, Micari F., Hirt G., Bramley A., Duflou J., Allwood J., "AsymmetricSingle Point Incremental Forming of Sheet Metal, CIRP Manufacturing Technology", Volume 54, pp 88-114,2005

[26] Meier H., Buff B., Laurischkat R., Smukala V., "Increasing the part accuracy in dieless robot-based incremental sheet metal forming", CIRP Manufacturing Tecnology, Volume 58, pp 233-238, 2008

[27] Allwood J. M., King G., Duflou J. R., "Structured Search for Applications of the Incremental Sheet Forming Process by Product Segmentation", IMECH E, Proceedings Part B, Journal of Engineering and Manufacture, Volume 219, pp 239-244, 2004

[28] Duflou, J.R., Lauwers, B., Verbert, J.,"Medical application of single point incremental forming: cranial plate manufacturing", Proceedings of the 2005VRAP Conference, Leiria, pp 161-164, 2005

[29] Rauch M., Hascoet J. Y., Hamann J. C., Plennel Y., "Tool path programming optimization for incremental sheet forming applications", Computer-Aided Design, Volume 41, pp 877-885, 2009

[30] Jackson K.P., Allwood J.M., Landert M., "Incremental forming of sandwich panels", Journal of Materials Processing Technology, Volume 204, pp 290-303, 2008

[31] Durante M., Formisano A., Langella A., Minutolo F., "The influence of tool rotation on an incremental forming process", Journal of Materials Processing Technology, Volume 209, pp 4621-4626, 2009

[32] Bouffioux C., Eyckens P., Henrard C., Aerens R., Van Bael A., Sol H., Duflou J. R., Habraken A. M., "Identification of material parameters to predict Single Point Incremental Forming forces", Proceedings of IDDRG Conference, Gyor, 2007.

[33] Decultot N., Velay V., Robert L., Bernhart G., Massoni E., "Behaviour modeling of aluminium alloy sheet for Single Point Incremental Forming", International Journal of Material Forming, Volume 1 - Supplement, pp 1151-1154, 2008

[34] Silva M., Skjoedt M., Martins P., Bay N., "Revisiting the fundamentals of single point incremental forming by means of membrane analysis", International Journal of Machine Tools and Manufacture, Volume 48, pp 73-83, 2008

[35] Jeswiet J., Young D., "Forming limit diagrams for single point incremental forming of aluminum sheet", Journal of Engineering Manufacture, Volume 219, pp. 359-364, 2005

[36] Hirt G., Witulski N., "Incemental Sheet Forming: Quality Evaluation and Process Simulation". in Proceeding of 7th ICTP- International Conference on Technology of Plasticity, Yokohama, Japan, 2002

[37] Hussain G., G.L., "A novel method to test the thinning limits of sheet metals in negative incremental forming", International Journal of Machine Tools and Manufacture, Volume 47, pp 419-435, 2007

[38] Ham M., Jeswiet J., "Single Point Incremental Forming and the Forming Criteria for AA3003", Annals of the CIRP,Volume 55, pp 241-244 ,2006

[39] Allwood J. M., Houghton N. E., Jackson K. P., "The design of an Incremental Forming machine", 11th Conference on Sheet Metal, Erlangen, pp 471-478, 2005

[40] Suriyaprakan P., "Single Point Incremental Forming and Multi-Stage Incremental Forming on Aluminium Alloy 1050", Master Thesis - Faculdade de Engeharia da Universidade do Porto 2013.

[41] Meier H., Laurischkat R., Zhu J., "A model based approach to increase the part accuracy in robot based incremental sheet metal forming", AIP conference proceedings, Volume 1315, pp 1407-1412, 2011

[42] Amino H., Lu Y., Maki T., Osawa S., Fukuda K., "Dieless NC Forming, Prototype of Automotive Service Parts", Proceedings of the 2nd International Conference on Rapid Prototyping and Manufacturing (ICRPM), Beijing 2002.

[43] Sieczkarek P., Kwiatkowski L., Khalifa N., Tekkaya1 A, "Novel five-axis forming press for the incremental sheet-bulk metal forming", in Proceedings Esaform Conference 2013, Aveiro, Portugal

[44] Callegari M., Amodio D., Ceretti E., Giardini C., "Sheet incremental forming: advantages of robotised cells vs. CNC machines", Industrial Robotics: Programming, Simulation and Applications, Low Kin Huat Edition , ARS Publications, pp. 493-514, 2007

[45] www.giuntirotar.it/, last access at the 13th of January 2013

[46] www.parker.com/, last access at the 8th of March 2013

[47] Duflou J. R., Szekeres A., VanHerck A., "Force Measurements for Single Point Incremental Forming and experimental study", Journal of Materials Research, Volumes 6, pp 441-448, 2006

[48] Eyckens P., Moreau J. D., Duflou J. R., Van Bael A., Van Houtte P., "MK modelling of sheet formability in the incremental sheet forming process, taking into account through-thickness shear", International Journal of Material Forming , Volume 2, pp 379-382, 2009

[49] Soares P. "Aços - Carateristicas e Tratamentos", LivroLuz, 5th edition, 1992

[50] Obikawa T., Satou S., Hakutani T., "Dieless incremental micro-forming of miniature shell objects of aluminum foils", International Journal of Machine Tools and Manufacture, Volume 49, pp 906-915, 2009

[51] Ambrogio G., De Napoli L., Filice L., Gagliardi F., Muzzupappa M., "Application of Incremental Forming process for high customized medical product manufacturing", Journal of Materials Processing Technology, Volume 162, pp 156-162, 2005

[52] Dejardin S., Thibaud S., Gelin J.C., Michel G., "Experimental investigations and numerical analysis for improving knowledge of Incremental Sheet Forming process for sheet metal parts", Journal of Materials Processing Technology, Volume 210, Pages 363-369, 2010

[53] Bosh - Rexroth oil/air cooler Types KOL and KOLP catalogue RE 50111/12.06, 2012

[54] Cauchy A. L., "Deuxiéme Mémoire sur les polygones et les polyédres", Journal de l'Ecole Impériale Polytechnique, XVI Cahier, pp 87-99, 1813

[55] Gough, V. E., "Contribution to discussion of papers on research in Automobile Stability, Control and Tyre performance", Proc. Auto Div. Inst. Mech. Eng., 1956-1957

[56] Stewart, D. (1965-1966), "A Platform with Six Degrees of Freedom". Proc. Institution of Mechanical Engineers, Volume 180, 1965-1966

[57] Rehsteinera F., Neugebauerb R., Spiewakc S., Wielandb F.,"Putting Parallel Kinematics Machines (PKM) to Productive Work",CIRP Annals - Manufacturing Technology, Volume 48, Issue 1, pp 345-350, 1999

[58] Merlet, J.P. "Parallel Robots - Second Edition", Springer, 2006

[59] www.hexapods.net/, last access at the 27th February 2013

[60] Taylor J.C., "Six-axis deformity analysis and correction", Principles of Deformity Correction, Springer, Berlin Heidelberg New York, pp 411-436, 2002

[61] Su Y. X., Duan B. Y., "The mechanical design and kinematics accuracy analysis of a fine tuning stable platform for the large spherical radio telescope", Mechatronics, Volume 10, pp 819-834, 2000

[62] NASA Docking System (NDS) Technical Integration Meeting , 17 October 2010

[63] Gao X. S., Lei D., Liao Q., Zhang G. F.,"Generalized Stewart?Gough Platforms and Their Direct Kinematics", IEEE Transactions on Robotics, Volume 21, pp 141-151, 2005

[64] Santos V., "Robótica Industrial - Apontamentos teóricos", Departamento de Engenharia Mecânica, Universidade de Aveiro, 2003

[65] Schwab A. L., Meijaard J. P.,"How to draw Euler angles and utilize Euler parameters",ASME International Design Engineering Technical Conferences and Computers and Information in Engineering Conference, Philadelphia, Pennsylvania, USA, 10-13 September, 2006

[66] Dasgupta B, Mruthyunjaya T.S., "A Canonical Formulation of a Direct Position Kinematics Problem for a General 6-6 Stewart Platform", Mechanism and Machine Theory 31, Volume 6, pp 819-826, 1994

[67] Lee T. Y., Shim J. K.,"Algebraic Elimination-Based Real-Time Forward Kinematics of the 6-6 Stewart Platform with Planar Base and Platform", IEE International Conference on Robotics and Automation", Seoul, Korea, 21-26 May, 2001

[68] Huang X., Liao Q, Wei S, "Closed-form forward kinematics for a symmetrical 6-6 Stewart platform using algebraic elimination", Mechanism and Machine Theory, Volume 45 ,pp 327-334, 2010

[69] Wang S., Wan Y."A Mixed Real-time Algorithm for the Forward Kinematics of Stewart Parallel Manipulator",Journal of Electronic Science and Technology of China, Volume 4, pp 173-180, 2006

[70] Bonev I. A., Jeha Ryu J., "A new method for solving the direct kinematics of general 6-6 Stewart Platforms using three linear extra sensors", Mechanism and Machine Theory, Volume 35, pp 423-436, 2000

[71] Song S.K., Kwon D.S., "New Closed-Form Direct Kinematic Solution of the 3-6 Stewart-Gough Platform Using the Tetrahedron Approach", Proceedings of the International Conference on Control, Automation and Systems, October 17-21, Cheju National Univ. Jeju, Korea, pp 484-487, 2001

[72] Cruz P., Ferreira R., "Kinematic Modelling of Stewart-Gough Platforms" , ICINCO 2005 - Robotics and Automation, 2nd international conference on informatics in control, Automation and robotics , 14-17 of September, pp 93-99, 2005

[73] Lopes A. M. F. M. "Um dispositivo robótico para controlo de força-impedância de manipuladores industriais", Doctoral Thesis, FEUP, Universidade do Porto, 1999

[74] Yang J., Geng Z. J., "Closed Form Forward Kinematics Solution to a Class of Hexapod Robots", IEEE Transactions on Robotics and Automation, Volume 14, pp 503-508, 1998

[75] Ji P., Wu H., "A Closed-Form Forward Kinematics Solution for the 6-6p Stewart Platform", IEEE Transactions on Robotics and Automation, Volume 17, pp 522-526, 2001

[76] Bruyninckx H.,Schutter J., "Comments on: Closed Form Forward Kinematics Solution to a Class of Hexapod Robots", IEEE Transactions on Robotics and Automation, Volume 15, pp 788-789, 1999

[77] Melo A. P., "Teoria dos Sistemas de Controlo Linear", Departamento de Electrónica Telecomunicações e Informatica, Universidade de Aveiro, 2010

[78] Zadeh L.A., "Fuzzy sets", Journal of Information and Control, Volume 8, pp 338-353, 1965

[79] Sulc B., Jan J. A., "Non Linear Modelling and Control of Hydraulic Actuators", Acta Polytechnica, Volume 42, pp 41-47, 2002

[80] Aly A. A., El-Lail A. S. A., Shoush K. A., Salem F. A., "Intelligent PI Fuzzy Control of An Electro-Hydraulic Manipulator", I.J. Intelligent Systems and Applications, Volume 7, pp 43-49, 2012

[81] Zhu D., Mei T., Sun L., "Fuzzy Support Vector Machines Control for 6-DOF Parallel Robot", Journal of Computer, volume 6, pp 1926-1934, 2011

[82] Omurlu V. E., Yildiz I., "Self-tuning fuzzy PD-based stiffness controller of a 3x3 Stewart platform as a man-machine interface", Journal of Electrical Engineering and Computer Science, Volume 19, pp 743-752, 2011

[83] Zaitsev D.A., Sarbei V.G., Sleptsov A.I., "Synthesis of continuous-valued logic functions defined in tabular form", Cybernetics and Systems Analysis, Volume 34, pp 190-195, 1998

[84] http://www.speedgoat.ch/, last access at the 29th of April 2013

[85] SN1584 User's Manual, Speedgoat GmbH

[86] Zhu H., Li N., Liu Z.J., "The effect of pressing direction on the 5-axis CNC incremental forming quality", International Journal of Material Forming, Volume 5, pp 227-233, 2012

[87] Marabuto S.R., Sena J.I.V., Afonso D., Martins M.A.B.E., Coelho R.M., Ferreira J.A.F., Valente R.A.F, Alves de Sousa R.J., "Estudo numérico e experimental de processos de estampagem incremental", Congress on Numerical Methods in Engineering - CMNE, 14-17 June, Coimbra, Portugal, 2011.

[88] Ha J, Lee M. G., Barlat F.,"Strain hardening response and modeling of EDDQ and DP780 steel sheet under non-linear strain path", Mechanics of Materials, Volume 64, pp 11-26, 2013

[89] Yoon J.W., Barlat F., Gracio J. J., Rauch E.,"Anisotropic strain hardening behavior in simple shear for cube textured aluminum alloy sheets", International Journal of Plasticity, Volume 21, pp 2426-2447, 2005

[90] Ambrogioa G., Gagliardia F., Bruschib S., Filicea L., "On the high-speed Single Point Incremental Forming of titanium alloys", CIRP Annals - Manufacturing Technology, Volume 62, pp 243-246, 2013

[91] http://www.boschrexroth.de/, last access at 17th of June 2013

[92] Threadgill P.L., Leonard A.J., Shercliff H.R., Withers P.J., "Friction stir welding of aluminium alloys", International Materials Reviews, Volume 54, pp 49-93, 2009

Appendix A

FMS calibration data

Load cell - TR3D-A-5K-605

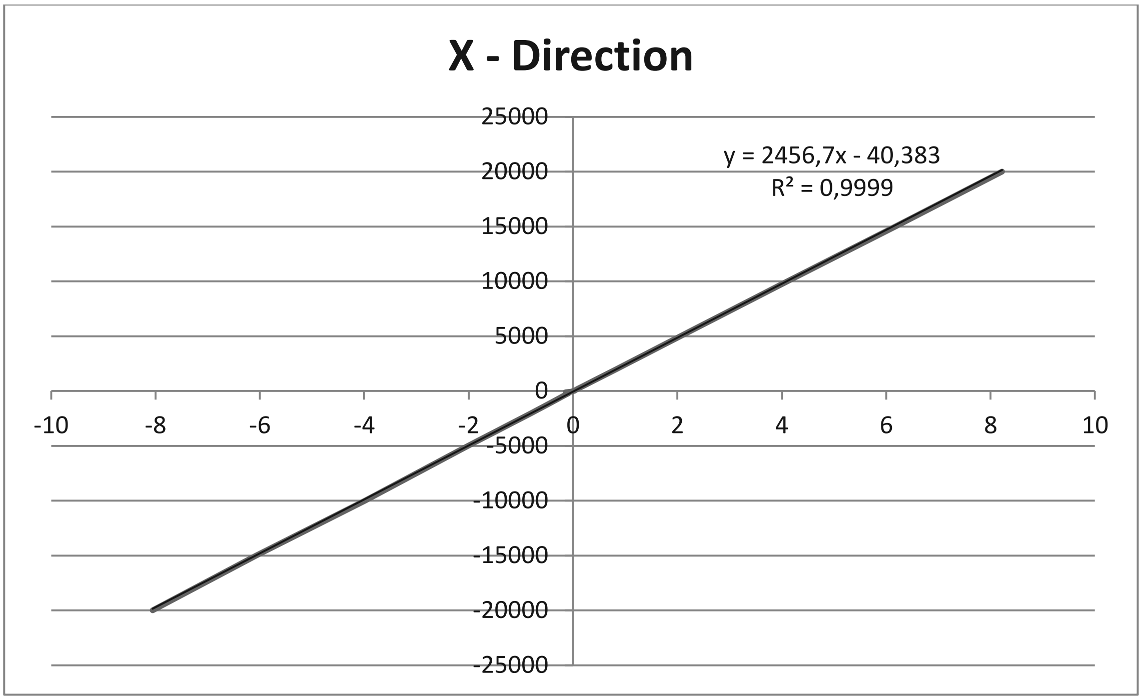

	Positive				Negative			
Load (N)	1'	2'	3'	Mean	1'	2'	3'	Mean
0	0,0003	0,0002	0,0002	0,0002	0,0001	0,0002	0,0001	0,0001
20	0,0187	0,0191	0,0189	0,0189	-0,0121	-0,0129	-0,0132	-0,0127
50	0,0277	0,0282	0,0279	0,0279	-0,0254	-0,0261	-0,0258	-0,0258
100	0,0471	0,0473	0,0472	0,0472	-0,0348	-0,0353	-0,3510	-0,1404
200	0,0894	0,0882	0,0888	0,0888	-0,0831	-0,0849	-0,0838	-0,0839
500	0,2150	0,2120	0,2150	0,2140	-0,1997	-0,2001	-0,1999	-0,1999
1.000	0,4150	0,4170	0,4160	0,4160	-0,3990	-0,4070	-0,4050	-0,4037
2.000	0,8320	0,8240	0,8290	0,8283	-0,7890	-0,8020	-0,8010	-0,7973
5.000	2,0600	2,0500	2,0500	2,0533	-2,0100	-2,0200	-2,0200	-2,0167
10.000	4,1100	4,1000	4,1100	4,1067	-3,9800	-3,9900	-3,9900	-3,9867
15.000	6,1900	6,1500	6,1700	6,1700	-6,0800	-6,0700	-6,0700	-6,0733
20.000	8,2300	8,2100	8,2200	8,2200	-8,0500	-8,0600	-8,0600	-8,0567

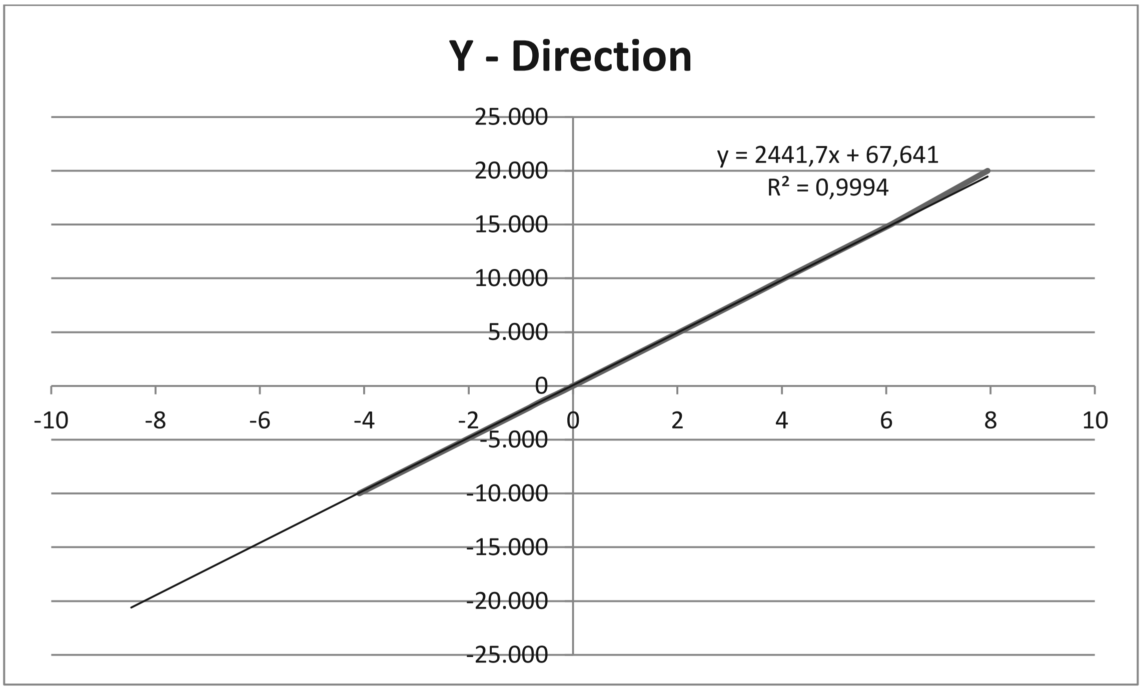

	Positive				Negative			
Load (N)	1'	2'	3'	Mean	1'	2'	3'	Mean
0	-0,0001	-0,0001	-0,0002	-0,0001	-0,0001	-0,0002	-0,0001	-0,0001
20	0,0195	0,0194	0,0191	0,0193	-0,0122	-0,0137	-0,0125	-0,0128
50	0,0274	0,0272	0,0269	0,0272	-0,0247	-0,0296	-0,0259	-0,0267
100	0,0466	0,0464	0,0461	0,0464	-0,0438	-0,0498	-0,0440	-0,0459
200	0,0895	0,0892	0,0887	0,0891	-0,0871	-0,0927	-0,0877	-0,0892
500	0,2090	0,2110	0,2080	0,2093	-0,2070	-0,2190	-0,2090	-0,2117
1.000	0,4130	0,4160	0,4140	0,4143	-0,4111	-0,4230	-0,4180	-0,4174
2.000	0,8150	0,8140	0,8140	0,8143	-0,8160	-0,8370	-0,8250	-0,8260
5.000	2,0400	2,0400	2,0300	2,0367	-2,0520	-2,0600	-2,0500	-2,0540
10.000	4,0700	4,0600	4,0400	4,0567	-4,1000	-4,0900	-4,0900	-4,0933
15.000	6,1000	6,0900	6,0800	6,0900	-6,2700	-6,2700	-6,2700	-6,2700
20.000	7,9600	7,9400	7,9300	7,9433	-8,2700	-8,2700	-8,2700	-8,2700

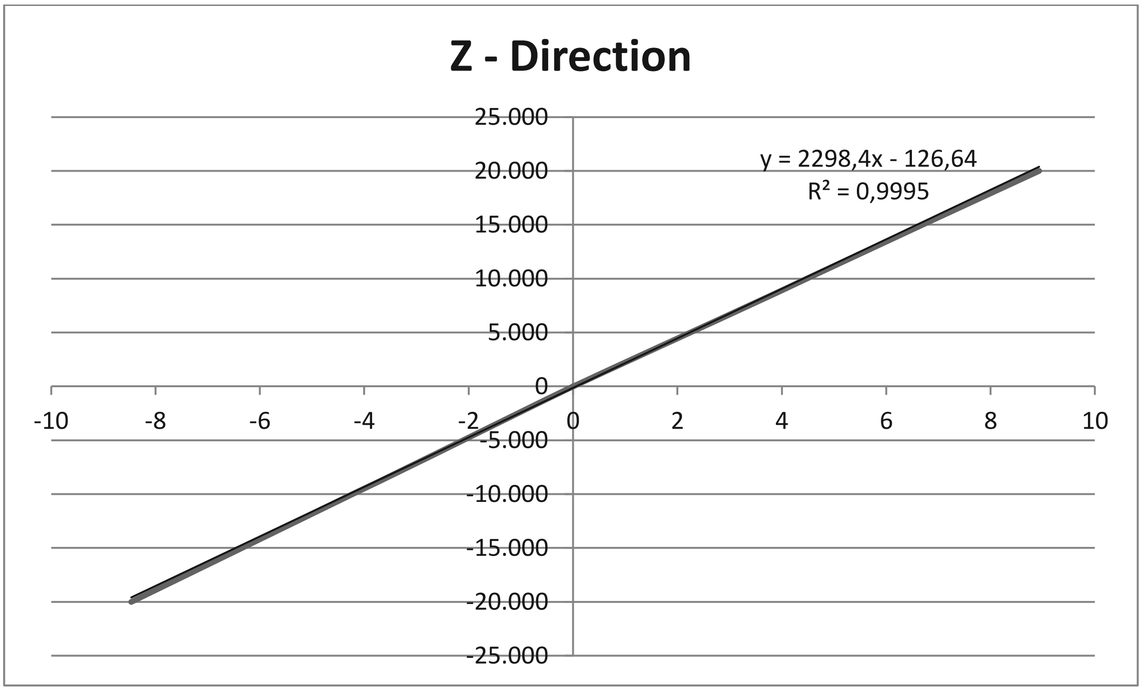

	Positive				Negative			
Load (N)	1'	2'	3'	Mean	1'	2'	3'	Mean
0	0,0000	0,0001	0,0001	0,0001	0,0001	0,0002	0,0001	0,0001
20	0,0103	0,0121	0,0114	0,0113	-0,0087	-0,0096	-0,0086	-0,0090
50	0,0212	0,0255	0,0223	0,0230	-0,0200	-0,0208	-0,0201	-0,0203
100	0,0552	0,0548	0,0549	0,0550	-0,0418	-0,0444	-0,0439	-0,0434
200	0,0981	0,0947	0,0976	0,0968	-0,0826	-0,0839	-0,0825	-0,0830
500	0,2210	0,2240	0,2182	0,2211	-0,2090	-0,2150	-0,2120	-0,2120
1.000	0,4440	0,4520	0,4470	0,4477	-0,4240	-0,4290	-0,4290	-0,4273
2.000	0,8940	0,8980	0,8920	0,8947	-0,8460	-0,8450	-0,8460	-0,8457
5.000	2,2500	2,2500	2,2400	2,2467	-2,1100	-2,1100	-2,1100	-2,1100
10.000	4,4800	4,4800	4,4700	4,4767	-4,2300	-4,2200	-4,2300	-4,2267
15.000	6,7000	6,7000	6,7000	6,7000	-6,3400	-6,3400	-6,3400	-6,3400
20.000	8,9300	8,9300	8,9300	8,9300	-8,4700	-8,4600	-8,4600	-8,4633

Load cell - TR3D-A-5K-683

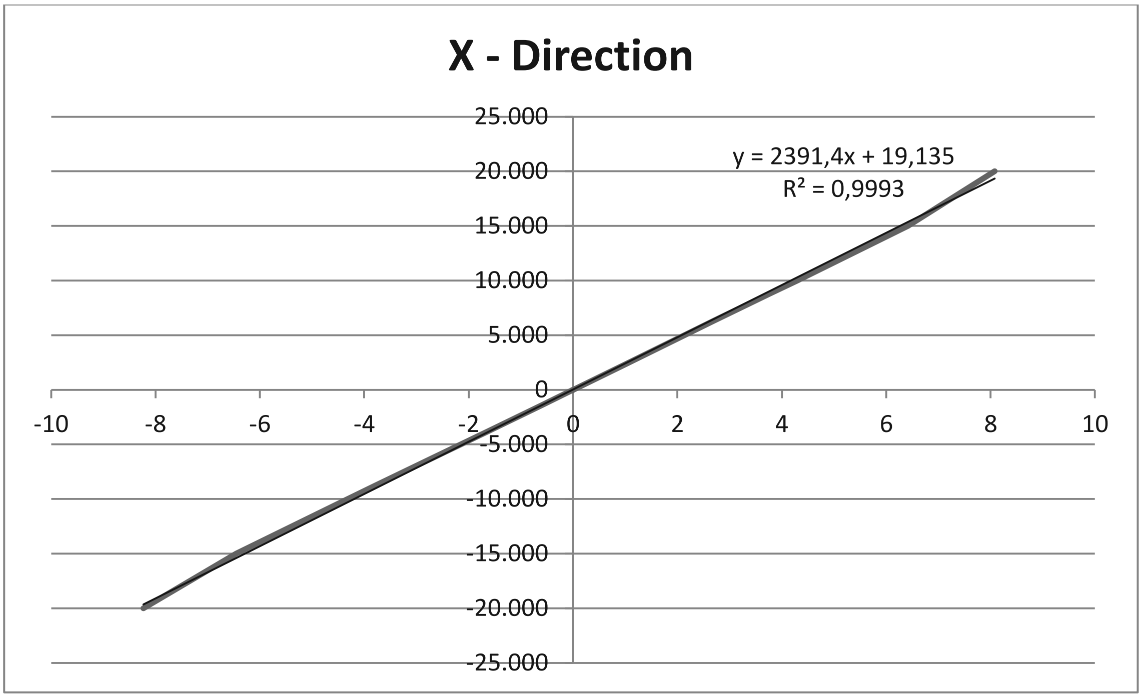

	Positive				Negative			
Load (N)	1'	2'	3'	Mean	1'	2'	3'	Mean
0	0,0003	0,0001	0,0002	0,0002	0,0002	0,0003	0,0002	0,0002
20	0,0112	0,0108	0,0113	0,0111	-0,0110	-0,0109	-0,0117	-0,0112
50	0,0223	0,0218	0,0221	0,0221	-0,0229	-0,0222	0,0237	-0,0071
100	0,0448	0,0428	0,0423	0,0433	-0,0421	-0,0427	-0,0433	-0,0427
200	0,0837	0,0863	0,0835	0,0845	-0,0845	-0,0834	-0,0856	-0,0845
500	0,2160	0,2140	0,2130	0,2143	-0,2150	-0,2160	-0,2140	-0,2150
1.000	0,4320	0,4330	0,4330	0,4327	-0,4230	-0,4250	-0,4240	-0,4240
2.000	0,8600	0,8630	0,8590	0,8607	-0,8610	-0,8580	-0,8610	-0,8600
5.000	2,1300	2,1300	2,1400	2,1333	-2,1400	-2,1500	-2,1400	-2,1433
10.000	4,2900	4,3000	4,3000	4,2967	-4,3100	-4,3100	-4,3200	-4,3133
15.000	6,4100	6,4200	6,4200	6,4167	-6,4500	-6,4500	-6,4600	-6,4533
20.000	8,0700	8,0800	8,0800	8,0767	-8,2300	-8,2300	-8,2300	-8,2300

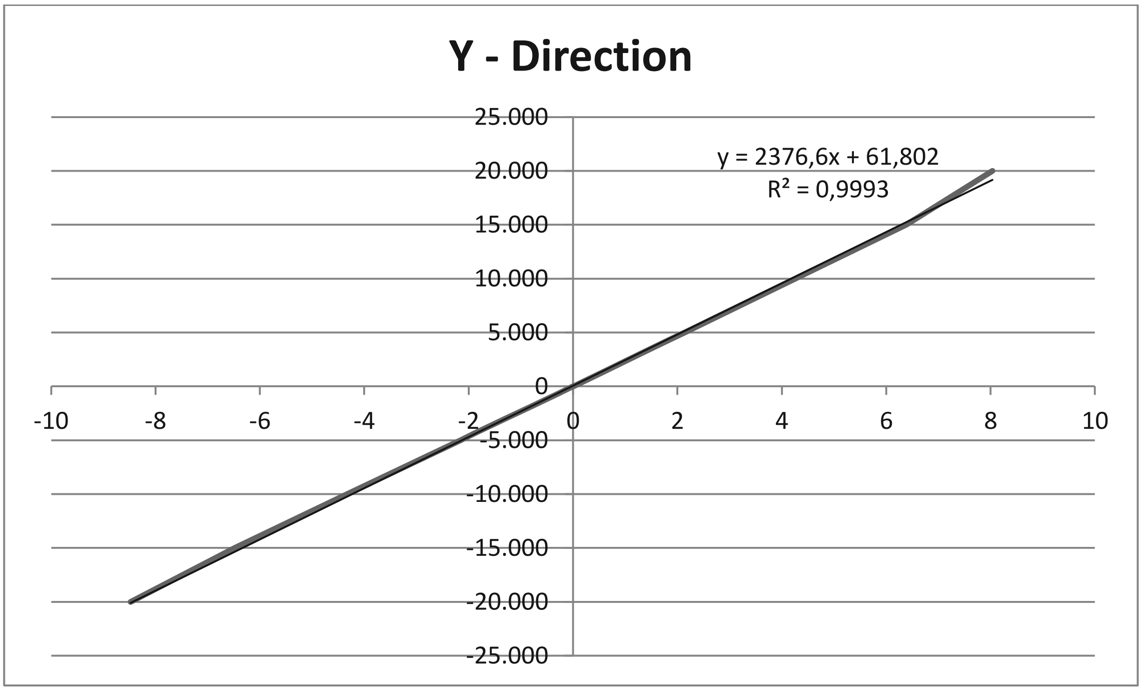

	Positive				Negative			
Load (N)	1'	2'	3'	Mean	1'	2'	3'	Mean
0	0,0002	0,0002	0,0001	0,0002	0,0002	0,0001	0,0003	0,0002
20	0,0106	0,0111	0,0113	0,0110	-0,0112	-0,0119	-0,0128	-0,0120
50	0,0206	0,0215	0,0216	0,0212	-0,0223	-0,0228	-0,0242	-0,0231
100	0,0425	0,0434	0,0437	0,0432	-0,0421	-0,0423	-0,0429	-0,0424
200	0,0833	0,0843	0,0847	0,0841	-0,0859	-0,0861	-0,0865	-0,0862
500	0,2170	0,2180	0,2190	0,2180	-0,2140	-0,2160	-0,2190	-0,2163
1.000	0,4310	0,4310	0,4320	0,4313	-0,4230	-0,4250	-0,4270	-0,4250
2.000	0,8610	0,8580	0,8620	0,8603	-0,8590	-0,8630	-0,8640	-0,8620
5.000	2,1400	2,1300	2,1400	2,1367	-2,1500	-2,1600	-2,1600	-2,1567
10.000	4,2600	4,2500	4,2600	4,2567	-4,3300	-4,3300	-4,3300	-4,3300
15.000	6,3900	6,3800	6,3900	6,3867	-6,4800	-6,4800	-6,4800	-6,4800
20.000	8,0400	8,0300	8,0400	8,0367	-8,4800	-8,4700	-8,4800	-8,4767

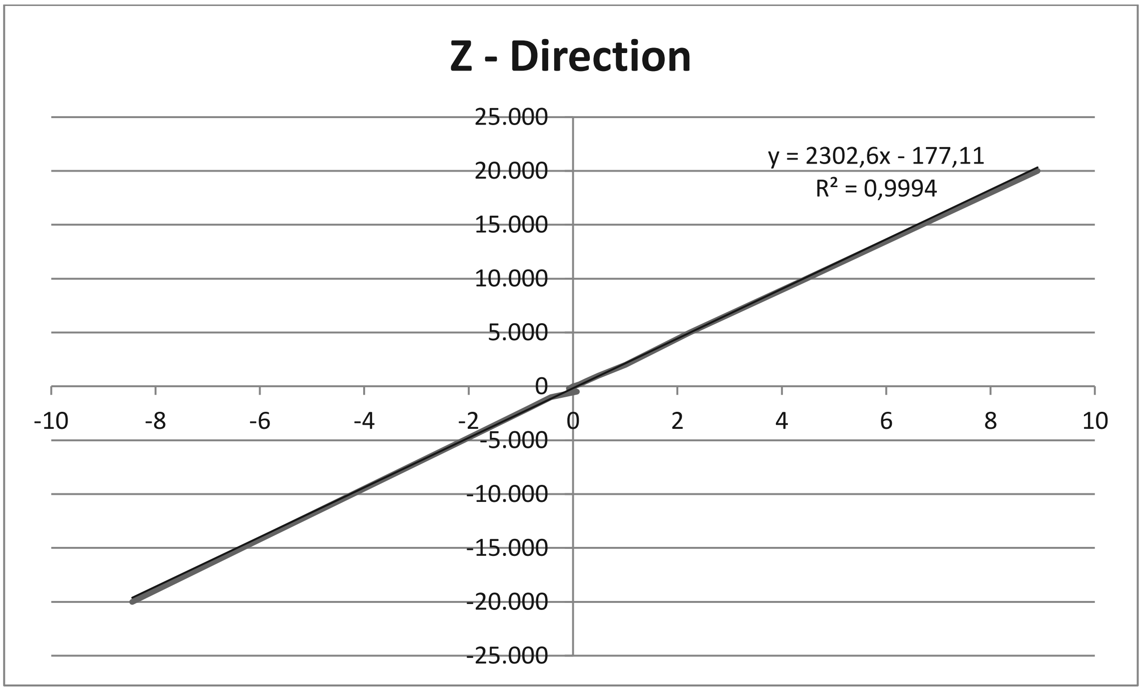

	Positive				Negative			
Load (N)	1'	2'	3'	Mean	1'	2'	3'	Mean
0	0,0003	0,0002	0,0002	0,0002	0,0004	0,0002	0,0003	0,0003
20	0,0188	0,0226	0,0249	0,0221	-0,0065	-0,0088	-0,0078	-0,0077
50	0,0353	0,0294	0,0323	0,0323	-0,0169	-0,0180	-0,0173	-0,0174
100	0,0758	0,0539	0,0687	0,0661	-0,0378	-0,0417	-0,0410	-0,0402
200	0,1350	0,1042	0,1271	0,1221	-0,0793	-0,0814	-0,0799	-0,0802
500	0,2710	0,2310	0,2550	0,2523	-0,2060	0,2190	0,2080	0,0737
1.000	0,5350	0,4600	0,4650	0,4867	-0,4140	-0,4300	-0,4210	-0,4217
2.000	1,0750	0,9120	1,0310	1,0060	-0,8330	-0,8470	-0,8460	-0,8420
5.000	2,2400	2,2400	2,2400	2,2400	-2,1000	-2,1000	-2,1000	-2,1000
10.000	4,4600	4,4800	4,4700	4,4700	-4,2200	-4,2200	-4,2200	-4,2200
15.000	6,6800	6,6900	6,6900	6,6867	-6,3400	-6,3300	-6,3300	-6,3333
20.000	8,9000	8,9000	8,9000	8,9000	-8,4500	-8,4500	-8,4500	-8,4500

Load cell - TR3D-A-5K-711

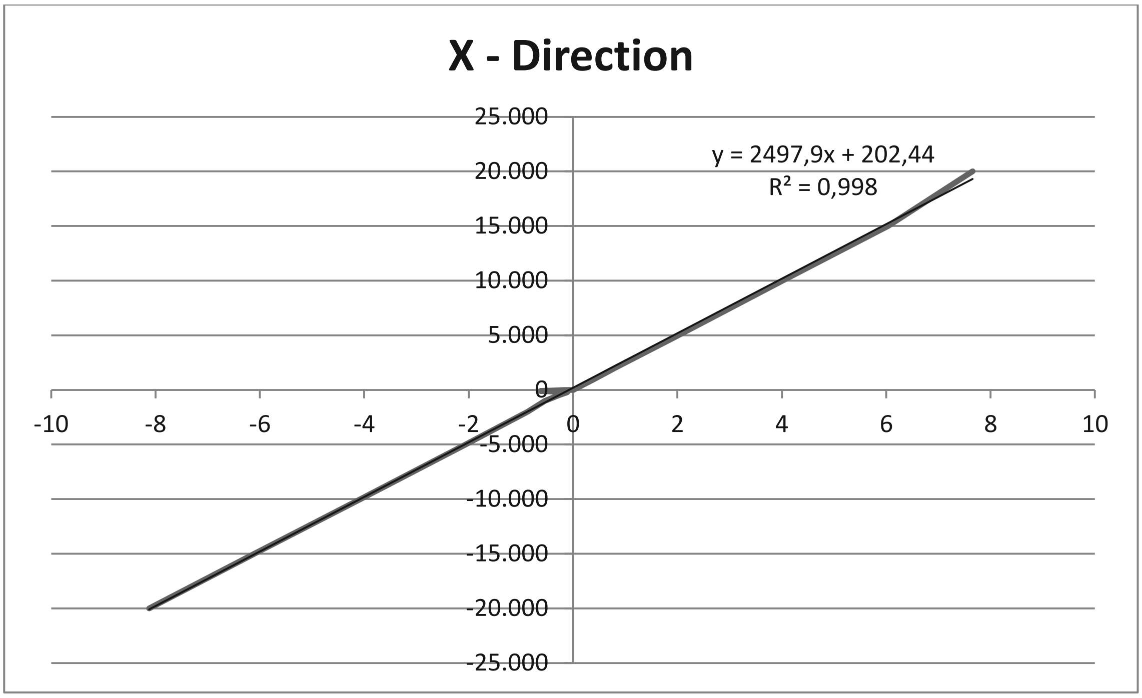

	Positive				Negative			
Load (N)	1'	2'	3'	Mean	1'	2'	3'	Mean
0	0,0001	0,0002	0,0004	0,0002	0,0001	0,0001	0,0001	0,0001
20	0,0162	0,0157	0,0169	0,0163	-0,1630	-0,1630	-0,1690	-0,1650
50	0,0242	0,0238	0,0251	0,0244	-0,3140	-0,3180	-0,3290	-0,3203
100	0,0475	0,0479	0,0436	0,0463	-0,6060	-0,6110	-0,6520	-0,6230
200	0,0849	0,0852	0,0836	0,0846	-0,1054	-0,1068	-0,1104	-0,1075
500	0,2020	0,2080	0,1998	0,2033	-0,2790	-0,2780	-0,2830	-0,2800
1.000	0,4010	0,4080	0,4090	0,4060	-0,5420	-0,5450	-0,5400	-0,5423
2.000	0,7980	0,8110	0,8040	0,8043	-0,8670	-0,8660	-0,8740	-0,8690
5.000	2,0100	2,0200	2,0200	2,0167	-2,0500	-2,0500	-2,0600	-2,0533
10.000	4,0100	4,0300	4,0100	4,0167	-4,0700	-4,0700	-4,0800	-4,0733
15.000	6,0400	6,0400	6,0400	6,0400	-6,1000	-6,1100	-6,1000	-6,1033
20.000	7,6500	7,6600	7,6500	7,6533	-8,1200	-8,1200	-8,1200	-8,1200

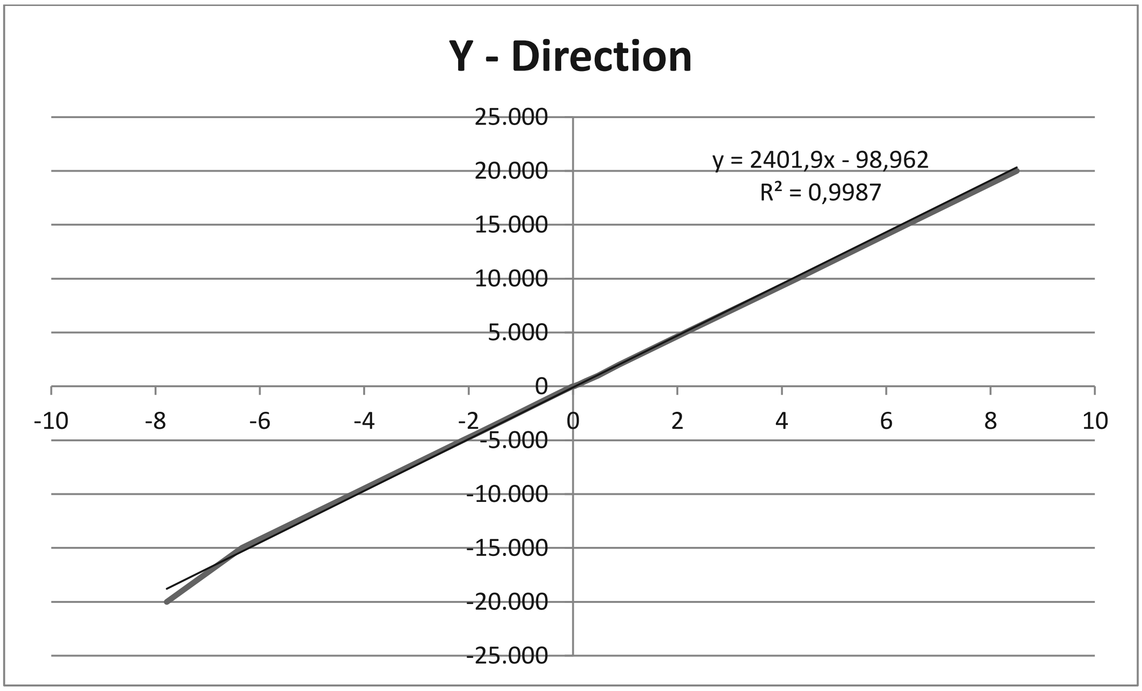

	Positive				Negative			
Load (N)	1'	2'	3'	Mean	1'	2'	3'	Mean
0	0,0002	0,0002	0,0002	0,0002	0,0002	0,0001	0,0002	0,0002
20	0,0183	0,0234	0,0192	0,0203	-0,0189	-0,0192	-0,0188	-0,0190
50	0,0343	0,0417	0,0387	0,0382	-0,0285	-0,0315	-0,0303	-0,0301
100	0,0656	0,0585	0,0613	0,0618	-0,0508	-0,0526	-0,0512	-0,0515
200	0,1091	0,1098	0,1115	0,1101	-0,0919	-0,0945	-0,0928	-0,0931
500	0,2380	0,2440	0,2390	0,2403	-0,2170	-0,2230	-0,2250	-0,2217
1.000	0,4750	0,4770	0,4750	0,4757	-0,4240	-0,4340	-0,4410	-0,4330
2.000	0,8850	0,8670	0,8850	0,8790	-0,8490	-0,8550	-0,8520	-0,8520
5.000	2,1500	2,1600	2,1500	2,1533	-2,1100	-2,1200	-2,1200	-2,1167
10.000	4,2900	4,2900	4,2900	4,2900	-4,2300	-4,2300	-4,2200	-4,2267
15.000	6,3900	6,4000	6,3900	6,3933	-6,3500	-6,3500	-6,3400	-6,3467
20.000	8,5000	8,5100	8,5000	8,5033	-7,7900	-7,7900	-7,7800	-7,7867

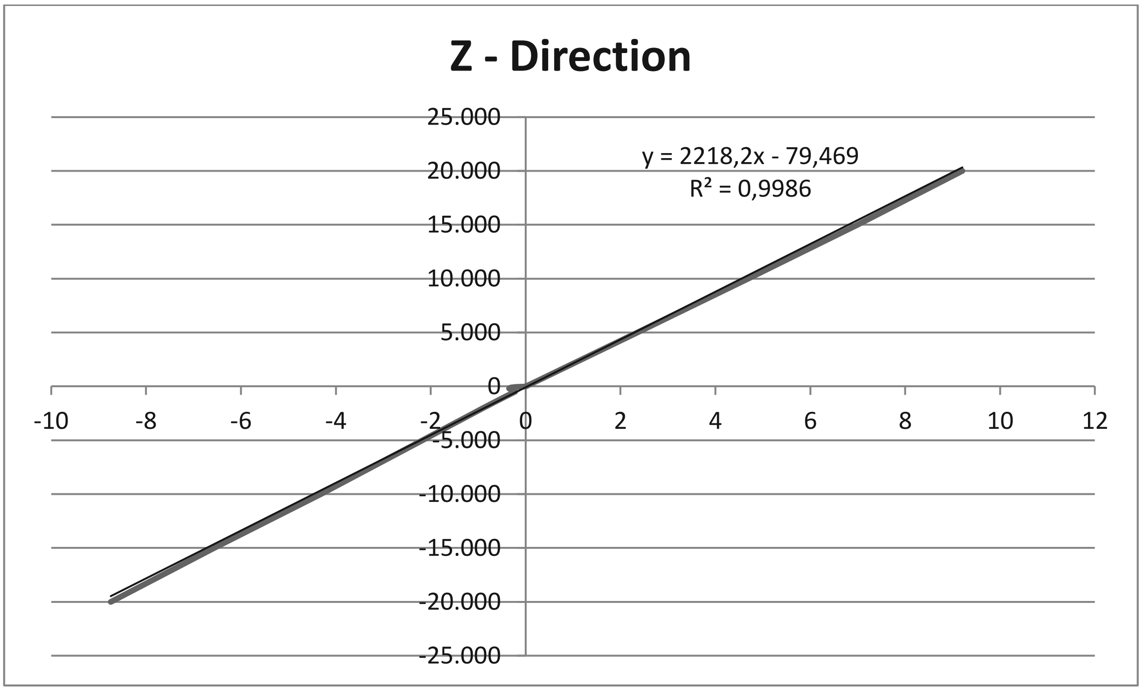

	Positive				Negative			
Load (N)	1'	2'	3'	Mean	1'	2'	3'	Mean
0	0,0007	0,0001	0,0004	0,0004	0,0002	0,0001	0,0003	0,0002
20	0,0150	0,0129	0,0141	0,0140	-0,0166	-0,0184	-0,0173	-0,0174
50	0,0265	0,0250	0,0252	0,0256	-0,0267	-0,2940	-0,2840	-0,2016
100	0,0466	0,0518	0,0510	0,0498	-0,0452	-0,4490	-0,4430	-0,3124
200	0,0960	0,0973	0,0966	0,0966	-0,8780	-0,0882	-0,0879	-0,3514
500	0,2380	0,2420	0,2410	0,2403	-0,2150	-0,2270	-0,2180	-0,2200
1.000	0,4720	0,4780	0,4750	0,4750	-0,4440	-0,4510	-0,4490	-0,4480
2.000	0,9430	0,9490	0,9470	0,9463	-0,8970	-0,8910	-0,8950	-0,8943
5.000	2,3600	2,3500	2,3600	2,3567	-2,1800	-2,1800	-2,1700	-2,1767
10.000	4,6900	4,6900	4,6800	4,6867	-4,3600	-4,2900	-4,2900	-4,3133
15.000	7,0000	7,0100	7,0000	7,0033	-6,5500	-6,5600	-6,5600	-6,5567
20.000	9,2000	9,2100	9,2000	9,2033	-8,7400	-8,7500	-8,7500	-8,7467

Appendix B

Blank holder CAD

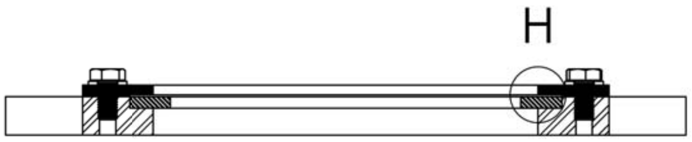

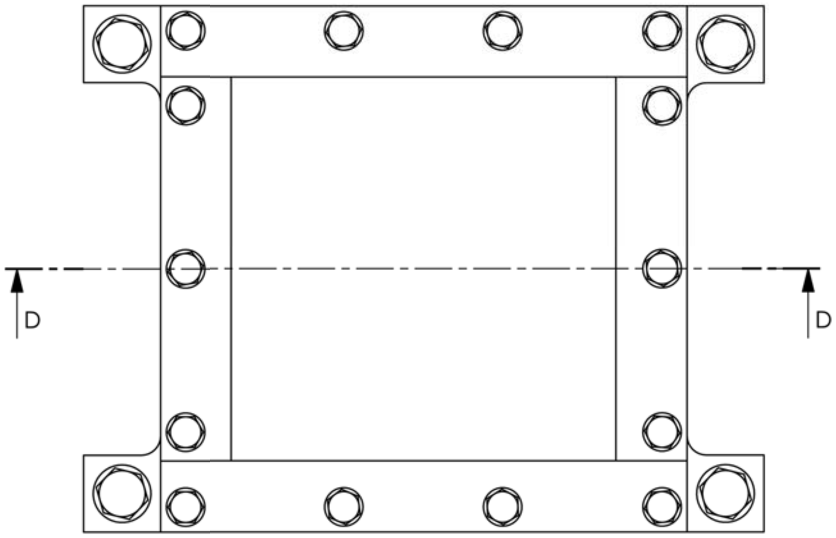

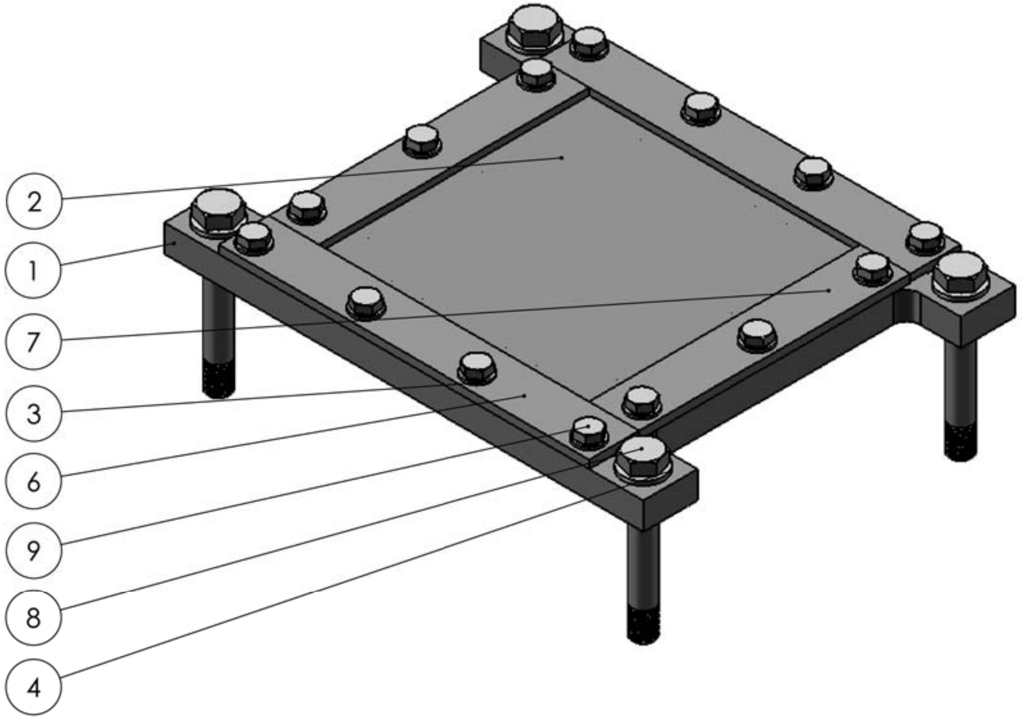

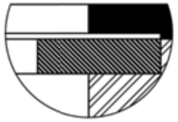

ITEM NO.	PART NUMBER	Material	Backing plate encaixado/QTD.
1	Placa inferior	AISI 1020	1
2	chapa		1
3	Washer DIN 125 - A 10.5		14
4	Washer DIN 125 - A 17		4
5	Backing plate_square	AISI 1020	1
6	Tira superior 1	AISI 1020	2
7	Tira superior 2	AISI 1020	2
8	DIN 7990 - M16 x 110-WS		4
9	ISO 4017 - M10 x 20-S		14

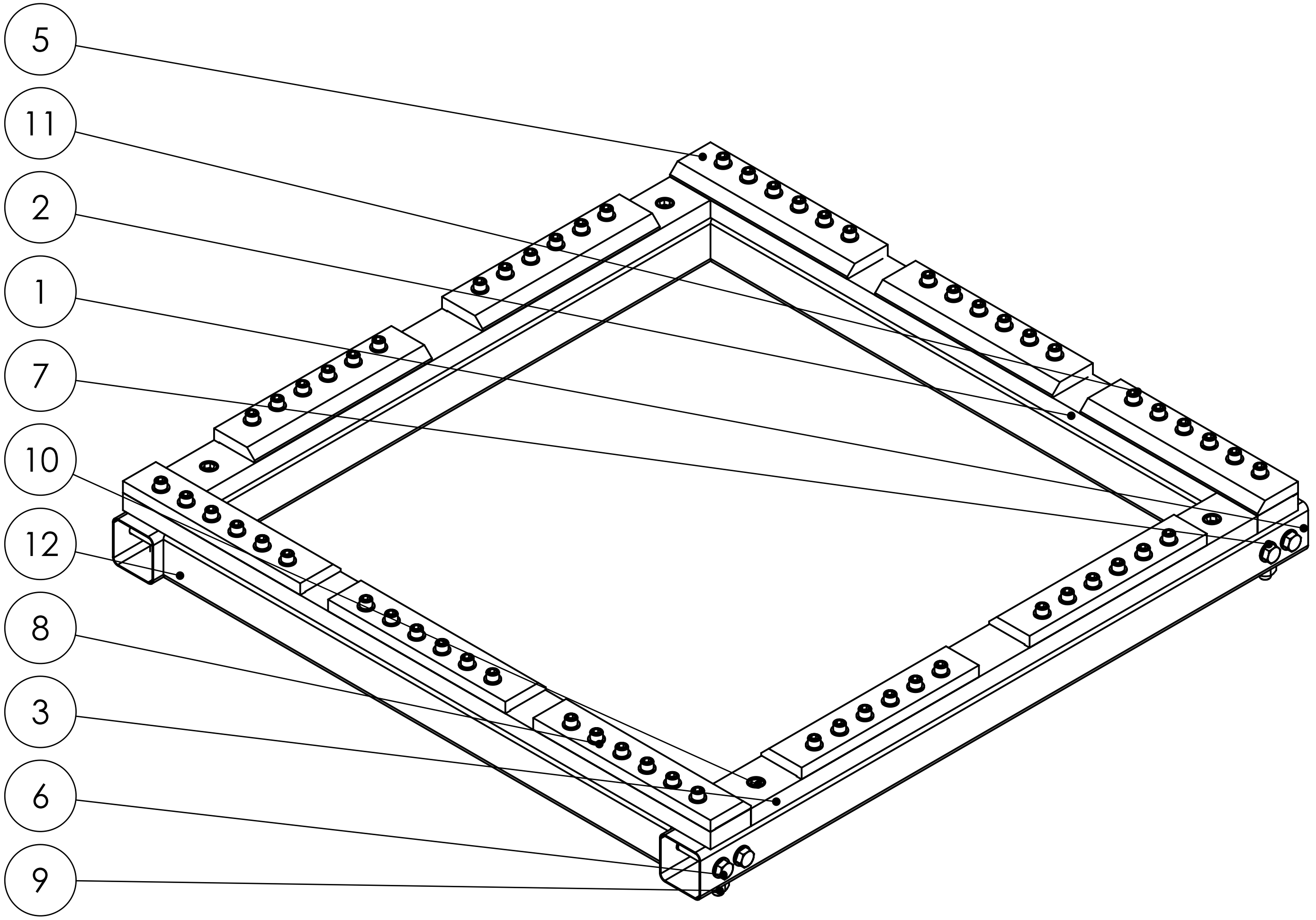

ITEM	PART NUMBER	QTY.	Material	Dimensões
1	Tubo Estrutura	2		
2	Base1	2	AISI 1020	30x80x1160
3	Base2	2	AISI 1020	30x80x1000
5	prensa chapa	10	AISI 1020	20x80x350
6	DIN 7990 - M16 x 100-NS	8		
7	Washer DIN 125 - A 17	16		
8	Washer DIN 125 - A 13	60		
9	Hexagon Nut DIN 6915 - M16 - C	8		
10	DIN 912 M16 x 120 --- 44C	8		
11	DIN 912 M12 x 35 --- 35S	60		
12	tubo de reforço	2		80x80x1000

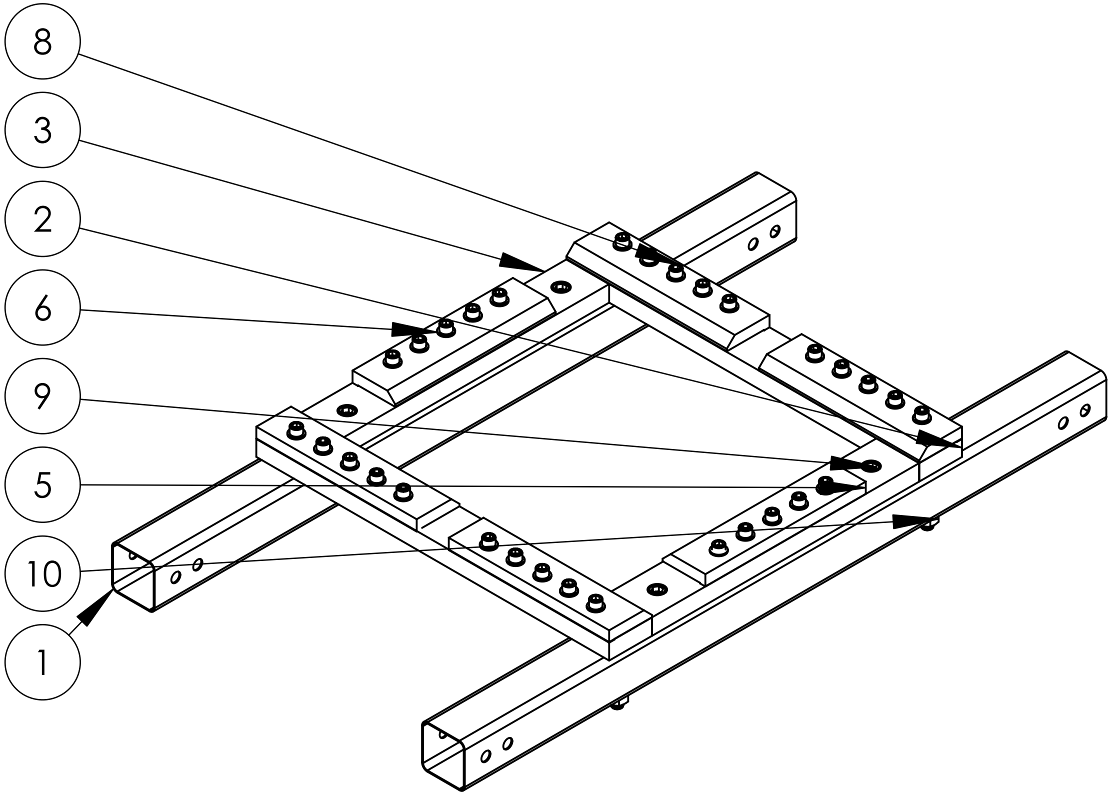

ITEM NO.	PART NUMBER	QTY.	Material	Dimensões
1	Tubo Estrutura	2		
2	Base_1	2	AISI 1020	30x80x660
3	Base_2	2	AISI 1020	30x80x500
5	prensa_chapa	6	AISI 1020	20x80x300
6	Washer DIN 125 - A 13	30		
7	Washer DIN 125 - A 17	8		
8	DIN 912 M12 x 35 --- 35S	30		
9	DIN 912 M16 x 120 --- 44S	8		
10	Hexagon Nut DIN 6915 - M16 - C	8		

Appendix C

Electrical plan

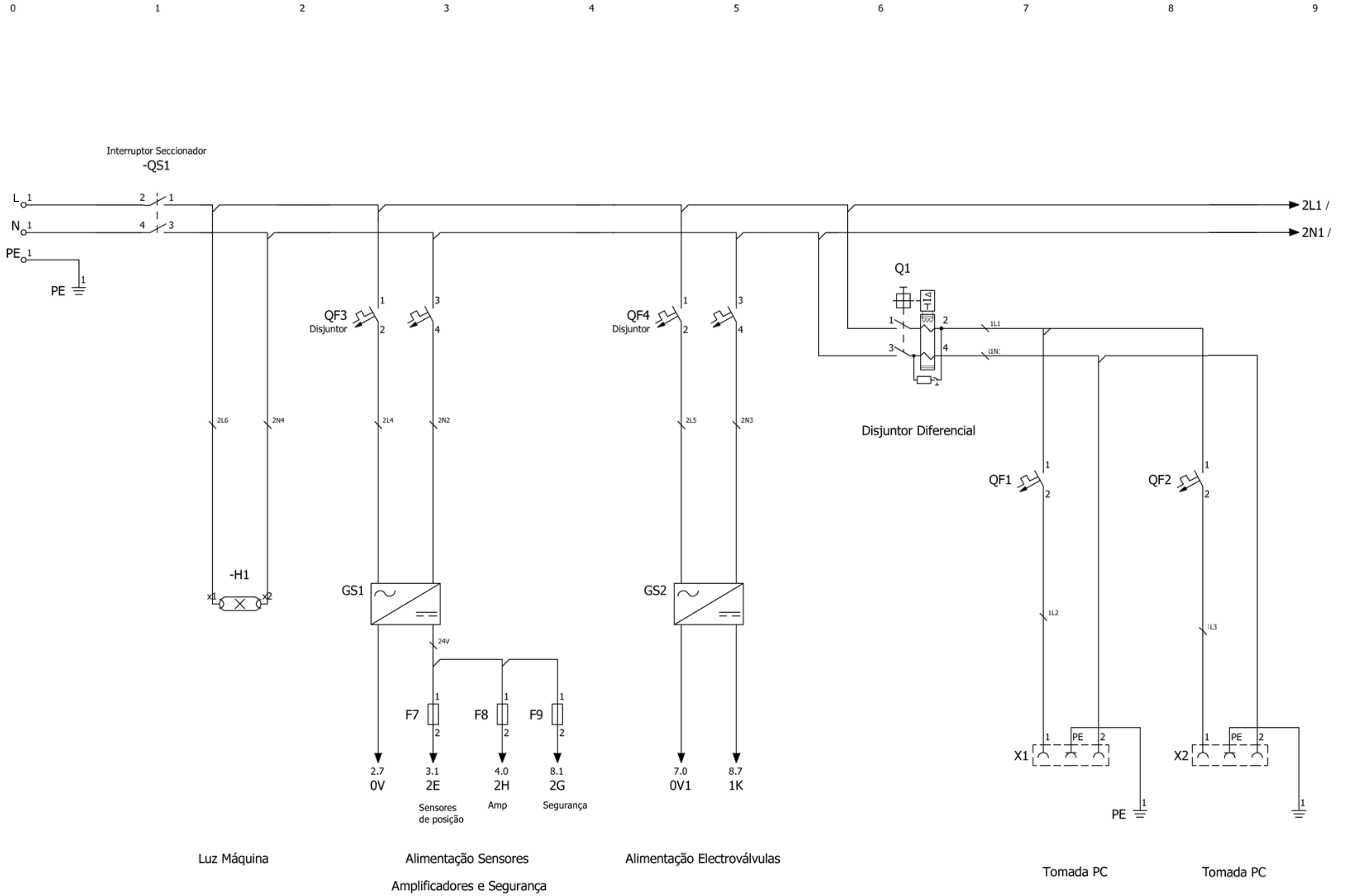
0
1
2
3
4
5
6
7
8
9
Interruptor Seccionador
-QS1
L
N
PE
PE
2L1 /
2N1 /
Q1
Disjuntor Diferencial
QF3
Disjuntor
QF4
Disjuntor
QF1
QF2
2L6
2N4
2L4
2N2
2L5
2N3
1L1
1N
1L2
1L3
-H1
x1
x2
GS1
GS2
24V
F7
F8
F9
2.7
0V
3.1
2E
4.0
2H
8.1
2G
7.0
0V1
8.7
1K
Sensores de posição
Amp
Segurança
X1
X2
PE
Luz Máquina
Alimentação Sensores Amplificadores e Segurança
Alimentação Electroválvulas
Tomada PC
Tomada PC

Próxima página
1

Plano Electrico SPIF-A
Nº 1

SPIFA

Departamento de Engenharia Mecânica

EPLAN

Potencia

Data de modificação
Alterado por

Verif
Formulário

=
+

Folha 2

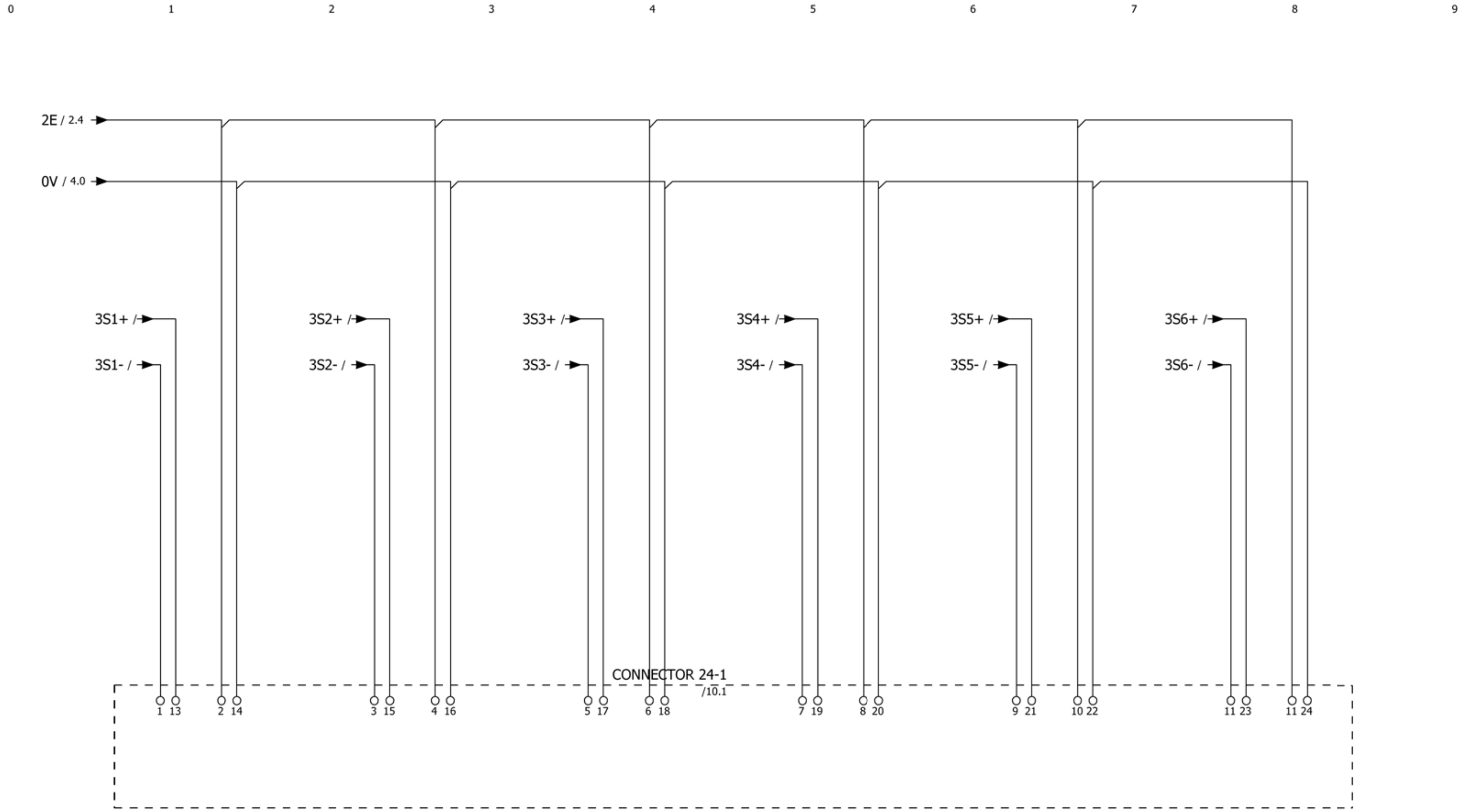
0
1
2
3
4
5
6
7
8
9
2E / 2.4
0V / 4.0
3S1+ /
3S1- /
3S2+ /
3S2- /
3S3+ /
3S3- /
3S4+ /
3S4- /
3S5+ /
3S5- /
3S6+ /
3S6- /
CONNECTOR 24-1
/10.1
1 13
2 14
3 15
4 16
5 17
6 18
7 19
8 20
9 21
10 22
11 23
11 24

Parte interna do conector

Próxima página
4

Página anterior
1

Plano Electrico SPIF-A Nº 1	SPIFA	Departamento de Engenharia Mecânica	ePLAN	Sensores de Posição	=	+
				Data de modificação Alterado por	Verif Formulário	Folha 3

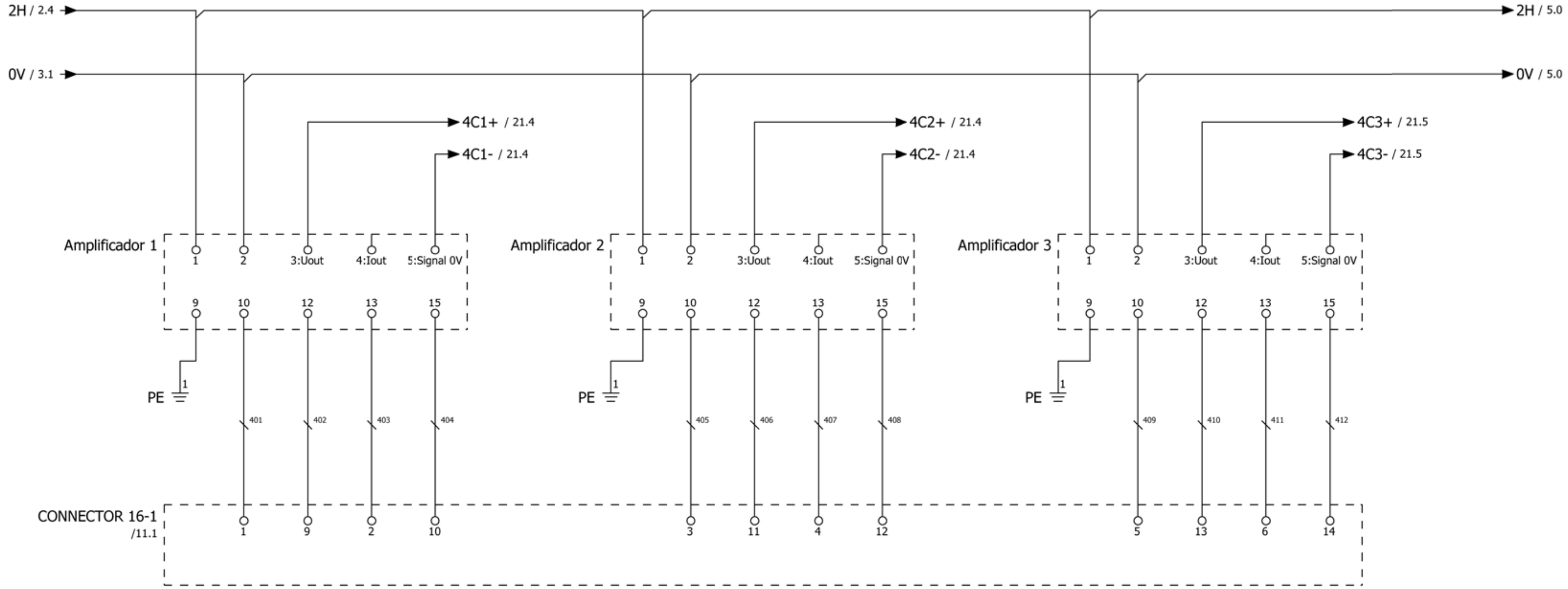
0 1 2 3 4 5 6 7 8 9
2H / 2.4
0V / 3.1
2H / 5.0
0V / 5.0
4C1+ / 21.4
4C1- / 21.4
4C2+ / 21.4
4C2- / 21.4
4C3+ / 21.5
4C3- / 21.5
Amplificador 1
Amplificador 2
Amplificador 3
1
2
3:Uout
4:Iout
5:Signal 0V
9
10
12
13
15
PE
1
401
402
403
404
405
406
407
408
409
410
411
412
CONNECTOR 16-1
/11.1
1
9
2
10
3
11
4
12
5
13
6
14

Parte interna do conector

Página anterior
3

Próxima página
5

Plano Electrico SPIF-A
Nº 1

SPIFA

Departamento de Engenharia Mecânica

Amp 1-3

Data de modificação
Alterado por

Verif
Formulário

=
+

Folha 4

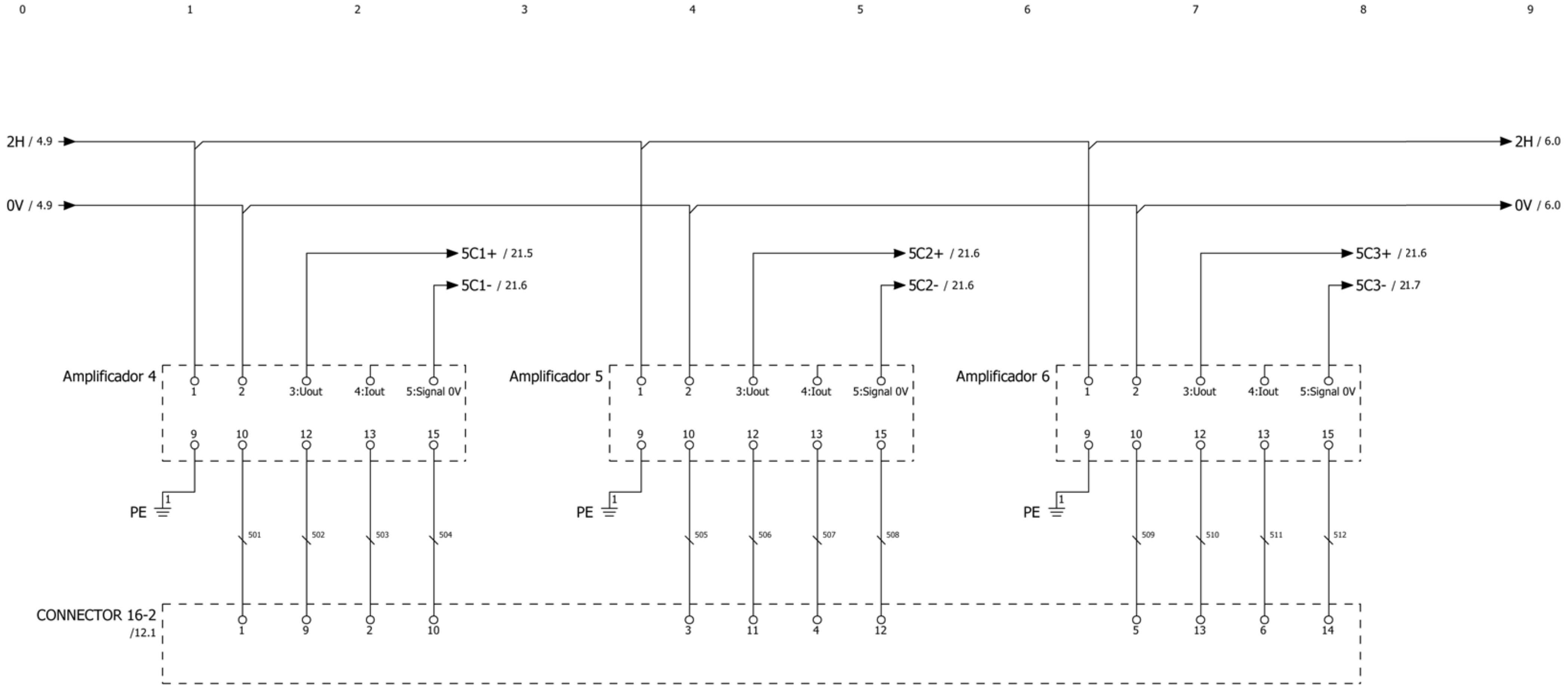
0
1
2
3
4
5
6
7
8
9
2H / 4.9
0V / 4.9
2H / 6.0
0V / 6.0
5C1+ / 21.5
5C1- / 21.6
5C2+ / 21.6
5C2- / 21.6
5C3+ / 21.6
5C3- / 21.7
Amplificador 4
Amplificador 5
Amplificador 6
1
2
3:Uout
4:Iout
5:Signal 0V
9
10
12
13
15
PE
1
501
502
503
504
505
506
507
508
509
510
511
512
CONNECTOR 16-2
/12.1
1
9
2
10
3
11
4
12
5
13
6
14

Parte interna do conector

Página anterior
4

Próxima página
6

Plano Electrico SPIF-A Nº 1	SPIFA	Departamento de Engenharia Mecânica	Amp 4-6		=	
			Data de modificação Alterado por	Verif Formulário	+	Folha 5

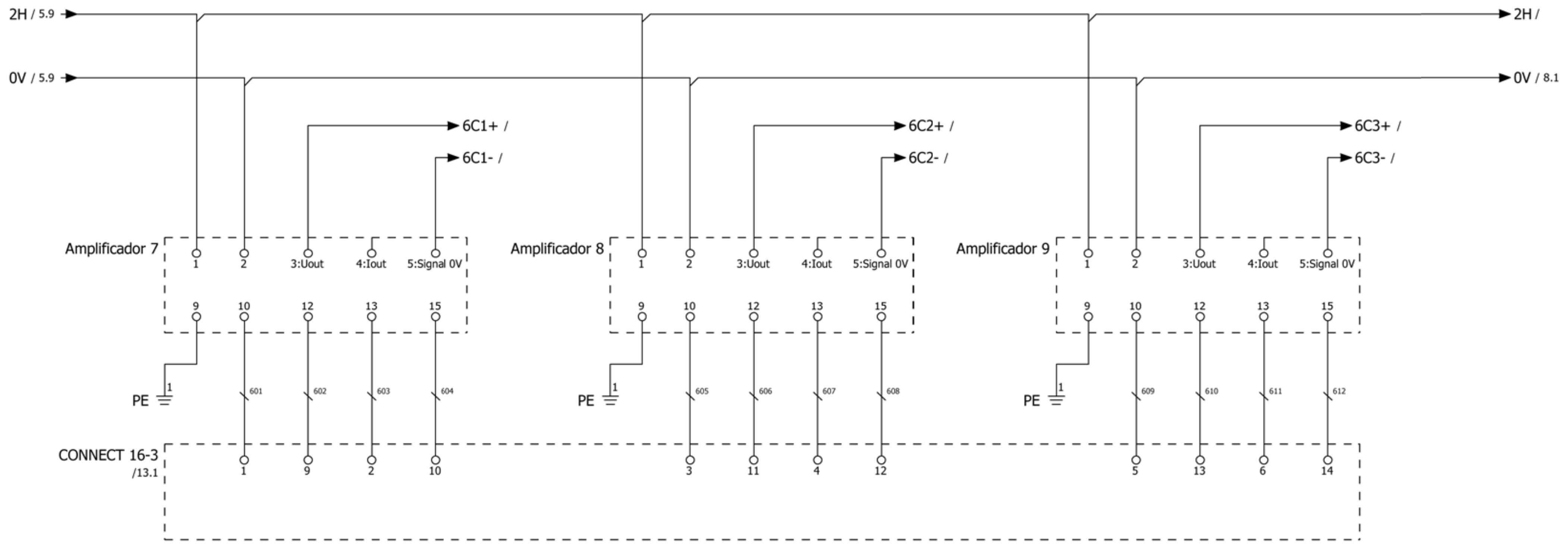
2H / 5.9
0V / 5.9
2H /
0V / 8.1
6C1+ /
6C1- /
6C2+ /
6C2- /
6C3+ /
6C3- /
Amplificador 7
Amplificador 8
Amplificador 9
1
2
3:Uout
4:Iout
5:Signal 0V
9
10
12
13
15
PE
601
602
603
604
605
606
607
608
609
610
611
612
CONNECT 16-3
/13.1
1
9
2
10
3
11
4
12
5
13
6
14

Parte interna do conector

Plano Electrico SPIF-A
Nº 1

SPIFA

Departamento de Engenharia Mecânica

Amp 7-9

Data de modificação
Alterado por

Verif
Formulário

=
+

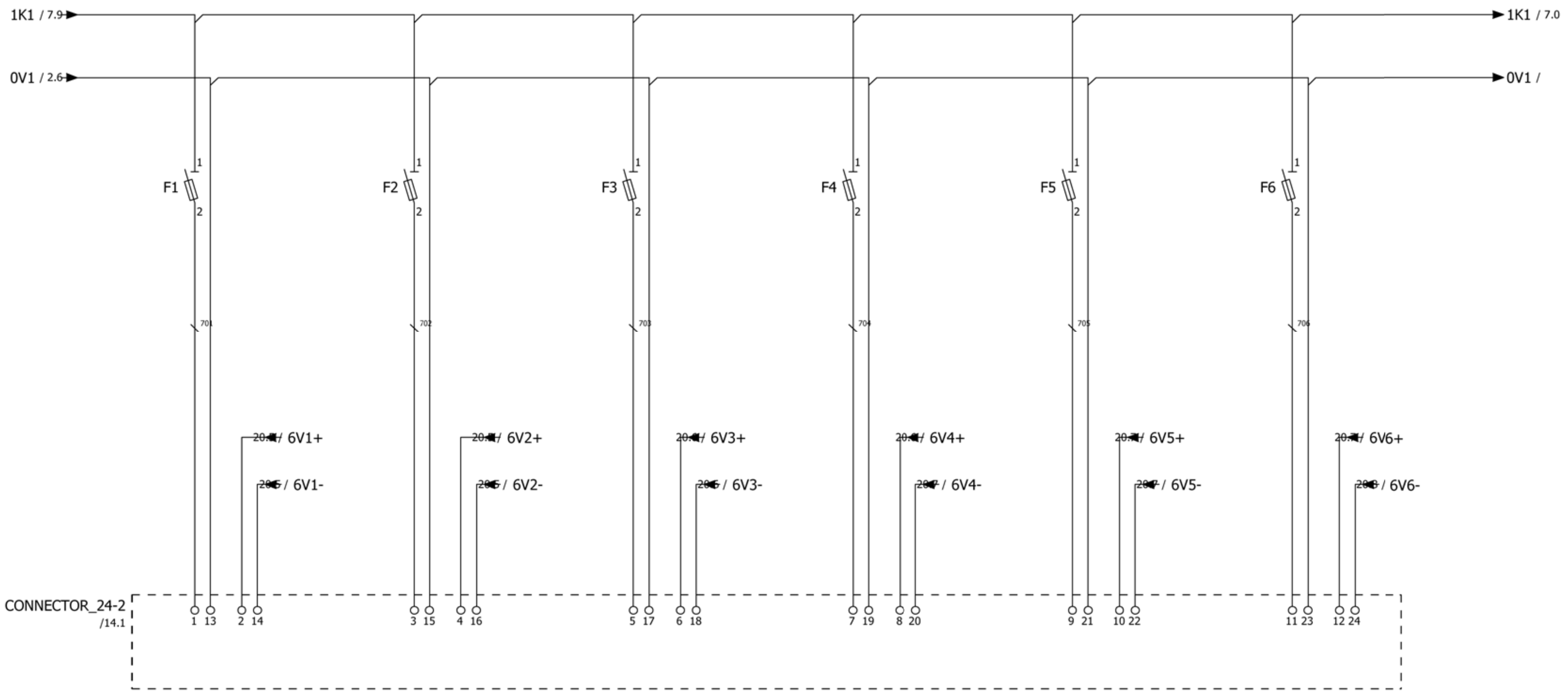
1K1 / 7.9
0V1 / 2.6
1K1 / 7.0
0V1 /
F1
F2
F3
F4
F5
F6
1
2
701
702
703
704
705
706
/ 6V1+
/ 6V1-
/ 6V2+
/ 6V2-
/ 6V3+
/ 6V3-
/ 6V4+
/ 6V4-
/ 6V5+
/ 6V5-
/ 6V6+
/ 6V6-
CONNECTOR_24-2
/14.1
1 13 2 14
3 15 4 16
5 17 6 18
7 19 8 20
9 21 10 22
11 23 12 24

Parte interna do conector

Plano Electrico SPIF-A
Nº 1

SPIFA

Departamento de Engenharia Mecânica

Electroválvulas

Data de modificação
Alterado por

Verif
Formulário

=
+

Parte externa do conector

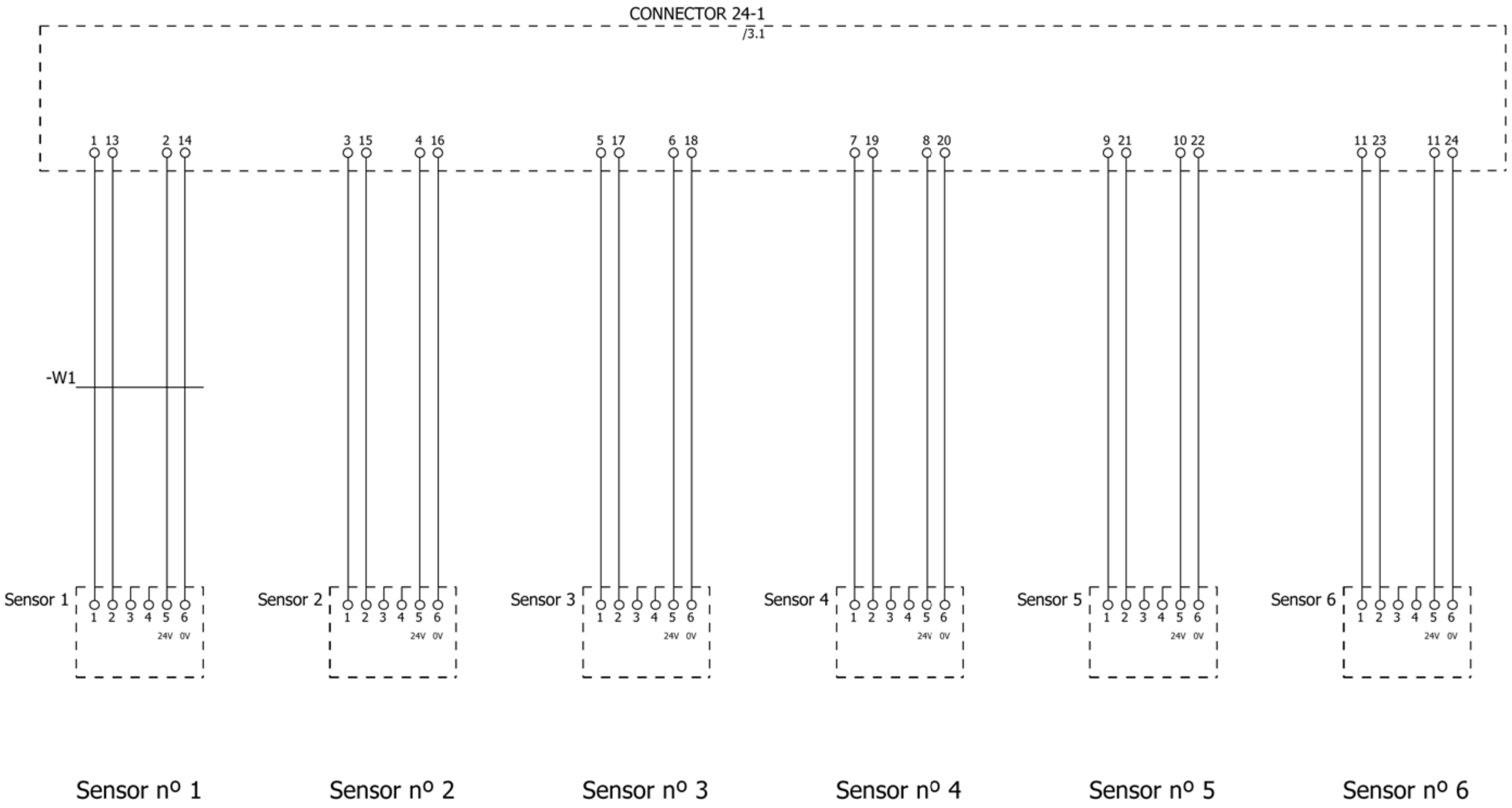
CONNECTOR 24-1
/3.1
1 13
2 14
3 15
4 16
5 17
6 18
7 19
8 20
9 21
10 22
11 23
11 24
-W1
Sensor 1
Sensor 2
Sensor 3
Sensor 4
Sensor 5
Sensor 6
1 2 3 4 5 6
24V 0V
Sensor nº 1
Sensor nº 2
Sensor nº 3
Sensor nº 4
Sensor nº 5
Sensor nº 6

Página anterior
7

Próxima página
11

Plano Electrico SPIF-A Nº 1	SPIFA	Departamento de Engenharia Mecânica	SENSORES Data de modificação Alterado por	Verif Formulário	= + Folha 10

Parte externa do conector

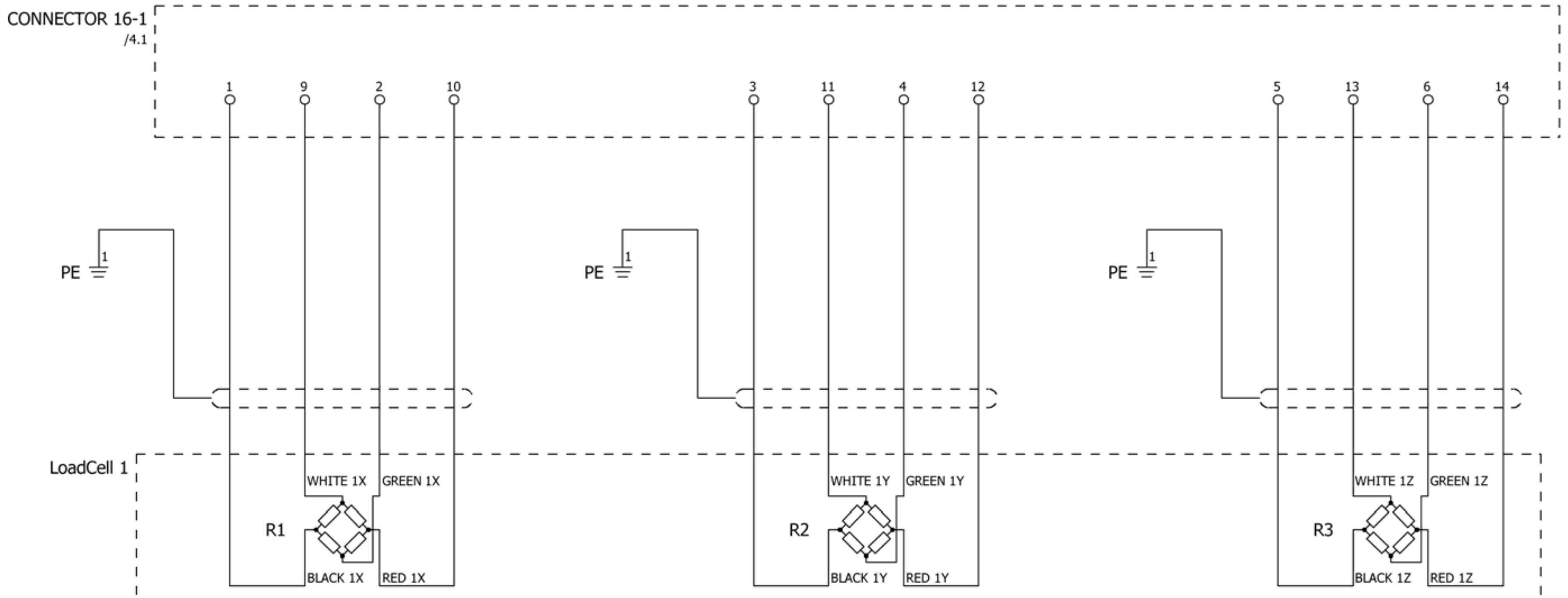
CONNECTOR 16-1
/4.1
1
9
2
10
3
11
4
12
5
13
6
14
PE
1
PE
1
PE
1
LoadCell 1
WHITE 1X
GREEN 1X
R1
BLACK 1X
RED 1X
WHITE 1Y
GREEN 1Y
R2
BLACK 1Y
RED 1Y
WHITE 1Z
GREEN 1Z
R3
BLACK 1Z
RED 1Z

Ponte de Wheatstone para medição de deslocamentos em XX

Ponte de Wheatstone para medição de deslocamentos em YY

Ponte de Wheatstone para medição de deslocamentos em ZZ

Parte externa do conector

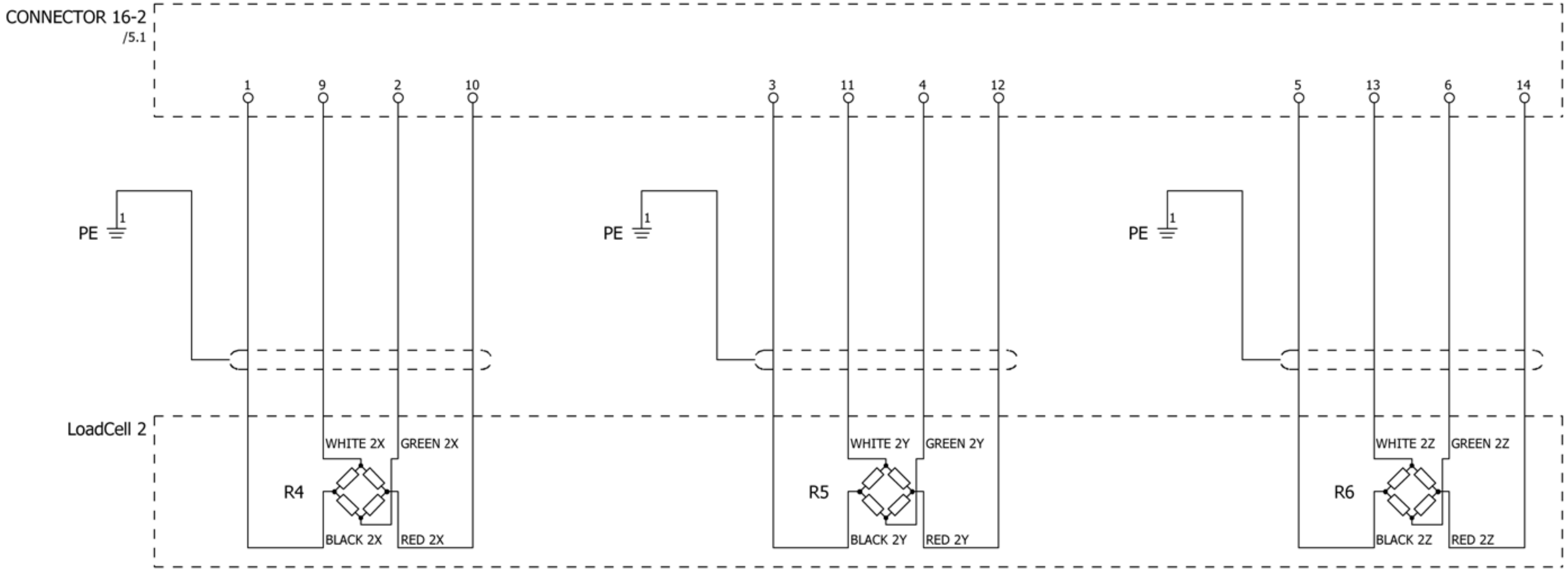
CONNECTOR 16-2
/5.1
1
9
2
10
3
11
4
12
5
13
6
14
PE
1
PE
1
PE
1
LoadCell 2
WHITE 2X
GREEN 2X
R4
BLACK 2X
RED 2X
WHITE 2Y
GREEN 2Y
R5
BLACK 2Y
RED 2Y
WHITE 2Z
GREEN 2Z
R6
BLACK 2Z
RED 2Z

Ponte de Wheatstone para medição de deslocamentos em XX

Ponte de Wheatstone para medição de deslocamentos em YY

Ponte de Wheatstone para medição de deslocamentos em ZZ

Parte externa do conector

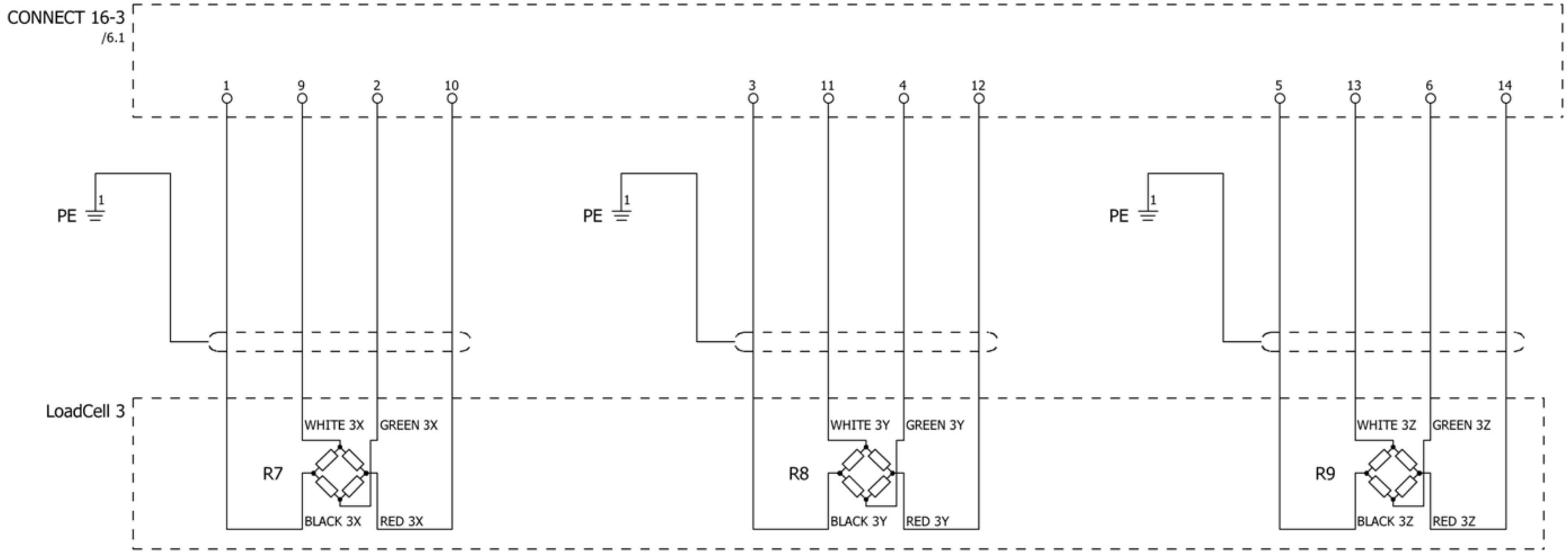
CONNECT 16-3
/6.1
1
9
2
10
3
11
4
12
5
13
6
14
PE
1
PE
1
PE
1
LoadCell 3
WHITE 3X
GREEN 3X
R7
BLACK 3X
RED 3X
WHITE 3Y
GREEN 3Y
R8
BLACK 3Y
RED 3Y
WHITE 3Z
GREEN 3Z
R9
BLACK 3Z
RED 3Z

Ponte de Wheatstone para medição de deslocamentos em XX

Ponte de Wheatstone para medição de deslocamentos em YY

Ponte de Wheatstone para medição de deslocamentos em ZZ

Plano Electrico SPIF-A
Nº 1

SPIFA

Departamento de Engenharia Mecânica

CÉLULA 3

Data de modificação
Alterado por

Verif
Formulário

=
+

Parte externa do conector

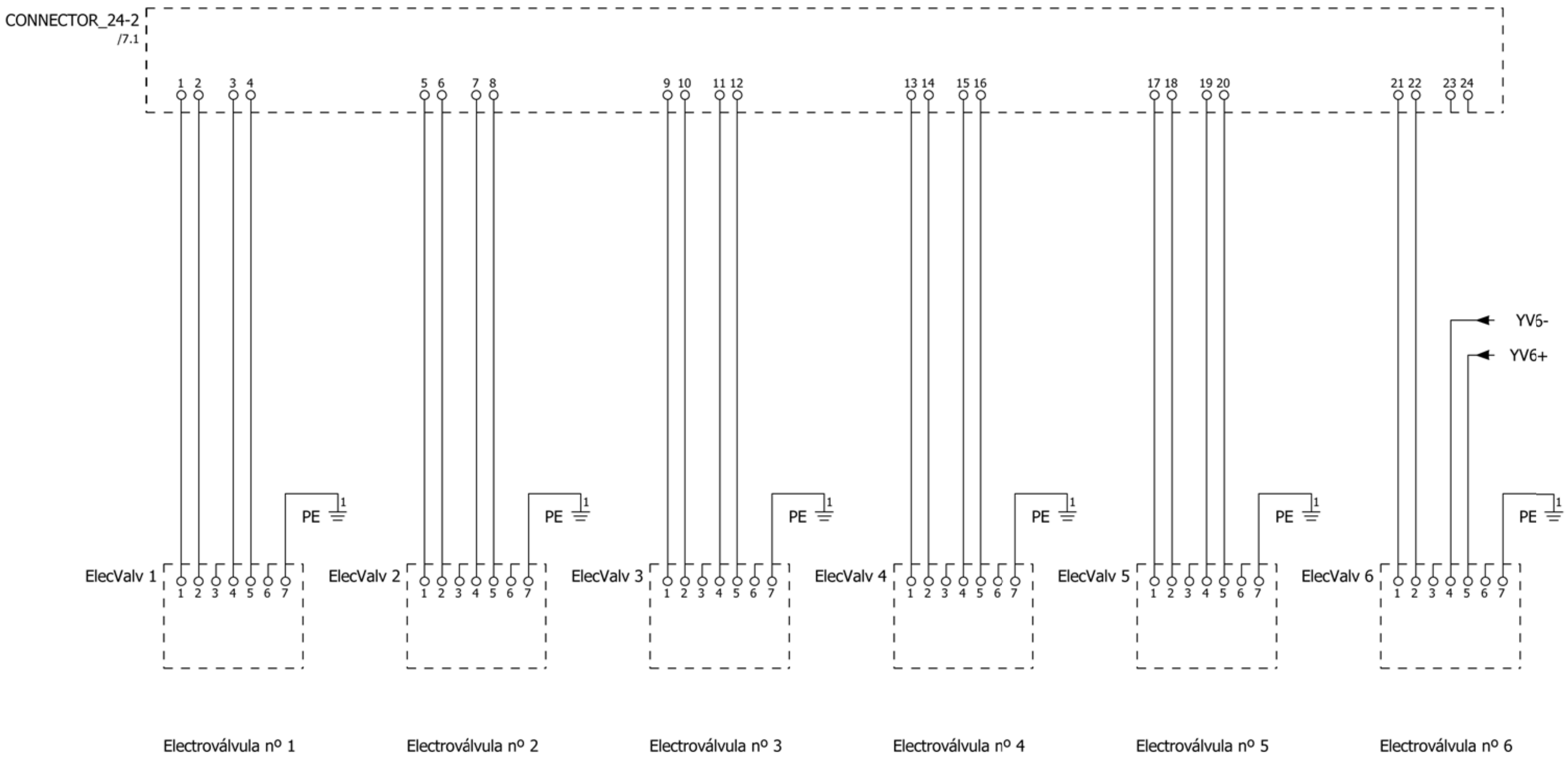
CONNECTOR_24-2
/7.1
1 2 3 4 5 6 7 8 9 10 11 12 13 14 15 16 17 18 19 20 21 22 23 24
YV6-
YV6+
PE 1
ElecValv 1
ElecValv 2
ElecValv 3
ElecValv 4
ElecValv 5
ElecValv 6
1 2 3 4 5 6 7
Electroválvula nº 1
Electroválvula nº 2
Electroválvula nº 3
Electroválvula nº 4
Electroválvula nº 5
Electroválvula nº 6

Plano Electrico SPIF-A
Nº 1

SPIFA

Departamento de Engenharia Mecânica

VALVULAS

Data de modificação
Alterado por

Verif
Formulário

=
+

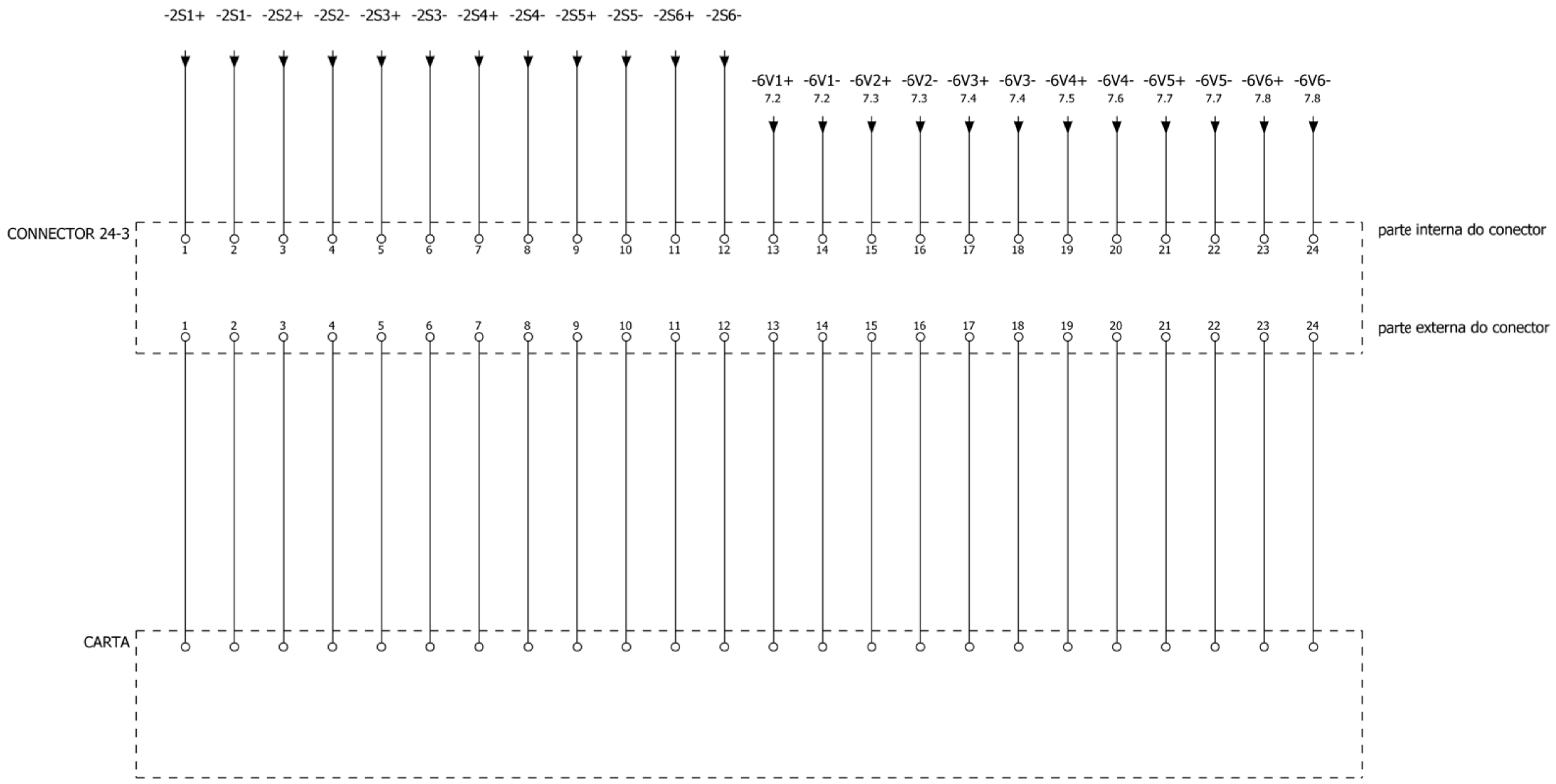
-2S1+
-2S1-
-2S2+
-2S2-
-2S3+
-2S3-
-2S4+
-2S4-
-2S5+
-2S5-
-2S6+
-2S6-
-6V1+ 7.2
-6V1- 7.2
-6V2+ 7.3
-6V2- 7.3
-6V3+ 7.4
-6V3- 7.4
-6V4+ 7.5
-6V4- 7.6
-6V5+ 7.7
-6V5- 7.7
-6V6+ 7.8
-6V6- 7.8
CONNECTOR 24-3
parte interna do conector
parte externa do conector
1 2 3 4 5 6 7 8 9 10 11 12 13 14 15 16 17 18 19 20 21 22 23 24
CARTA

Página anterior
14

Próxima página
21

Plano Electrico SPIF-A
Nº 1

SPIFA

Departamento de Engenharia Mecânica

Carta

Data de modificação
Alterado por

Verif
Formulário

=
+

Folha 20

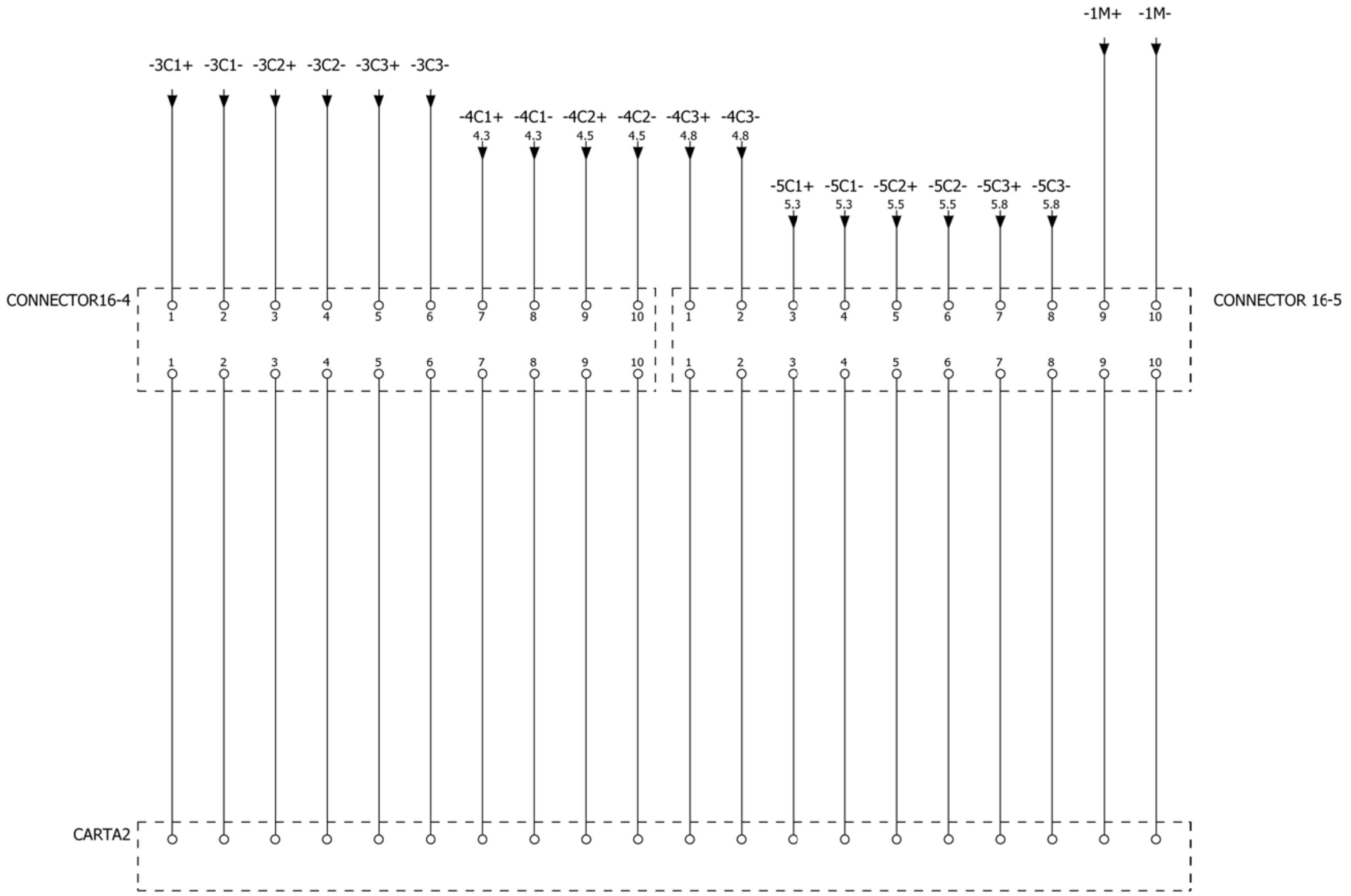
-3C1+
-3C1-
-3C2+
-3C2-
-3C3+
-3C3-
-4C1+ 4.3
-4C1- 4.3
-4C2+ 4.5
-4C2- 4.5
-4C3+ 4.8
-4C3- 4.8
-5C1+ 5.3
-5C1- 5.3
-5C2+ 5.5
-5C2- 5.5
-5C3+ 5.8
-5C3- 5.8
-1M+
-1M-
CONNECTOR16-4
1 2 3 4 5 6 7 8 9 10
CONNECTOR 16-5
1 2 3 4 5 6 7 8 9 10
CARTA2

Plano Electrico SPIF-A Nº 1	SPIFA	Departamento de Engenharia Mecânica	Carta2 Data de modificação Alterado por	Verif Formulário	= +

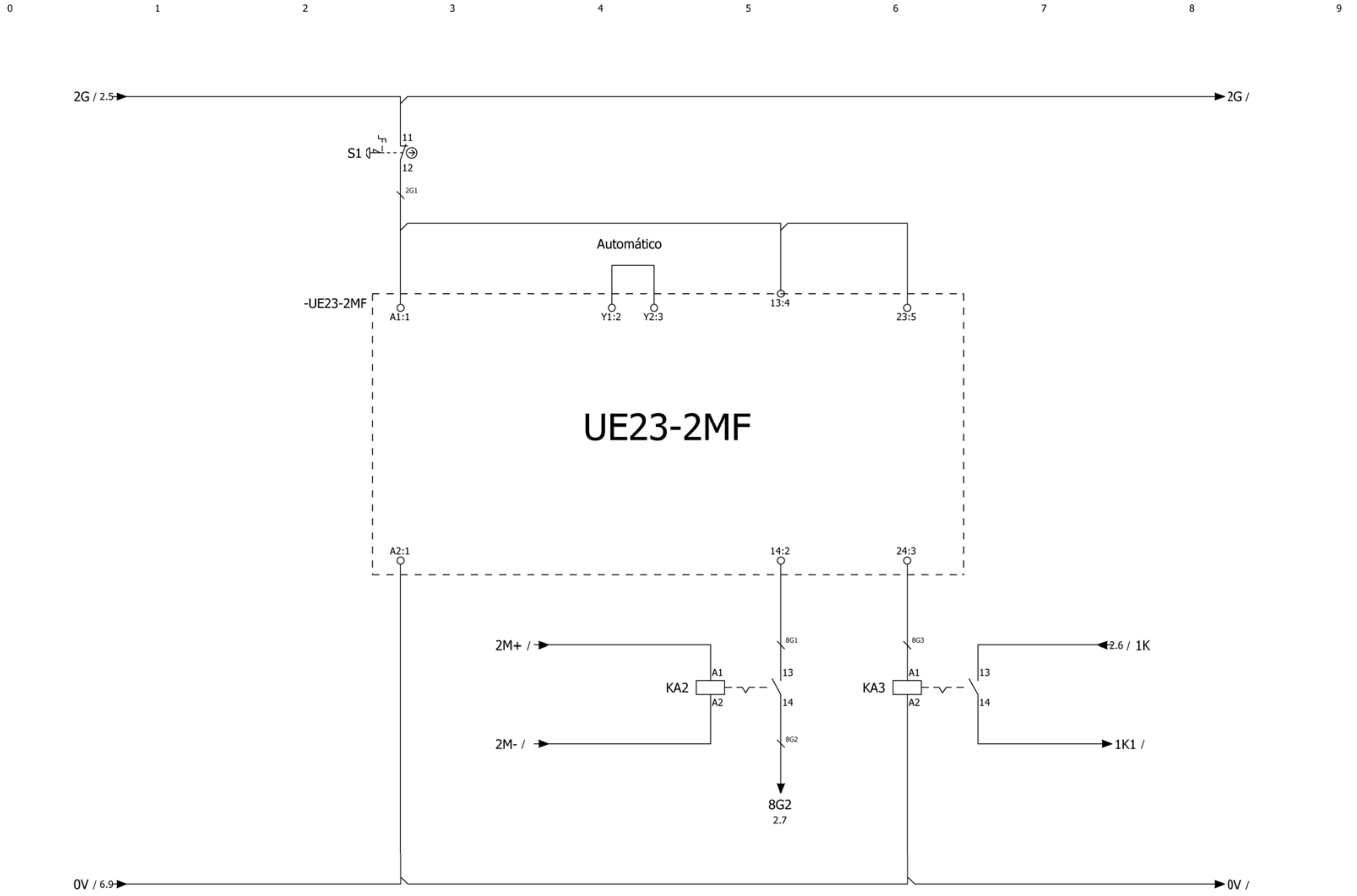
0
1
2
3
4
5
6
7
8
9
2G / 2.5
2G /
S1
11
12
2G1
Automático
-UE23-2MF
A1:1
Y1:2
Y2:3
13:4
23:5
UE23-2MF
A2:1
14:2
24:3
8G1
8G3
2M+ /
2.6 / 1K
KA2
A1
A2
13
14
KA3
A1
A2
13
14
2M- /
8G2
1K1 /
8G2
2.7
0V / 6.9
0V /

Próxima página

Página anterior
21

Plano Electrico SPIF-A
Nº 1

SPIFA

Departamento de Engenharia Mecânica

SEGURANÇA

Data de modificação
Alterado por

Verif
Formulário

=
+

Folha 8